Response to the comments of Referee #1:

Particle pollution has been raised wide attention in the world, and is quite prominent in China. Synoptic system is identified as one of the significant causes. This paper studied the relationship between particle pollution and weather pattern in the Yangtze River Delta region of China. The work is meaningful. The manuscript is well organized.

We appreciate the referee for the valuable and constructive reviews of our manuscript. We carefully revise the manuscript based on the following comments.

I suggest to publish the manuscript after addressing the comments and suggestions as below:

1) In Figure 2 and 3, it is better to mark the city name near each point.

Response: Thanks for the constructive comment. The city names have been added in Figs. 2-3 in the new revised manuscript.

2) The study is discussed the regional air pollution, but the used pollution data are mainly based on the surface monitoring records in 16 cities. 16 points cannot well reveal the spatial characteristics of air pollution. So, it is better to use the MODIS/AOD data and add some more discussion based on them. The satellite information can help to show the regional condition.

Response: Thanks for the constructive comment. In the new revised manuscript, the aerosol optical depth data from satellite observation (MODIS/AOD) are used to reveal the regional characteristics of aerosol pollution. The introduction of MODIS/AOD data has been added in Section 2.1. More discussion based on the AOD data has been added in Section 3.1.1, 3.1.2 and 3.3.1. These added data and discussion words can help us to understand the spatial distribution of aerosol in this region.

3) The analysis of transport processes of particle pollution is limited to the geopotential height fields and wind fields at 850 hPa. It is better to give a more comprehensive comparison between different layers, for example, at surface layer, 850 hPa layer, and 500 hPa layer, etc.

Response: Thanks for the constructive comment.

We have added the comparison of geopotential height fields and wind fields between different layers (500, 850 and 1000 hpa) in Section 3.3.2 of the new revised manuscript.

Meanwhile, in the new revised manuscript, we also removed Figs. 6-10 of the original manuscript, and replaced them with Figs. 7-11, which present the averaged condition of all days for each weather pattern.

4) There are many grammar errors in this manuscript, including Lines 99-100, “a great deal of” are not a good choice of words. May be replaced by “a lot of researches”? Line 110, “focuses the pollution” should be replaced by “focuses on the pollution”. Line 271, “the most importance source” should be replaced by “the most important source”. Line 383, “occur for 14.3% of the days” may be revised as “occur in 14.3% of the days”. Line 389, “are less frequently” should be replaced by “are

less frequent”. Lines 398-399, “Fig. 6 to 10” should be replaced by “Figs. 6 to 10”. Many other errors are not pointed out here. Please improve the English of the manuscript with the aid of native speaker.

Response: Sorry for these grammatical errors in the original manuscript. The errors listed above are corrected as follows.

The words “a great deal of” on lines 99-100 of the original manuscript are revised as “many”. Please see line 105 in the new revised manuscript.

The words “focuses the pollution” on line 110 of the original manuscript are revised as “focuses on the pollution”. Please see line 115 in the new revised manuscript.

The words “the most importance source” on line 271 of the original manuscript are revised to “the most important source”. Please see line 322 in the new revised manuscript.

The words “occur for 14.3% of the days” on line 383 of the original manuscript are revised to “occur on 14.3% of the days”. Please see line 428 in the new revised manuscript.

The words “are less frequently” on line 389 of the original manuscript are revised to “are less frequent”. Please see line 434 in the new revised manuscript.

The words “Fig. 6 to 10” on lines 398-399 of the original manuscript are revised to “Figs. 7 to 11”. Please see lines 493-496 in the new revised manuscript.

Additionally, a professional language correcting company (Wiley Editing Services) has helped to modify and improve the English in the new manuscript carefully. Please see the revised manuscript with marks and the "language editing certificate".

Response to the comments of Referee #2:

In this manuscript, the regional characteristic of aerosol and its relation with synoptic weather patterns were discussed over the Yangtze River Delta region China. There are a lot of previous studies about PM10 and PM2.5 pollution in China. However, only a few of them have focused on the potential impacts of weather patterns on this kind of pollution. The results of this manuscript may be of great interests to the ACP audiences. Also, the study may be able to provide some useful views for the government on the air pollution control.

We would like to thank the referee for the valuable and affirmative comments of our manuscript. We carefully revise the manuscript based on the following comments.

Several comments and suggestions should be addressed before the publication of this paper.

(1) Section 3.1.1 and 3.1.3. Apart from the in-situ monitoring particle concentration records, the aerosol optical depth data (monitored records, satellite observation, etc.) can be analyzed to deep the discussion on the particle pollution in YRD.

Response: Thanks for the constructive comment. In the new revised manuscript, the aerosol optical depth data from satellite observation (MODIS/AOD) are used to reveal the regional characteristics of aerosol pollution and deep the discussion. The introduction of MODIS/AOD data has been added in Section 2.1. More discussion of AOD has been added in Section 3.1.1, 3.1.2 and 3.3.1. These added data and discussion words can help us to understand the spatial distribution of aerosol in this region.

(2) Section 3.2.2, the author only mentioned and analyzed the geopotential height fields and wind fields at 850 hPa on the key date. The results may be quite different when it comes to the averaged condition of all days corresponding to each weather pattern. It's suggested to add the averaged geopotential height fields and revise the discussion.

Response: Thanks for the constructive comment. In the new revised manuscript, we have removed Figs. 6-10 of the original manuscript, and replaced them with Figs. 7-11. Figs. 7-11 present the averaged condition of all days for each weather pattern. Meanwhile, according to the suggestion of Referee #1, we also added the comparison of geopotential height fields and wind fields between different layers (500, 850 and 1000 hpa) in Section 3.3.2 of the new revised manuscript.

(3) Section 3.3.1, the occurrence frequencies of five weather patterns during the regional particle pollution episodes are not yet enough to conclude the relationship between them. It's suggested to add more detailed analysis for the monitoring data of particles (PM2.5 and PM10) and their precursors (such as SO2, NO2, etc.) at surface corresponding to each weather pattern.

Response: Thanks for the constructive comment. More detailed analysis of the surface monitoring data of air pollutants (including $PM_{2.5}$, PM_{10}, O_3, NO_2, SO_2 and CO) for each weather pattern have been added in Section 3.3.1. Please see new Fig. 6 and the relevant discussion words in the new revised manuscript.

(4) Section 3.3.2, the wind speed and wind direction at surface are closely related to the transport processes. It's suggested to add the analysis of meteorological parameters from observational records corresponding to each weather pattern instead of NCEP reanalysis data.

Response: Thanks for the constructive comment. More detailed analyses for the surface monitoring data of meteorological parameters (wind speed, temperature, surface pressure and relative humidity) have been added in Section 3.3.1 of the new revised manuscript (new fig. 6 and the relevant discussion). In addition, the wind rose plots based on the daily data at the Nanjing site corresponding to each weather pattern from December 2013 to November 2014 are added in Figs. 7-11. The relevant discussion has also been added in Section 3.3.2 of the new revised manuscript. Besides, we also added the discussion of sea-level pressure field and wind field at 1000 hPa layer based on the NCEP reanalysis data, which can to some extent reflect the transport processes at the surface.

(5) The English should be polished. Some grammatical errors in this paper are listed as follows, Line 75, "Eastern Asian monsoon circulation" should be "East Asia monsoon circulation", "increasing aerosol loading" should be "increased aerosol loading". Line 110, "focuses the pollution" should be "focuses on the pollution". Line 271-272, "the most importance source" should be "the most important source". Line 577, "it also confirmed" should be "it was also confirmed". It is suggested to correct the errors with the aid of a professional language correcting company.

Response: Sorry for these grammatical errors in the original manuscript. The errors listed above are corrected as follows.

The words "Eastern Asian monsoon circulation" on line 75 of the original manuscript are revised as "East Asia monsoon circulation". The words "increasing aerosol loading" are revised as "increased aerosol loading". Please see lines 80-81 in the new revised manuscript.

The words "focuses the pollution" on line 110 of the original manuscript are revised as "focuses on the pollution". Please see line 115 in the new revised manuscript.

The words "the most importance source" on lines 271-272 of the original manuscript are revised as "the most important source". Please see line 322 in the new revised manuscript.

The words "it also confirmed" on line 577 of the original manuscript are revised as "these results also confirm ". Please see line 725 in the new revised manuscript.

Additionally, a professional language correcting company (Wiley Editing Services) has helped to modify and improve the English in the new manuscript carefully. Please see the revised manuscript with marks and the "language editing certificate".

Regional severe particle pollution and its association with synoptic weather patterns in the Yangtze River Delta region, China

Lei Shu [1], Min Xie [1*], Da Gao [1], Tijian Wang [1*], Dexian Fang [2], Qian Liu [3], Anning Huang [1], Liwen Peng [1]

[1] School of Atmospheric Sciences, CMA-NJU Joint Laboratory for Climate Prediction Studies, Jiangsu Collaborative Innovation Center for Climate Change, Nanjing University, Nanjing 210023, China

[2] Chongqing Institute of Meteorology and Science, Chongqing 401147, China

[3] Jiangsu Provincial Academy of Environmental Science, Nanjing 210036, China

----

*Corresponding to Min Xie (minxie@nju.edu.cn) and Tijian Wang (tjwang@nju.edu.cn)

Abstract: Regional air pollution is significantly associated with ~~the~~ dominant weather systems. In this study, the relationship between the particle pollution over the Yangtze River Delta (YRD) region and ~~the~~ weather patterns is investigated. ~~Firstly,~~ First, the pollution characteristics of particles in the YRD are studied ~~by~~ using ~~the in-situ~~in situ monitoring data ($PM_{2.5}$ and PM_{10}) in 16 cities and Terra/MODIS AOD (aerosol optical depth) products collected from December 2013 to November 2014. The results show that the regional mean value of AOD is high in the YRD, with ~~the~~ an annual mean value of 0.71±0.57. The annual mean particle concentrations in the cities of Jiangsu Province all exceed the national air quality standard. The pollution level is higher in ~~the~~ inland areas, ~~with~~ and the highest concentrations of $PM_{2.5}$ and PM_{10} ~~respectively being~~are 79 and 130 $\mu g \cdot m^{-3}$~~–~~, respectively, in Nanjing. The $PM_{2.5}/PM_{10}$ ratios are ~~usually~~ typically high, thus indicating that $PM_{2.5}$ is the overwhelmingly dominant particle pollutant in the YRD. The wintertime peak of particle concentrations is tightly linked to the increased emissions ~~in~~ during the heating season, as well as ~~the~~ adverse meteorological conditions. ~~Secondly,~~ Second, based on NCEP reanalysis data, synoptic weather classification is conducted, and five typical synoptic patterns are objectively identified.~~to reveal the weather patterns that are easy to~~~~can easily cause severe particle pollution in the YRD. Five typical synoptic patterns are objectively identified,~~

~~including the East Asian trough rear pattern, the depression inverted trough pattern, the transversal trough pattern, the high-pressure controlled pattern, and the northeast cold vortex pattern.~~ Finally, the synthetic analysis of meteorological fields and backward trajectories are applied to further clarify how these patterns impact particle concentrations. It is demonstrated that air pollution is more or less influenced by high-pressure systems. The relative position~~s~~ of the YRD to the anti-cyclonic circulation~~s are quite~~exerts significant ~~to~~ effects on the air quality of the YRD. The YRD is largely influenced by polluted air masses from the northern and the southern inland areas when it is located at the rear of the East Asian major trough. The s~~S~~ignificant downward motion of air masses results in stable weather conditions, ~~and~~ thereby ~~hinders~~ hindering the diffusion of air pollutants. Thus, this~~e East Asian trough rear~~ pattern is quite favorable for the accumulation of pollutants in the YRD, ~~and causes~~resulting in higher regional mean PM_{10} (116.5±66.9 μg·m^{-3}), $PM_{2.5}$ (75.9±49.9 μg·m^{-3}) and AOD (0.74) values. Moreover, this pattern is also responsible for the ~~most~~ occurrence of most large-scale regional $PM_{2.5}$ (70.4%) and PM_{10} (78.3%) pollution episodes. High wind speed and ~~the~~ clean marine air masses may also play important roles in the mitigation of ~~the~~ pollution in the YRD. Especially when the clean marine air masses account for a large proportion of all trajectories (i.e., when the YRD is ~~controlled~~affected by the cyclonic system or ~~high-pressure controlled pattern and the northeast~~oceanic circulation ~~cold vortex pattern~~), the air in the YRD has ~~less~~ a smaller chance of being polluted. The ~~found~~ observed correlation between weather patterns and particle pollution can provide valuable ~~views~~ insight ~~in the~~into making decision~~s-making~~ ~~on~~ about pollution control and mitigation strategies.

Keywords: $PM_{2.5}$; PM_{10}; air pollution meteorology; synoptic weather pattern; the Yangtze River Delta region

1. Introduction

The ~~high~~ common occurrence of regional particle pollution ~~is~~ has acquired worldwide attention in the scientific community (Malm et al., 1994; Putaud et al., 2004; Chan and Yao, 2008) due to its adverse impacts on visibility (Singh and Dey, 2012; Green et al., 2012) and public health (Kappos et al., 2004; Brook et al., 2010). Generally, the causes ~~for~~ of this kind of pollution involve diverse aspects. Two major contributors ~~Among them~~to this pollution~~,~~ include the emission of pollutants and weather conditions ~~are two major contributors~~ (Oanh and Leelasakultum, 2011;

Young et al., 2016). Particle pollution in urban agglomerations is primarily attributed to ~~the hugevery~~ very large amounts of the anthropogenic emissions of primary particles and their precursors (e.g., SO_2, NO_x, ~~and~~ VOCs~~, etc.~~). However, these emissions are normally quasi-stable within a certain period of time (Kurokawa et al., 2013). Thus, the pollution level in a certain region generally depends on the regional weather conditions (~~namely~~ namely, weather patterns), which are strongly correlated with ~~the~~ synoptic-scale atmospheric circulation (Buchanan et al., 2002; Chuang et al., 2008; Flocas et al., 2009; Zhang et al., 2012; Zhao et al., 2013; Russo et al., 2014; Grundstrom et al., 2015; Zheng et al., 2015a; 2015b; Li et al., 2016).

~~Until now~~To date, researchers have gained an improved knowledge of the relationship between weather patterns and particle pollution. For example, Buchanan et al. (2002) observed ~~the~~ significantly elevated concentrations of Black Smoke and PM_{10} under the anti-cyclonic, southerly and southeasterly weather types in the city of Edinburgh in the UK between 1981 and 1996. Russo et al. (2014) ~~showed~~ presented an objective classification scheme ~~of~~ for the atmospheric circulation affecting Portugal between 2002 and 2010~~,~~ and revealed that higher concentrations of PM_{10}, O_3 and NO_2 are predominantly associated with synoptic circulation that is characterized by an eastern component and the advection of dry air masses. Previous studies have confirmed that ~~the~~ different levels of air pollution ~~have close relations~~are closely related with weather patterns~~, and also~~ and they ~~showed~~ ascribed its great spatial variability ~~ascribed~~ to the fact that the dominant weather pattern differs ~~among~~ between different regions (Flocas et al., 2009; Grundstrom et al., 2015).

In recent decades, the air pollution caused by PM_{10} and $PM_{2.5}$ has become ~~the~~ an extremely prominent air quality problem in the urban areas of China (Deng et al., 2011; Huang et al., 2012; Ji et al., 2012; Cheng et al., 2013; Kang et al., 2013; Huang et., 2014; Zhang et al., 2014; Xie et al., 2016a; 2016c; Zhu et al., 2017). Many studies have tried to reveal the meteorological contributions ~~of meteorology~~ to these severe particle pollution episodes. Chuang et al. (2008) identified seven weather patterns for aerosol events occurring from March 2002 to February 2005 in the Taipei B~~b~~asin~~,~~ and suggested that weather systems and their associated terrain blocking played important roles in the accumulation of $PM_{2.5}$ ~~accumulation~~ during the days of events~~ days~~. Niu et al. (2010) revealed the potential impacts of the weakening of the East Asian monsoon circulation and increased aerosol loading on the increase ~~of~~ in wintertime fog in China. Zhao et al.

(2013) analyzed a regional haze episode in the North China Plain from 16 to 19 January 2010~~,~~ and ~~pointed out~~noted that ~~the~~ strong temperature inversion, weak surface wind speed and descending air motions in the boundary layer were responsible for the accumulation of pollutants in a shallow layer ~~and~~ that produced high pollutant concentrations within the source region. Zheng et al. (2015a) found that ~~the~~ favorable atmospheric circulation conditions are responsible for the severe winter haze over northeastern China. Li et al. (2016) ~~pointed out~~noted that the fog-haze days over central and eastern China ~~shows a~~exhibited the clear features of inter-annual variations~~,~~ and that the strong (weak) East Asian winter monsoon may result in less (more) fog-haze days ~~across the~~throughout this region.

~~Located in the southeast coastal area of East China, t~~The Yangtze River Delta (YRD) region, which is located in the southeastern coastal area of East China, is one of the most developed urban economic ~~circles~~ regions in the world; it~~,~~ generally includes Shanghai, Jiangsu Province and Zhejiang Province, and it occupies over 20% of China's total gross domestic product (GDP) (Shu et al., 2016; Xie et al., 2016a; 2017). In recent years, ~~like~~ similar to other megacity clusters in China, such as the Beijing-Tianjin-Hebei (BTH) region (He et al., 2001; Chan and Yao, 2008; Ji et al., 2012; Zhang et al., 2012; 2014; Zhao et al., 2013; Zheng et al., 2015a) and the Pearl River Delta (PRD) region (Ho et al., 2003; Chan and Yao, 2008; Xie et al., 2016c; Zhu et al., 2017), the YRD has ~~also been suffering~~suffered from severe air pollution problems ~~brought~~ caused by an ~~accelerated~~ increasing population, urban expansion, and industrialization (Chan and Yao, 2008; Fu et al., 2008; 2010; 2014; Deng et al., 2011; Li et al., 2011; Huang et al., 2012; Kang et al., 2013; Wang et al., 2013; 2014; 2015; Xie et al., 2014; 2016a, 2016b, 2017; Feng et al., 2015; Zheng et al., 2015b; Shu et al., 2016; Xu et al., 2016; Ming et al., 2017). ~~Especially~~In particular, ~~the~~ severe particle pollution episodes are widely recognized as one of the major air pollution issues in the YRD (Fu et al., 2008; 2010; Deng et al., 2011; Huang et al., 2012; Kang et al., 2013; Kong et al., 2013; Wang et al., 2013; 2014; 2015; Fu et al., 2014; Feng et al., 2015; Zheng et al., 2015b; Xu et al., 2016; Ming et al., 2017). Thus, ~~a lot of~~ many ~~researches~~studies have been conducted to ~~figure out~~determine the contamination status (Fu et al., 2010; Kang et al., 2013; Wang et al., 2013; 2015; Feng et al., 2015; Ming et al., 2017), possible source (Fu et al., 2010; 2014; Kong et al., 2013; Wang et al., 2013; 2014; Xu et al., 2016), ~~or~~ and causes ~~and~~ or features (Fu et al., 2008; 2010; Huang et al., 2012; Wang et al., 2015; Zheng et al., 2015a) of these episodes. However, ~~among~~

these studies, the workstudies that have attempted to determine trying to figure out how particle pollution in the YRD is associated with synoptic weather patterns areis still quite limited. Zheng et al. (2015b) once summarized the synoptic-scale atmospheric circulations influencing the distribution of particles over eastern China in during autumn from 2001 to 2010. They found that there are six polluted weather types and three clean ones, and revealed that heavy pollution events particularly most commonly occur when the study areas are located at the rear of the anticyclone. However, tTheirhis study considerededs the influence of pollution in a region that is larger than YRD, only focusedds on the pollution in October, and is was mainly on basisbased of on satellite aerosol optical depth (AOD) data. Ground-based monitoring particle concentration data can better represent the status of particle pollution in the urban atmosphere of the YRD. Thus, to better understand the relationship between the pollution in the planetary boundary layer and the synoptic weather patterns over the YRD, further study studies should be conducted based on surface monitoring the data collected over a time period of at least over a one year from the surface monitoring inin the YRD.

This work attempts to enhance the our understanding of particle pollution in the YRD and, and provides the scientific knowledge for about the association of regional severe particle pollution and synoptic weather patterns. Firstly, First, we analyze the spatial and temporal distribution of PM_{10}, $PM_{2.5}$ and AOD in the YRD from December 2013 to November 2014 , aimed to illustrate the characteristics of particle pollution over the this region. Secondly, Second, synoptic weather classification is conducted to reveal the weather patterns related to heavy pollution. Finally, the synthetic analyseis of meteorological fields and backward trajectories are used to further clarify the impact mechanism. In this paper, Section 2 describes the observed data, the synoptic weather classification method and the trajectory model. Section 3 presents our main findings, including the a detailed analysis of the characteristics of particle pollution in the YRD, the synoptic weather patterns affecting the this pollution, and the mechanism how by which weather systems impact the pollution. In the endFinally, a brief summary is addressed presented in Section 4.

2. Data and methods

2.1 Observed data

The observed air quality data used in this study are obtained from the National Environmental Monitoring Center (NEMC) of China. The in situ monitoring data for of the hourly concentrations of $PM_{2.5}$, PM_{10}, CO, NO_2, SO_2 and O_3 can beare acquired from the national air quality real-time publishing platform (http://106.37.208.233:20035). Sixteen cities are selected as the representative research objects sites to better reflect the status of particle pollution over the YRD region. They These cities are include Shanghai, Changzhou, Nanjing, Nantong, Suzhou, Taizhoushi, Wuxi, Yangzhou, Zhenjiang, Hangzhou, Huzhou, Jiaxing, Ningbo, Shaoxing, Taizhou, and Zhoushan (here, Taizhou in Jiangsu Province is renamed referred to as Taizhoushi to distinguish it from the city of Taizhou in Zhejiang Province). Fig. 1 shows the locations of the 16 cities in the YRD. In order to better characterize the pollution levels of each city, The the hourly pollutant concentration for of a each city is calculated as the average value of the pollutant concentrations from measured in several of the national monitoring sites in that city, which can better characterize the pollution levels of the city. The sampling methods and the quality assurance and quality control (QA/QC) procedures used at each site act are in accordance with the Chinese national standard HJ/T193-2005 (State Environmental Protection Administration of China, 2006; Xie et al., 2016b). Furthermore, manual inspection is conducted in during data processing;, including this inspection includes the removal of the absentmissing and the abnormal values (such ase.g., $PM_{2.5}$ values that are higher than PM_{10} values). The period of this study startsThe study period lasts from December 2013 to November 2014. In the following analysis, winter refers to the period from December 2013 to February 2014. Accordingly, spring, summer and fall represent the periods from March to May, June to August, and September to November in 2014, respectively.

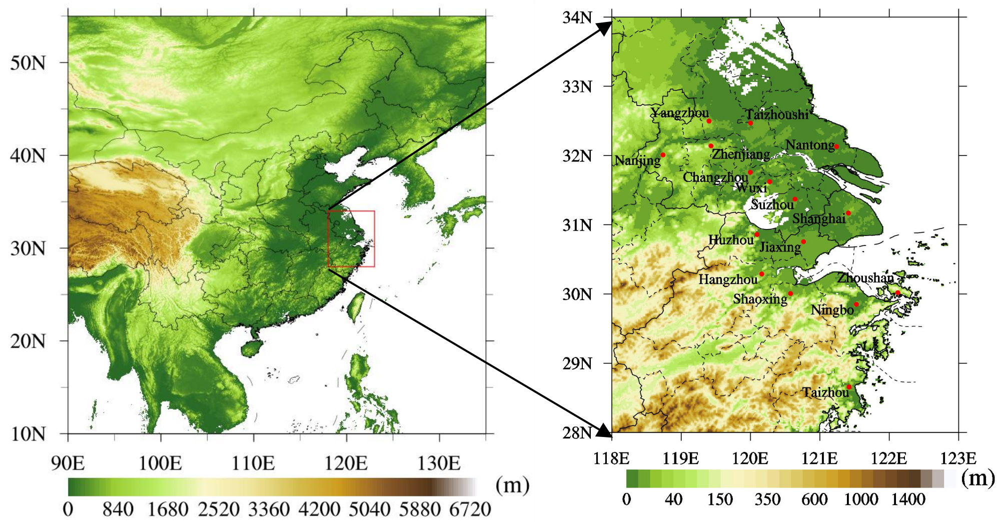

Figure 1. The location of the YRD in China (a) and 16 typical cities in the YRD (b), with ~~the~~ terrain elevation~~s~~ data. The terrain elevation~~s~~ data are obtained from the website (https://www.ngdc.noaa.gov/mgg/global/relief/ETOPO1/data/bedrock/cell_registered/).

The use of Moderate Resolution Imaging Spectroradiometer (MODIS) aerosol products can help ~~to~~ us comprehensively analyze the spatial and temporal variations ~~of~~ in aerosol loading over China. In this study, we use the aerosol optical depth (AOD) data obtained at a wavelength of 550 nm ~~wavelength~~ in the Terra/MODIS daily global Level 3 products (MOD08_D3). ~~They~~ These data can be obtained from the MODIS collection 6 (C6) dataset (https://ladsweb.nascom.nasa.gov/search/index.html). MODIS aerosol products are derived ~~by~~ using two entirely independent retrieval algorithms:~~,~~ one is used for deriving aerosols over land (Chu et al, 2002; 2003) and another is used for deriving aerosols over the ocean (Remer et al, 2002; 2005; Chu et al., 2005). Here, we use the C6 Deep Blue (DB) products ~~for deriving~~to derive aerosols over land, with ~~the~~ a spatial resolution of ~~1°~~ 1° × ~~1°~~ 1°, during the period from December 2013 to November 2014. ~~The~~ For detailed descriptions of the retrieval algorithms and their~~,~~ accuracy and validation, ~~can further~~ refer to the work of Hsu et al. (2013).

~~In order to~~To illustrate ~~the real~~actual weather situations, the hourly monitored meteorological parameter records in each of the 16 typical cities are also applied~~ as well~~. These data include 2 m temperature (T), 2 m relative humidity (RH), 10 m wind speed (WS), 10 m wind direction (WD) and surface air pressure (P). ~~They~~ These data are collected from the National Meteorological Center (http://www.nmc.cn).

2.2 Synoptic weather classification

Synoptic weather classification refers to the analysis of historical weather charts and the characterization of weather systems. It is more effective for ~~the~~ producing disastrous weather forecasts due to its ability to reveal ~~the~~ atmospheric circulation situations. With the gradual popularization of computer analysis and the ~~greater~~ increased sharing of data, synoptic weather classification has great practical value in ~~many other~~a wide variety of research fields. For example, it has widespread applications in the field of analyzing ~~the~~ weather patterns related to air pollution (Mcgregor and Bamzelis, 1995; Zhang et al., 2012; Santurtún et al., 2015).

Methods of synoptic weather classification can ~~be~~ generally be divided into ~~the~~ objective and ~~the~~ subjective methods (El-Kadi and Simithson, 1992). In this study, we apply the sums-of-squares technique, which is ~~one of the~~an objective classification method~~s~~ ~~and~~ that was established in 1973 by Kirchhofer (Kirchhofer, 1973). The sums-of-squares technique can effectively categorize more than 90% of ~~the~~ analyzed weather maps, which ~~is~~ represents an improvement over ~~the~~ other correlation techniques (Yarnal, 1984). ~~The steps of a~~The application of~~pplying~~ this technique ~~are threefold~~involves three steps. ~~Firstly,~~ First, the daily pressure data at each grid point~~s~~ are normalized as follows:

$$Z_i = \frac{(X_i - \overline{X})}{s} \qquad (1)$$

where Z_i is the normalized value of ~~the~~ grid point i, X_i is the value at grid point i, $\overline{X}$ is the mean value of the study domain, and s is the standard deviation. Data normalization removes the effects of the magnitude of pressure ~~magnitude~~ and improves the seasonal comparability of different weather types. ~~Secondly,~~ Second, each normalized grid point is compared to all other grid points~~s~~ ~~on the basis of~~based on the Kirchhofer score (S) ~~for~~ of each grid point:

$$S = \sum_{i=1}^{N} (Z_{ai} - Z_{bi}) \qquad (2)$$

where Z_{ai} is the normalized value ~~in~~ of grid point i on ~~the~~ day a, Z_{bi} is the normalized value ~~in~~ of grid point i on ~~the~~ day b, and N is the number of grid points. The Kirchhofer score (S) is calculated for each row (denoted as S_R), each column (S_C) and the entire study domain (S_T) to ensure the pattern similarity between any pair of patterns for all grid points. Finally, all days are separated into one of the identified synoptic weather patterns ~~according to the~~based on these three values and their empirically derived thresholds. ~~Thereinto~~Thus, the values of S_R, S_C and S_T must be lower than their respective threshold values ~~so that~~for these patterns ~~can~~ to be accepted as similar (Barry et al., 1981). For each daily grid, the lowest significant Kirchhofer score (S) is recorded with the associated key day, thus denoting the synoptic type of ~~the~~ that day. All r~~R~~emaining days are considered ~~as~~ to be 'unclassified'.

The ~~dataset of~~ meteorological field dataset used in the sums-of-squares technique ~~is from~~contains NCEP–DOE AMIP-II Reanalysis 2 data (Kanamitsu et al., 2002), which are collected at 00:00, 06:00, 12:00, and 18:00 UTC (universal time coordinated) (https://www.esrl.noaa.gov/psd/data/gridded/data.ncep.reanalysis2.pressure.html). These data have 144×73 horizontal grids ~~of 144×73,~~ with a grid spacing of 2.5°. From the ground level to 10 hPa, there are 17 pressure levels in the vertical direction. The classification of synoptic weather maps is conducted ~~by~~ using the gridded data at ~~the~~ a geopotential height of 850 hPa during the same time period when the air quality data are recorded. The domain of interest is centered over the YRD region, covering an area of 25-40° N in latitude and 110-128°E in longitude.

2.3 HYSPLIT model

Backward trajectories can be adopted to help understand transport paths and identify the source regions of air masses. The Hybrid Single-Particle Lagrangian Integrated Trajectory (HYSPLIT) Model (Version 4) ~~is~~ was developed by the National Oceanic and Atmospheric Administration (NOAA) Air Resources Laboratory (ARL). It is one of the most extensively used atmospheric transport and dispersion models for the study of air parcel trajectories (Draxler and Rolph, 2013; Rolph, 2013; Stein et al., 2016), and it has been ~~well~~ widely applied in simulations of the complex transport, diffusion, chemical transformation and deposition~~al~~ processes ~~simulations~~ of atmospheric pollutants (Mcgowan and Clark, 2008; Wang et al., 2011; Huang et al., 2015; Xie et al., 2016b).

In this study, HYSPLIT is used to compute the ~~air parcel~~ backward trajectories of air parcels, reveal the possible source regions of air masses, and establish ~~the~~ source-receptor relationships for each synoptic weather pattern. For each synoptic weather pattern, the terminus of ~~the~~ each trajectory~~ies~~ is considered to be located at the observation site in Nanjing (32°N, 118.8°E). The 72-h backward trajectories are then calculated and clustered. The ending point is ~~set~~ defined ~~at~~ as

1500 m above sea level. The NCEP reanalysis data (http://ready.arl.noaa.gov/archives.php) are used to drive the backward trajectory calculation. The NCEP data contain 6-hourly basic meteorological fields on pressure surfaces with ~~the~~ a spatial resolution of 2.5°. In this study, these data are also converted to hemispheric 144 by 73 polar stereographic grids;~~,~~ ~~which is~~these data thus have the same grid configuration as the dataset applied in the synoptic weather classification.

3. Results and discussion

3.1 Characteristics of particle pollution in the YRD

3.1.1 Spatial distributions of particle pollution

Fig. 2a displays the annual mean values of AOD observed at a wavelength of 550 nm ~~wavelength in~~throughout most ~~areas~~ of China. The highest values (i.e., larger than 0.6) generally occur in the BTH, the YRD, the Sichuan Basin (SCB), and some of the central and southern provinces in China (i.e., Hubei, Hunan and Guangxi provinces). AOD is mainly governed by fine particles in industrialized urban conditions (Kim et al., 2006);~~,~~ thus, the abovementioned areas should ~~be suffering~~suffer from high columnar aerosol loading. In the YRD, with the development of modern industrialization and urbanization, ~~the~~ contrasts ~~of~~ in the atmospheric pollution levels among ~~the~~ different cities gradually decrease~~ gradually~~, and severe air pollution episodes tend to exhibit significant regional pollution characteristics.

Fig. 2b shows the temporal variations ~~of~~ in the regional average~~d~~ AOD values ~~of AOD~~ in the YRD (covering 16 cities within the area of 25-40°N and 110-128°N). The annual mean value is 0.71±0.57. The maximum seasonal value is 0.98±0.83 in summer, followed by 0.81±0.57 in winter, 0.59±0.24 in spring, and 0.48±0.35 in autumn. ~~Though~~ Although the peak ~~of~~ particle concentrations ~~occurs~~are observed in winter (as shown in Fig. 3 and 5~~ show~~), the above results demonstrate that the maximum regional mean AOD values occur~~s~~ in summer, ~~with~~ as they reach their~~the~~ highest value of 1.60 in June. ~~The~~ This result is similar to that found by Kim et al. (2006), who~~.~~ ~~It is~~ reported that the value of AOD is not only associated with the pollution levels of fine particles~~, but also~~ but is also strongly affected by other factors (~~such as~~e.g., solar radiation, water vapor~~ and etc.~~). The fact that the maximum AOD values occur in hot seasons should be ascribed to the combined effects of ~~an~~ the increase ~~of~~ in fine aerosol production (i.e., due to secondary aerosol formation by gas-to-particle conversion, the hygroscopic growth of hydrophilic aerosols ~~and~~ or biomass burning emissions) and humid weather (Kim et al., 2006). Consequently, the aerosol optical depth data obtained from satellite observations can reveal the spatial distribution of aerosols to some extent, but they cannot exactly reflect ~~the~~ pollution levels ~~and~~ or replace ~~the~~ concentration data.

Figs. 2c and 2d show the spatial distributions of the annual mean particle concentrations in 16 typical cities over the YRD from December 2013 to November 2014. Generally, the spatial distributions of $PM_{2.5}$ (Fig. 2c) and PM_{10} (Fig. 2d) ~~present a~~exhibit overall similar pattern~~s as a whole~~. The annual mean $PM_{2.5}$ and PM_{10} values decrease progressively ~~along~~ in the northwest-southeast direction, which means that particle concentrations are comparatively high in the northwest inland areas and low in the southeast coastal areas. The pollution levels in most cities ~~have~~ exhibit a positive correlation with their proximity ~~from the city~~ to the sea. The farther ~~the~~ a city is from the sea, the higher ~~the~~ its particle concentrations are. The maximum particle concentrations occur in Nanjing, with ~~the~~ values of 79 $\mu g \cdot m^{-3}$ for $PM_{2.5}$ and 130 $\mu g \cdot m^{-3}$ for PM_{10}. ~~Given the p~~Previous ~~researches~~studies ~~on~~ of major climatic features in the YRD have demonstrated that~~,~~ the southeast coastal area is dramatically affected by the land-sea breeze and marine air masses. The clean marine air masses are advantageous to the dilution and ~~the~~ diffusion of atmospheric pollutants, thus ~~leading to~~producing lighter air pollution. However, in the inland region, ~~the~~ clustered cities and ~~the~~ industrial districts tend to emit more pollutants, ~~and~~ thereby resulting in ~~more~~ the accumulation of ~~accumulated~~ more air pollutants around these cities.

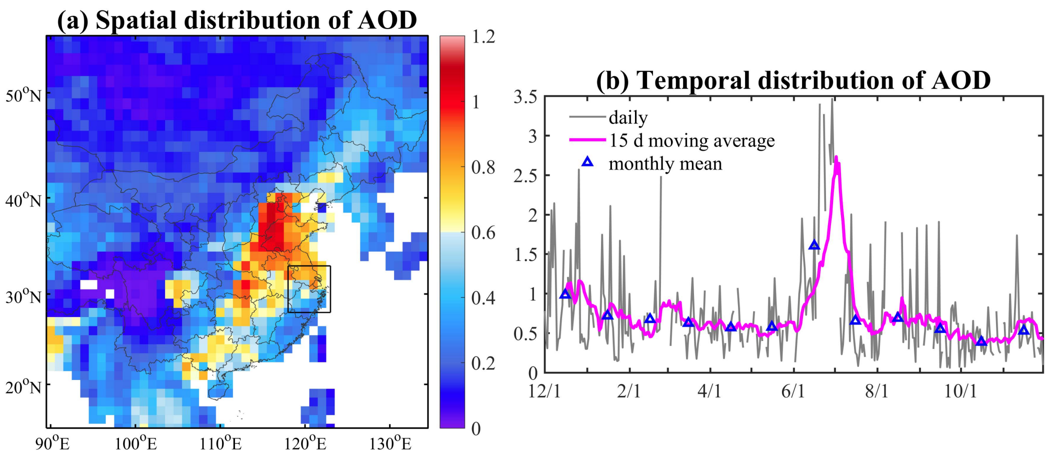

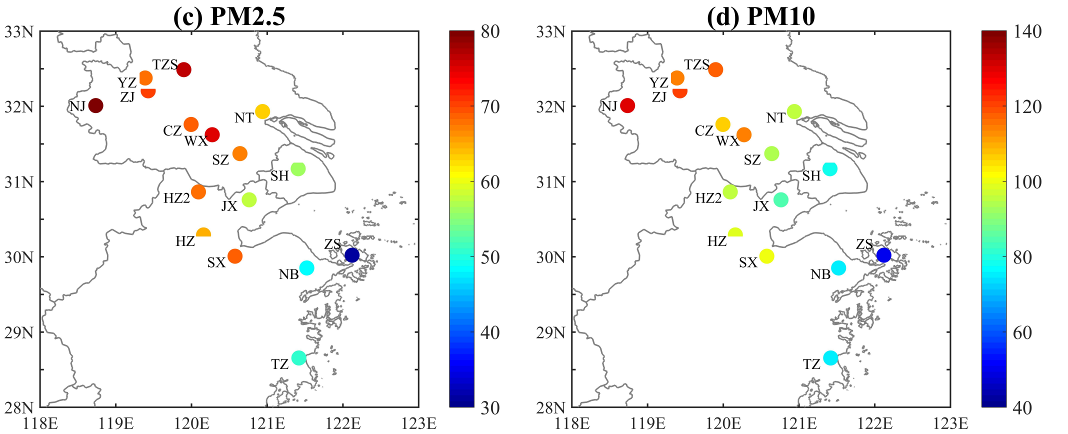

Figure 2. The spatial distribution of annual mean AOD values (at a wavelength of 550 nm ~~wavelength~~) ~~values~~ over the YRD (a);~~,~~ the temporal variations ~~of~~ in regional averaged~~d~~ AOD values over ~~(~~28-33°N and ~~,~~ 118-123°N~~)~~ (b);~~,~~ the spatial distribution of annual mean $PM_{2.5}$ concentrations (c);~~,~~ and the spatial distribution of annual mean PM_{10} concentrations (d). In (b), the gray line represents the daily value, the blue markers represent the monthly mean values, and the magenta line represents the 15-~~-~~days moving average value. In (c) and (d), the acronyms of each city are marked, including Shanghai-SH, Changzhou-CZ, Nanjing-NJ, Nantong-NT, Suzhou-SZ, Taizhoushi-TZS, Wuxi-WX, Yangzhou-YZ, Zhenjiang-ZJ, Hangzhou-HZ, Huzhou-HZ2, Jiaxing-JX, Ningbo-NB, Shaoxing-SX, Taizhou-TZ, and Zhoushan-ZS.

Fig. 3 illustrates the spatial distribution of the seasonal mean $PM_{2.5}$ in 16 cities over the YRD. The pattern observed ~~in~~ during each season is similar to the annual mean pattern (Fig. 2c). The $PM_{2.5}$ pollution levels are much higher in inland cities, and they decrease ~~along~~ in the northwest-southeast direction. ~~For the seasonal variation ,~~ $PM_{2.5}$ concentrations exhibit seasonal variations; they are highest in winter, ~~with the~~reaching a maximum value ~~being up to~~of 120 μg·m^{-3}, and they decrease throughout ~~the~~ spring, ~~and show the~~yielding their lowest values ~~in~~ during summer and autumn. The difference between the $PM_{2.5}$ concentration in summer and that in autumn is relatively small;~~,~~ this difference ranges from~~both~~ ~~with the~~a maximum value of lower than 60 μg·m^{-3} in Nanjing ~~and~~ to ~~the~~ a minimum value of close to 20 μg·m^{-3} in Zhoushan.

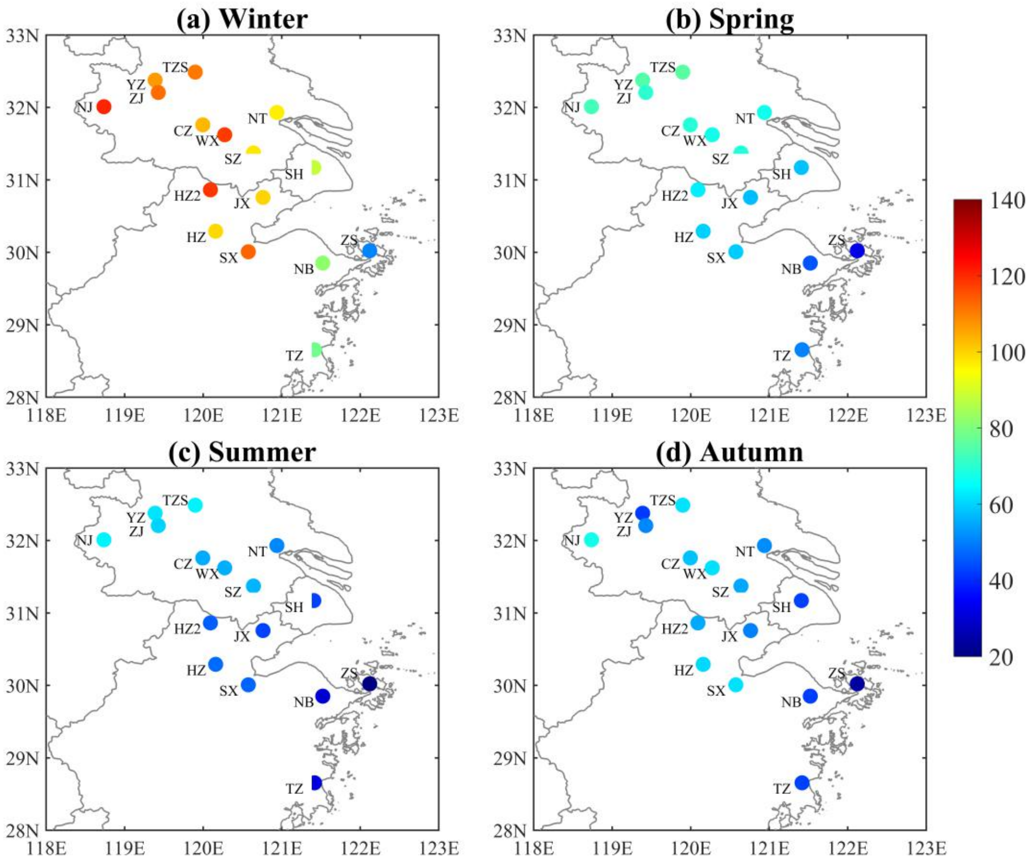

Figure 3. The spatial distribution of seasonal mean $PM_{2.5}$ over the YRD in (a) winter, (b) spring, (c) summer, and (d) autumn (unit: μg·m^{-3}). The acronyms for each city are the same as those in Figure 2.

Table 1 quantitatively ~~demonstrates~~ lists the annual mean concentrations of $PM_{2.5}$ and PM_{10} in 16 cities over the YRD. It also ~~shows~~ demonstrates that the particle pollution levels are relatively higher in inland cities~~ are relatively higher~~. The concentrations of $PM_{2.5}$ and PM_{10} in 8 cities ~~of~~ in Jiangsu ~~province~~ Province are all higher than 60 μg·m^{-3} ($PM_{2.5}$) and 80 μg·m^{-3} (PM_{10}), respectively. However, these concentrations are comparatively lower in the cities located in the coastal area (~~such as~~e.g., Ningbo, Taizhou and Zhoushan)~~ are comparatively lower~~. Only the air quality of Zhoushan meets the national standard, which may be attributed to the fact that it is located on ~~the~~ an island, where ~~the~~ its air is ~~more~~ most likely influenced by ~~the~~ clean marine air masses.

To reveal the important role of $PM_{2.5}$ in particle pollution, the ratios of $PM_{2.5}$ concentration to PM_{10} concentration ($PM_{2.5}/PM_{10}$) are calculated over the YRD. As listed in Table 1, the maximum annual mean value of the $PM_{2.5}/PM_{10}$ ratio is 0.72 in Shanghai, followed by Huzhou and Suzhou (0.71), thus implying that the $PM_{2.5}$ fraction is overwhelmingly dominant ~~of~~ relative to the PM_{10}

mass in these cities. The $PM_{2.5}/PM_{10}$ ratios in other cities ~~are between~~range from 0.60 ~~and~~ to 0.69, with ~~the~~ a minimum value of 0.58 in Zhenjiang. These values are comparable to those in other cities, ~~like~~ such as Beijing (He et al., 2001), Shanghai (Wang et al., 2013), Taibei (Chen et al., 1999), and Hong Kong (Ho et al., 2003), thus suggesting that the formation of $PM_{2.5}$ from gases is the most important source of particles in the cities of China. Table 1 also ~~presents~~ indicates that the $PM_{2.5}/PM_{10}$ ratios in all cities exhibit ~~show a~~ distinct seasonal variation. It is remarkable that the values of $PM_{2.5}/PM_{10}$ are much higher in winter than they are in other seasons, ~~with~~ reaching ~~the~~ a maximum value ~~reaching~~ of 0.85 in Shanghai, ~~and~~ followed by a value of 0.82 in Suzhou. The highest concentrations of $PM_{2.5}$ usually occur in winter (Fig. 3a), and high values of the $PM_{2.5}/PM_{10}$ ratio also ~~appear~~ occur ~~in~~ during the same season (Table 1), thus indicating that $PM_{2.5}$ poses a greater threat to human health in cold seasons, ~~that~~ which may be related to ~~the~~ heating activities. In summer, the values of $PM_{2.5}/PM_{10}$ in the 16 cities are medium, with ~~the~~ a mean value of 0.67. The lowest ratios usually occur in spring and autumn, ~~with~~ when the mean ratios of all cities ~~being~~ are 0.61 (spring) and 0.63 (autumn). The minimum value occurs in the autumn ~~of~~ in Yangzhou, with ~~the~~ a value of 0.51, followed by a value of 0.52 in the spring ~~of~~ in Nanjing and the autumn ~~of~~ in Zhenjiang. The above discussion ~~on~~ of the spatial and temporal variations ~~of~~ in $PM_{2.5}/PM_{10}$ ratios also implies that particles originate from various kinds of sources and are variedly emitted.

Table 1. Annual mean concentrations of $PM_{2.5}$ and PM_{10}, and the annual and seasonal mean values of $PM_{2.5}/PM_{10}$ ratio, in 16 cities over the YRD.

Cities		$PM_{2.5}$ ($\mu g \cdot m^{-3}$)	PM_{10} ($\mu g \cdot m^{-3}$)	$PM_{2.5}/PM_{10}$				
				Annual	Winter	Spring	Summer	Autumn
Shanghai		56	78	0.72	0.85	0.68	0.72	0.66
Jiangsu Province	Nanjing	79	130	0.61	0.64	0.52	0.70	0.60
	Changzhou	69	106	0.65	0.73	0.60	0.67	0.62
	Nantong	63	95	0.66	0.72	0.62	0.71	0.64
	Suzhou	67	94	0.71	0.82	0.68	0.71	0.67
	Taizhoushi	76	117	0.65	0.66	0.58	0.72	0.66
	Wuxi	75	114	0.66	0.73	0.59	0.67	0.62
	Yangzhou	68	114	0.60	0.69	0.58	0.59	0.51
	Zhenjiang	70	121	0.58	0.71	0.54	0.58	0.52
Zhejiang	Hangzhou	65	99	0.66	0.74	0.59	0.63	0.66

Province	Huzhou	68	96	0.71	0.78	0.66	0.68	0.69
	Jiaxing	58	84	0.69	0.75	0.65	0.68	0.69
	Ningbo	48	75	0.64	0.69	0.62	0.63	0.62
	Shaoxing	68	100	0.68	0.72	0.62	0.71	0.68
	Taizhou	50	75	0.67	0.69	0.66	0.66	0.65
	Zhoushan	31	50	0.63	0.66	0.62	0.66	0.55

3.1.2 Temporal variations ~~of~~ in particle pollution

Fig. 4 shows the annual mean diurnal variations ~~of~~ in $PM_{2.5}$ (Fig. 4a) and PM_{10} (Fig. 4b) in 16 cities over the YRD. Obviously, the diurnal cycles of particle concentrations in most cities follow ~~the~~ a similar pattern. The $PM_{2.5}$ concentrations maintain comparably high values from 0:00 to 8:00~~ –~~. ~~From t~~Then ~~on~~, coinciding with more vehicle emissions ~~in~~ during rush hours, these concentrations ~~go up~~increase rapidly from 8:00 to 12:00. After reaching their peak, the $PM_{2.5}$ concentrations decrease and ~~keep the~~remain at low values until ~~the~~ sunset. During ~~the~~ nighttime, the pollutants ~~get~~ accumulate~~d~~ until ~~the~~ midnight, which ~~should~~ can be attributed to the more stable atmospheric stratification in the boundary layer. In comparison, there are two peaks in the diurnal cycles of the PM_{10} concentrations in several cities. The broad morning peak of PM_{10} concentrations is more evident from 8:00 to 12:00, and the evening ~~one~~ peak occurs at ~~around 2~~approximately 20:00. ~~Besides,~~ In addition, the diurnal change ~~of~~ in particle concentrations in the southeast coastal area, ~~like~~ such as Zhoushan, is much smaller. As discussed in Section 3.1.1, ~~the~~ this difference might be related to its special geographic location, which exhibits ~~less~~ fewer emissions of precursors and lower pollution levels.

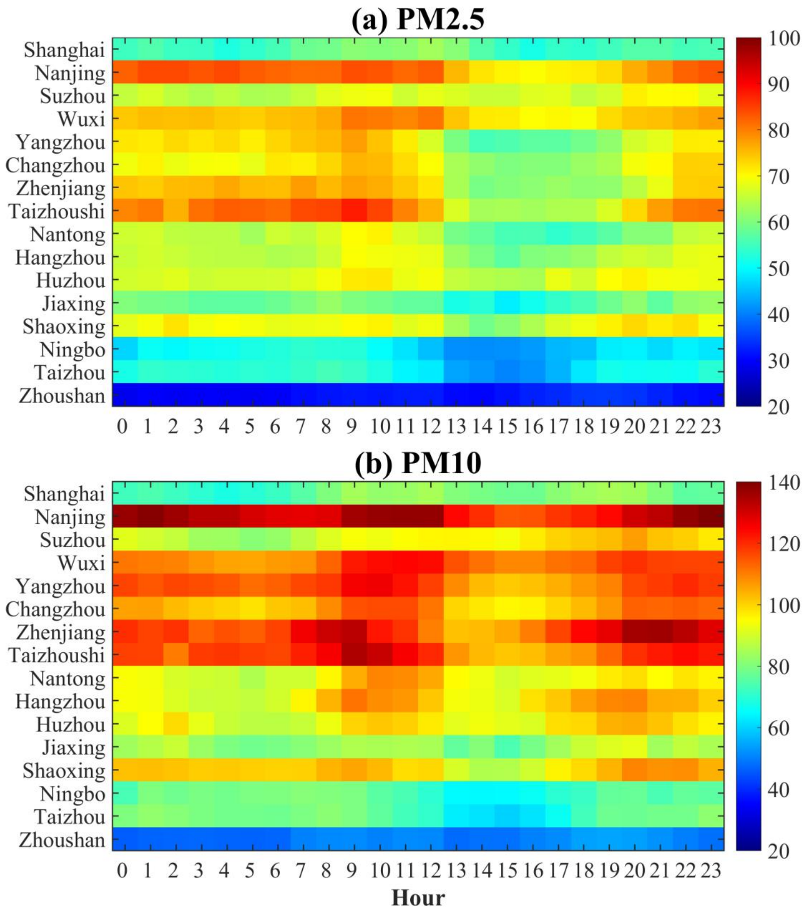

Figure 4. Diurnal variations ~~of~~ in $PM_{2.5}$ (a) and PM_{10} (b) concentrations in 16 cities of the YRD (unit: $\mu g \cdot m^{-3}$).

Fig. 5 ~~demonstrates~~ shows the monthly mean concentrations of $PM_{2.5}$ and PM_{10} in 16 cities of the YRD. As illustrated in ~~the~~ this figure, there are three peaks in the seasonal variations ~~of~~ in particles. These three peaks occur in December, March, and May/June. This monthly variation pattern is more obvious for PM_{10}. The causes resulting in the wintertime peak of particle concentrations can be explained by two factors. One is the enhanced emissions of pollutants ~~emissions~~ from residential heating. The other is the stable and poor meteorological conditions that limit the diffusion of atmospheric pollutants. ~~For~~ The drivers of the peak appearing in March~~, the drivers~~ may be associated with dust storm~~s~~ events in spring (Zhuang et al., 2001; Fu et al., 2010; 2014). As discussed in Section 3.1.1, the values of the $PM_{2.5}/PM_{10}$ ratio in 16 cities are lowest in spring~~,~~ with ~~the~~ a mean ratio~~s~~ of 0.61. High PM_{10} concentrations during this period further ~~prove~~ demonstrate that dust storms can bring more coarse dust particles to the YRD. ~~For t~~The peak in May/June~~, it~~ is probably caused by the field burning of crop residue in rural areas of China, which is regarded ~~as~~ to be an important source of biomass burning (Yan et al., 2006; Yang et al., 2007;

Zhu et al., 2012).

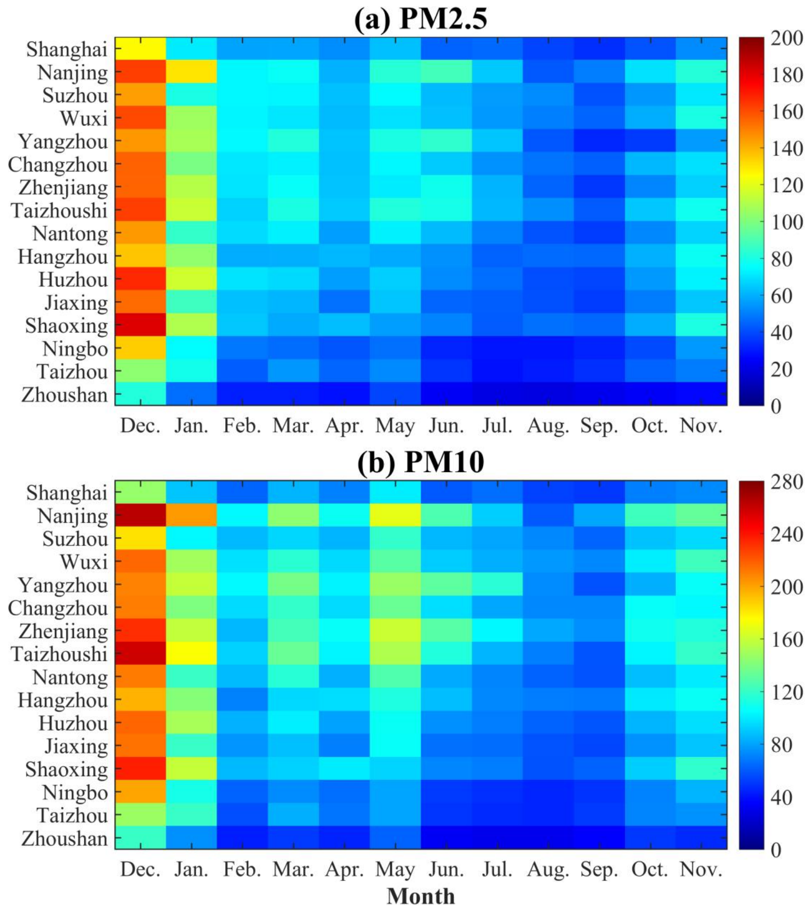

Figure 5. Monthly variations ~~of~~ in $PM_{2.5}$ (a) and PM_{10} (b) concentrations in 16 cities of the YRD (unit: μg·m^{-3}).

3.1.3 Regional severe particle pollution in the YRD

According to the National Ambient Air Quality Standard (NAAQS) of China, ~~the~~ urban air quality ~~needs to~~must meet the second standard, with ~~the~~ daily mean concentrations of $PM_{2.5}$ and PM_{10} that are lower than 75 μg·m^{-3} and 150 μg·m^{-3}, respectively. In this study, when the daily mean $PM_{2.5}$ (PM_{10}) concentrations exceed the national air quality standard in most (i.e., 8 or more) of the 16 cities, we define ~~that there is a~~this as large-scale regional $PM_{2.5}$ (PM_{10}) pollution. Consequently, from December 2013 to November 2014, there were 98 (46) days when ~~the~~ large-scale regional $PM_{2.5}$ (PM_{10}) pollution episodes ~~occurred are~~were identified. That is, the YRD suffered from ~~the~~ regional $PM_{2.5}$ (PM_{10}) pollution ~~in~~ during nearly 28.0% (13.1%) of the days of the year.

Table 2 shows the typical regional severe particle pollution episodes (that lasted no less than 3 days) in the YRD from December 2013 to November 2014. As illustrated in ~~the~~ this table, ~~there~~

~~are~~ dozens of continuous large-scale particle pollution episodes occurred. For example, $PM_{2.5}$ concentrations exceeded the national standard in all 16 cities from December 1 to 5, ~~in~~ 2013, and there were more than 14 cities facing heavy PM_{10} pollution at the same time. From May 26 to 30, ~~in~~ 2014, serious $PM_{2.5}$ and PM_{10} pollution episodes were ~~found~~ observed in more than 10 cities. It ~~seems~~ appears that high-~~-~~$PM_{2.5}$ pollution episodes are remarkably associated with high-~~-~~PM_{10} pollution episodes. Moreover, regional $PM_{2.5}$ pollution episodes occurred much more frequently than PM_{10} pollution episodes. ~~It might be owing~~This may be due to the fact that fine particles dominate the composition of particles in the YRD (as discussed in Section 3.1.2).

Table 2. The typical regional severe particle pollution episodes (lasting for no less than 3 days) in the YRD from December 2013 to November 2014.

Episodes of $PM_{2.5}$ pollution	Episodes of PM_{10} pollution
1-6 Dec.	1-6 Dec.
11-15 Dec.	12-15 Dec.
24-26 Dec.	24-26 Dec.
28 Dec. - 6 Jan.	29 Dec. - 5 Jan.
15-20 Jan.	17-20 Dec.
30 Jan. - 2 Feb.	26-30 May
20-24 Feb.	
16-18 Mar.	
8-10 Apr.	
20-22 May	
26-30 May	
5-7 Jun.	
28 Jun. - 1 Jul.	
10-12 Nov.	

3.2 Synoptic weather classification

In this study, ~~To~~ to examine the relationship between regional severe particle pollution in the YRD and weather situations, synoptic weather classification is carried out from December 2013 to November 2014~~ in this work~~. ~~Following~~ Using the method described in Section 2.2, we conduct the classification of the synoptic weather pattern by using the dataset of geopotential height at 850 hPa collected from the NCEP reanalysis data. As shown in Table 3, five weather patterns are finally identified.~~, including the East Asian trough rear pattern (Pattern 1), the depression inverted trough pattern (Pattern 2), the transversal trough pattern (Pattern 3), the high-pressure controlled~~

~~pattern (Pattern 4), and the northeast cold vortex pattern (Pattern 5).~~ ~~The u~~Unknown ~~type is~~patterns are defined as 'the unclassified pattern'.~~During the study period,~~ The weather situation on 95.6% of the days during the study period is classified as one of the five typical synoptic weather patterns.

Table 3 lists the typical date, ~~the~~ number of days, and seasonal occurrence frequencies of each synoptic weather pattern. As demonstrated in ~~the~~ this table, Pattern 1 is the dominant weather pattern in the YRD, which accounts for 47.6% of all of the days of the year (from December 2013 to November 2014). The occurrence frequencies of Patterns 2 and 3 are 20.0% and 18.1%, respectively. Patterns 4 and 5 are identified on the fewest number of days, with ~~the~~ occurrence frequencies of 4.1% and 5.8%, respectively.

Table 3 also shows the seasonal occurrence frequencies of each pattern from December 2013 to November 2014. Obviously, they are distinctly different. Pattern 1 tends to occur in winter, with ~~the~~ a frequency of 30.5%, followed by spring (25.9%), summer (21.8%) and autumn (21.8%). Pattern 2 is the most popular weather pattern in summer, with ~~the~~ an occurrence frequency of 37.0%, followed by spring (30.1%), autumn (21.9%) and winter (11.0%). ~~As for~~ For Pattern 3, the seasonal frequencies ~~are~~ occur in the order of winter (36.4%), spring (27.3%), autumn (19.7%) and summer (16.7%). Both ~~For~~ Pattern 4 and Pattern 5~~,~~ ~~they~~ are ~~both~~ most likely to ~~take place~~occur in autumn, with ~~the~~ occurrence frequencies ~~being~~ of 53.3% and 42.9%, respectively. The occurrence frequencies of Pattern 4 and Pattern 5 ~~in~~ during other seasons account for nearly 50%.

Table 3. The typical date, ~~the~~ number of days, and ~~the~~ seasonal occurrence frequencies of each synoptic weather pattern.

Type	Typical date	Number of days	Occurrence frequency (%)			
			Spring	Summer	Autumn	Winter
~~East Asian trough rear pattern (~~Pattern 1~~)~~	2014-05-12	174 (47.7%)	25.9	21.8	21.8	30.5
~~Depression inverted trough pattern (~~Pattern 2~~)~~	2014-05-09	73 (20.0%)	30.1	37.0	21.9	11.0
~~Transversal trough pattern (~~Pattern 3~~)~~	2014-02-18	66 (18.1%)	27.3	16.7	19.7	36.4
~~High-pressure controlled pattern (~~Pattern 4~~)~~	2014-10-07	15 (4.1%)	13.3	26.7	53.3	6.7
~~Northeast cold vortex pattern (~~Pattern	2014-09-14	21 (5.8%)	19.0	23.8	42.9	14.3

5~~)~~						
Unclassified pattern	—	16 (4.4%)	—	—	—	—

3.3 Effects of synoptic weather patterns on particle pollution

3.3.1 Relationship between synoptic weather pattern and particle pollution

To ~~figure out~~determine the relationship between synoptic weather patterns and particle pollution, the occurrence frequencies of the five typical synoptic patterns during the regional severe particle pollution episodes are calculated. As shown in Table 4, during the days with regional $PM_{2.5}$ (PM_{10}) pollution episodes~~ days~~, Pattern 1 is the dominant synoptic weather pattern, with ~~the~~ an occurrence frequency of 70.4% (78.3%). ~~For $PM_{2.5}$ pollution,~~ Pattern 2 and Pattern 3 both occur ~~in~~ on 14.3% of the days with $PM_{2.5}$ pollution episodes. ~~For~~ During PM_{10} pollution episodes, Pattern 2 (6.5%) appears less frequently than Pattern 3 (15.2%). The occurrence frequencies of Pattern 4 and Pattern 5 are less than 1%~~,~~ and can thus almost be ignored~~ on that account~~.

According to Table 3 and Table 4, the occurrence frequency of Pattern 1 during ~~the~~ regional particle pollution episodes is obviously higher than its occurrence ~~in~~ during the ~~whole~~ entire year. In contrast, the occurrences of Pattern 2 and Pattern 3 during these episodes are less frequent than those throughout the year. Moreover, Pattern 4 and Pattern 5 appear far less frequently during ~~the~~ regional particle pollution episodes than ~~their appearance~~they do ~~within~~ throughout ~~a~~ the year. ~~To sum up, it suggests~~In summary, these data suggest that the weather situation of Pattern 1 is more beneficial for the formation of large-scale regional particle pollution in the YRD.

Table 4. The occurrence frequencies of synoptic weather patterns during ~~the~~ regional severe $PM_{2.5}$ and PM_{10} pollution episodes

Type	$PM_{2.5}$		PM_{10}	
	Number of days	Frequency (%)	Number of days	Frequency (%)
Pattern 1	69	70.4	36	78.3
Pattern 2	14	14.3	3	6.5
Pattern 3	14	14.3	7	15.2
Pattern 4	0	0%	0	0
Pattern 5	1	1.0	0	0

Fig. 6 shows the ~~whisker-box~~box-and-whisker plot of the mean concentrations of ~~mean~~ air pollutants (PM_{10}, $PM_{2.5}$, O_3, NO_2, SO_2 and CO) ~~concentrations~~ and the meteorological parameters

(WS, T, P and RH) of 16 cities under the five synoptic weather patterns, as well as the corresponding spatial distribution of AOD over eastern China. These statistical results are also listed in Table 5~~ as well~~.

As shown in Figs. 6a-6f and Table 5, the highest average concentrations of the main air pollutants (except for O_3) ~~averaged for~~in the 16 cities in the YRD are ~~observed to be~~ associated with Pattern 1. Since aerosols can reflect and absorb solar radiation and thereby cause ~~the decrease of~~ the photochemical production of O_3 to decrease (Kaufman et al, 2002), the O_3 concentration is lowest for Pattern 1 (Fig. 6c). As ~~above~~ mentioned above, Pattern 1 is most likely to occur ~~in~~ during winter (30.5%) and spring (25.9%). Therefore, the weather situation of this pattern features the weakest surface wind, ~~the~~ lowest humidity, ~~the~~ second-highest surface pressure, and low temperature. All of these weather characteristics are conducive to ~~an~~ the accumulation of particles and their precursors (i.e., SO_2, NO_2 and CO). For Pattern 3, the concentrations of PM_{10}, $PM_{2.5}$ NO_2 and SO_2 are the second-highest compared to those of the other patterns. This pattern features the highest surface pressure and much stronger surface wind. The temperature is the lowest, as Pattern 3 also tends to ~~take place~~occur ~~in~~ during winter (37.0%) and spring (30.1%). Under the weather situation of Pattern 1 and Pattern 3, the YRD is both under the control of high-pressure~~,~~ and likely to suffer serious particle pollution. The strength of the surface wind for different weather patterns plays a key role in the occurrence frequency of regional severe particle pollution episodes. Pattern 1, which ~~With~~ has the weakest surface wind, ~~Pattern 1~~ is regarded as 'the most polluted pattern'. ~~As for Pattern 2, t~~The pollution levels of the main pollutants in Pattern 2 are in the middle and slightly lower than those ~~for~~ of Pattern 3. Due to ~~the~~ its high occurrence frequency in summer (37.0%) and spring (30.1), the weather condition of Pattern 2 is characterized ~~as~~ by its relatively high temperature, low pressure, and the lowest RH. In contrast, Pattern 4 and Pattern 5 are 'the clean patterns', ~~with~~ in which the concentrations of all of their pollutants are distinctly lower than those of the other three patterns. Their meteorological conditions of relatively high humidity, high temperature, strong wind (especially for Pattern 5) and much lower surface pressure are also favorable ~~to~~ for the mitigation of pollutants.

Figs. 6k to 6o display the spatial distribution of AOD over eastern China under different synoptic weather patterns. The regional mean values of AOD in the YRD (28-33°N, 118-123°N) are 0.74 for Pattern 1, 0.64 for Pattern 2, 0.81 for Pattern 3, 0.47 for Pattern 4 and 0.49 for Pattern

5~~, respectively~~. ~~It can also be found that~~Additionally, AOD ~~over YRD~~ is higher over the YRD for Pattern 3, Pattern 1 and Pattern 2. For these three patterns, high AOD values usually occur~~s~~ in the BTH, the YRD, and the SCB, as well as the provinces of Shanxi, Shandong, Hubei, Hunan, Anhui and Guangxi. The highest AOD values are mainly found in northeastern China. For Pattern 4 and Pattern 5, high AOD ~~is~~ values are mostly concentrated in the BTH and Shandong ~~province~~ Province, while relatively low AOD ~~is~~ values are found in the YRD. Since AOD is closely related to the concentrations of fine particles ~~concentrations~~, it can be concluded that the YRD is most heavily polluted under the weather situations of Pattern 1 and Pattern 3.

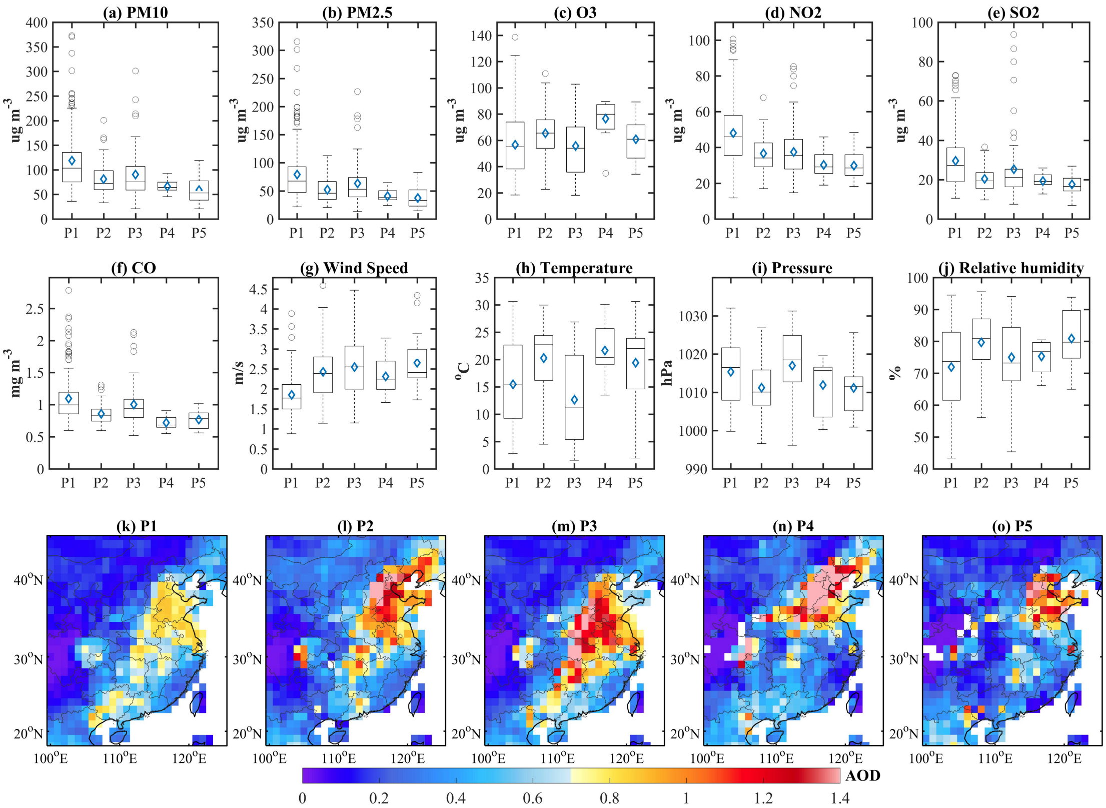

Figure 6. (a-j) ~~Whisker-box~~Box-and-whisker plots for the mean values of air pollutant concentrations and meteorological parameters of 16 typical YRD cities. The edges of each box in (a-j) are the 25th and 75th percentiles; the band inside the box is the median; the diamond is the average; and the whiskers extend to the most extreme data values. (k-p) Spatial distributions of AOD for the five synoptic weather patterns. P1, P2, P3, P4, and P5 represent Pattern 1, Pattern 2, Pattern 3, Pattern 4, and Pattern 5, respectively.

Table 5. The average values of air pollutant concentrations and meteorological factors for the 16 typical YRD cities under ~~the~~ different synoptic weather patterns.

Type	PM_{10}	$PM_{2.5}$	O_3	NO_2	SO_2	CO	SO_2	WS	T	P	RH
Pattern 1	116.5±66.9	75.9±49.9	57.7±27.3	46.9±19.2	29.3±17.1	1.08±0.41	29.3±17.1	1.84±0.67	15.8±7.8	1015.0±8.5	72.3±14.4

Pattern 2	81.5±38.4	52.3±27.4	65.5±23.6	36.1±13.4	20.6±9.9	0.86±0.24	20.6±9.9	2.38±0.88	20.3±6.3	1011.2±6.7	79.8±10.2
Pattern 3	86.9±49.5	59.1±37.3	58.5±25.5	35.1±15.5	23.3±15.9	0.96±0.35	23.3±15.9	2.59±0.87	13.4±8.2	1016.1±9.6	76.0±11.6
Pattern 4	66.1±18.8	40.7±15.9	76.8±19.6	29.4±9.8	19.4±6.4	0.72±0.17	19.4±6.4	2.29±0.64	21.7±4.9	1011.8±7.0	75.4±5.8
Pattern 5	58.7±31.3	37.4±22.5	61.1±20.6	29.1±11.1	17.8±8.4	0.77±0.22	17.8±8.4	2.63±0.93	19.4±8.0	1011.1±6.9	81.0±9.8

3.3.2 The impact mechanism of synoptic weather patterns on severe particle pollution

Figs. 7-11 present the meteorological fields and ~~the~~ backward trajectories under the weather situations of the Pattern 1 (northwestly inland wind), Pattern 2 (southwestly), Pattern 3 (northly inland wind), Pattern 4 (cyclone-related) and Pattern 5 (oceanic circulation related).~~five synoptic weather patterns.~~ The first two graphs of Figs. 7-11 illustrate the 850 hPa and 500 hPa geopotential height field and wind field, respectively. The third graphs display the sea level pressure field and 1000 hPa wind field. The highlighted boxes de~~point out~~note the ~~essential area~~study area (i.e., the YRD)~~ that we focus on~~. The fourth graphs demonstrate the height-latitude cross-sections of vertical velocity over the ~~in the~~ latitudes ~~(~~of 25-40°N~~)~~, which ~~is~~ are averaged from the longitudes of 110-128°E~~ in the longitude~~. The bold black lines show the latitude range of 16 cities (28.6-32.5°N) over the YRD. The positive wind speeds (10^2 Pa s^{-1}) ~~indicate that there are~~represent vertical downward atmospheric motions, while the negative wind speeds represent ~~the~~ upward motions. ~~Besides,~~ In addition, it is well known that ~~the~~ atmospheric pollutant transport trajectories are deeply affected by synoptic systems. As shown in the fifth graphs in Figs. 7-11, to reveal how the typical synoptic weather patterns influence the distribution of particles in the YRD, the 72-h backward trajectories are calculated and then clustered. Given that Nanjing is the most polluted city in the YRD, as described in Section 3.1, the observational site in Nanjing (32°N, 118.8°E) is chosen for the terminus of the trajector~~ies~~y ~~for~~ of each synoptic weather pattern.

As illustrated in Fig. 7a, Pattern 1 usually occurs when the YRD is located at the rear of the East Asian major trough and is under the control of a high-pressure ridge at 850 hPa. The center of the high-pressure system is ~~on~~ located in the northwestern Pacific Ocean. Meanwhile, northeastern China is strongly affected by a low-pressure system, ~~namely~~ namely, the Aleutian Low. The strong horizontal northwest wind at the rear of the East Asian major trough can transport ~~the~~ pollutants from the BTH (with high AOD, as shown in Fig. 6k) to the YRD. At the same time, the west and southwest wind at the rear of the high-pressure ridge can also transport ~~the~~ pollutants from central and southwestern China (such as the SCB and Guangxi P~~p~~rovince) to the YRD. The confluence of air flows may cause an accumulation of pollutants in the YRD. Accordingly, the atmospheric circulation at 500 hPa features a shallow through with a west-northwest flow (Fig. 7b). The sea level pressure pattern is ~~almost~~ nearly dominated by a uniform pressure field, ~~with~~ which exhibits relatively weak anti-cyclonic circulation over the YRD (Fig. 7c). The above discussion can be further explained by the 72-h backward trajectories displayed in Fig. 7e. When the YRD is under the control of Pattern 1, the air masses are mainly from northern China (44%), followed by the central ~~region~~ (36%) and ~~the~~ northeastern regions of the YRD (19%). ~~It~~ This suggests that ~~the~~ particle pollution is remarkably affected by the polluted air masses from the BTH and the central city clusters. Surface meteorological observation records also ~~shown~~ indicate that west-northwest-southwest surface winds ~~dominate~~ are dominant in Nanjing (Fig. 7f)~~,~~ and that high $PM_{2.5}$ is closely associated with the transport of polluted air masses in these wind directions. In the vertical section (Fig. 7d), the relatively weak upward air flows ~~dominate~~ are dominant ~~in~~ to the south of 30°N, while ~~the~~ clear downward air flows ~~prevail~~ are prevalent ~~in~~ to the north of 30°N. The largest descending velocity (~8×10^{-2} Pa s^{-1}) appears at ~~the~~ an altitude of 500 hPa and ~~in~~ a~~the~~ latitude of 37.5°N. Downward motion ~~dominates~~ is dominant above the YRD, which is in accordance with the 850 hPa circulation pattern represented by a high-pressure ridge. ~~For this reason~~Thus, the weather conditions are relatively stable near the surface~~,~~ ~~and~~ which is beneficial to the local accumulation of pollutants. Overall, Pattern 1 represents a stable synoptic weather pattern that ~~, and this weather situation~~ is extremely conduc~~t~~ive to the build~~t~~-up of atmospheric pollutants over the YRD. This result is consistent with the findings of Zheng et al (2015b).

Pattern 1

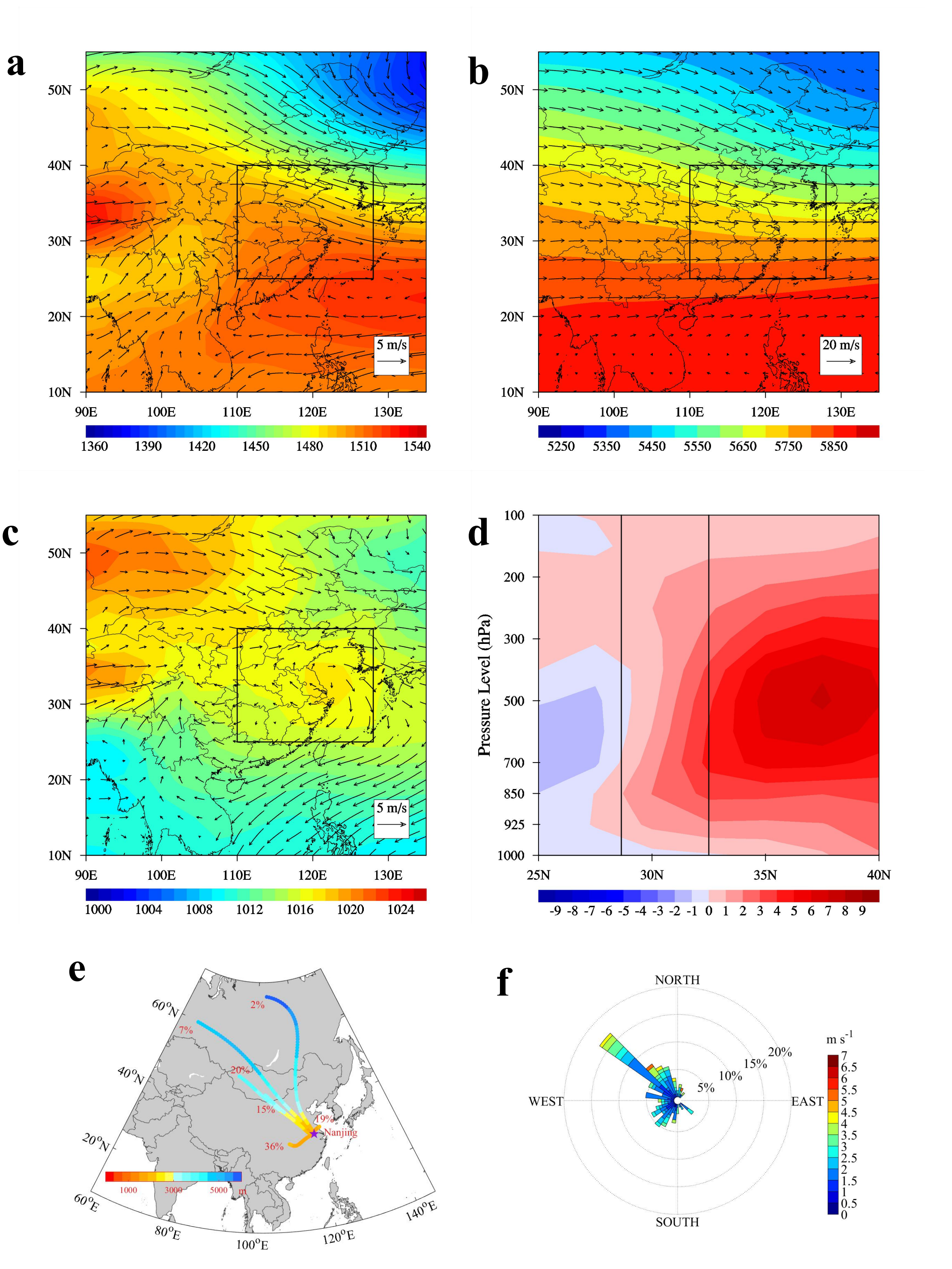

Figure 7. Weather condition in Pattern 1. (a) 850 hPa geopotential height field and wind field;~~ ,~~ (b) 500 hPa geopotential height field and wind field;~~,~~ (c) sea level pressure field and 1000 hPa wind field;~~,~~ (d) height-latitude cross-sections of vertical velocity (unit: 10^{-2} Pa/s) averaged from longitude of 110-128°E;~~,~~ (e) 72-h backward trajectory ending at ~~the~~ a height of 1500 m;~~,~~ and (f) observation wind rose plots in Nanjing. In (a)-(c), the highlighted boxes ~~depoint out~~note the ~~essential~~ study area (i.e., the YRD)~~ that we focus on~~. In (d), the black rectangular region represents the 16 cities in the YRD (28.6-32.5°N). In (e), the purple marker indicates the location of Nanjing (32°N, 118.8°E). These data ~~is~~ represent averages~~d~~ for all days

corresponding to Pattern 1.

~~As fo~~In~~r~~ Pattern 2, a low-pressure center (the Southeast Vortex) is centered in the SCB, the East China Sea is influenced by a high-pressure system, and a depression inverted trough extends and covers the YRD region ~~in~~ at a latitude at 850 hPa (Fig. 8a). Consequently, in the YRD, the strong southwest air flows from southern China meet with the southeast air flows from the East China Sea. After the convergence of these air masses, they jointly transport pollutants northwestward. ~~While~~ In contrast, at the surface (Fig. 8c), the study ~~domain~~ area is located at the bottom of a high-pressure system and is impacted by a strong southeast wind. In the middle troposphere (Fig. 8b), the sparse isopleths indicate that there is a small geopotential height gradient, while the shallow ridge causes westerly flows. Fig. 8e also illustrates these air pollutant transport paths. For the days when Pattern 2 ~~dominates~~is dominant, ~~about 4~~approximately 42% of the air masses are from the southwest and the south of China, and 15% are from the East China Sea. The air masses from the East China Sea are very important~~,~~ because the clean marine air masses may dilute the particle concentrations in the YRD. ~~Besides,~~ In addition, ~~there are~~ nearly 43% of air masses originat~~i~~e~~ng~~ from the local sources of the YRD, which may be related to ~~the~~ their short-range transport in the northwest direction. This is also in accordance with the dominant northwest surface wind in Nanjing (Fig. 8f). ~~When it comes to~~In regard to ~~the~~ its vertical structure (Fig. 8d), Pattern 2 is obviously different ~~from~~ than Pattern 1, as ~~the~~ upward air flows ~~dominate~~ are dominant ~~in~~ to the south of 37.5°N. The largest updraft~~s~~ zone (~7×10^{-2} Pa s^{-1}) appears above the YRD and between the altitude~~s~~ of 700 hPa and 500 hPa. The vertical velocity close to the surface is ~~relatively~~ weaker ~~compared to~~than that at higher levels over the YRD. ~~Meantime~~Meanwhile, ~~there is~~ stronger upward motion occurs near the surface ~~in the~~at a latitude of 37.5°N, with weak downward motion occurring above the 700 hPa layer. The above discussion suggests that atmospheric pollutants in the YRD are horizontally transported northwestward to a higher latitude~~,~~ and vertically transported upward to higher layers. Therefore, despite the transport of abundant pollutants to the YRD via southwest air flows and the short-range northwest transport of polluted air masses, the strong surface southeast wind and upward motion under the weather situation of Pattern 2 ~~determine that there~~result ~~is~~ in much ~~slighter~~ less particle pollution over the YRD compared to Pattern 1.

Pattern 2

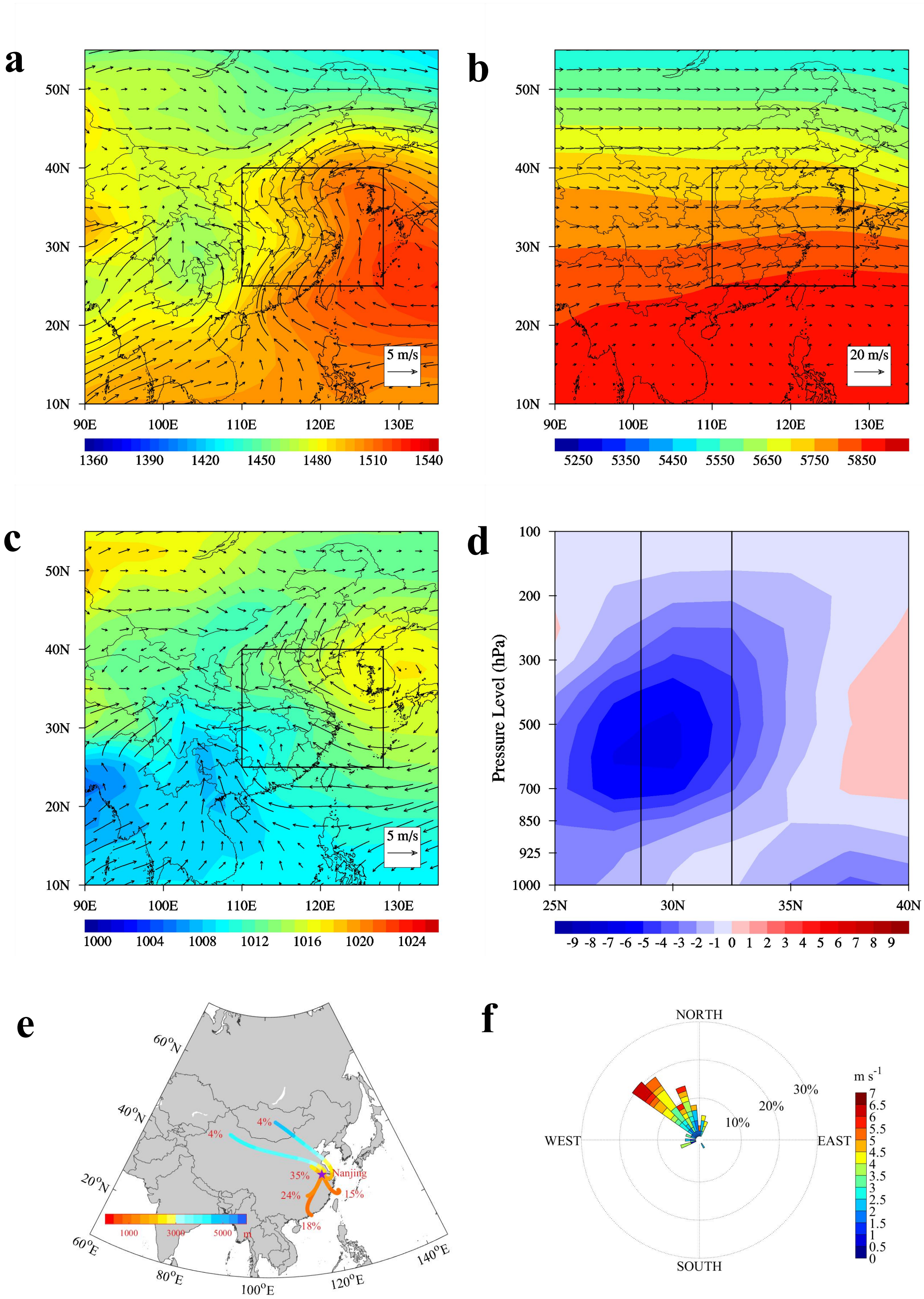

Figure 8. As in Fig. 7, but for Pattern 2.

~~For~~ Pattern 3~~,~~ ~~it~~ tends to occur in winter (36.4%, as displayed in Table 3). Under this circumstance, the YRD is mainly controlled by a high-pressure system that is centered in central China (Fig. 9a). Meanwhile, northeastern China is under the steering influence of the northwest air flows at the rear of the East Asian major trough, with its trough axis appearing along the eastern coastline of China. Affected by the strong northwest winds coming from northern China, the polluted air masses from the BTH are easily transported to the YRD. At the higher layer of 500 hPa (Fig. 9b), the circulation structure patterns are similar to those ~~for~~ of Pattern 1. A trough appears in the upper atmosphere, resulting in relatively strong west-northwest flows. The presence of dense isopleths indicates that there is a large geopotential height gradient and strong downward flows. ~~While a~~At the surface layer (Fig. 9c), the presence of strong northerly wind is also evident, and the YRD is located at the bottom of a high-pressure system centered in the remote Mongolian region. The above discussion is further ~~proved~~ supported by the results ~~from~~ of back trajectory calculations. As suggested in Fig. 9e, most air masses in clusters are from the Loess Plateau~~, with the percentage of~~(~~i.e.,~~ 31%). The transport path of this cluster is relatively short, which ~~might~~ may be attributed to ~~the~~ its strong anti-cyclonic circulation. Due to the strong northerly wind, the long-range transport of air masses from remote Mongolia and northern China account~~s~~ for 22% and 18% of all trajectories, respectively. ~~Besides,~~ In addition, the local transport of air masses from the southeast coastal area in the YRD accounts for 26% of all trajectories~~.~~, and ~~The~~ the marine air masses cluster that originates from the western Pacific via the Yellow Sea accounts for 4% of all trajectories. For the vertical structure (Fig. 9d), the distribution of the vertical flow field is similar to that of Pattern 1, whereas the vertical wind is slightly stronger ~~for~~ in the weather systems ~~in~~ of Pattern 3. Due to the influence of the high-pressure system, ~~it is observed that evident~~ downward air flows ~~dominate~~ are dominant ~~in~~ to the north of ~~around 2~~approximately 28°N (including the YRD) below ~~the~~ an altitude of 300 hPa. The largest descending velocity (~9×10^{-2} Pa s^{-1}) also appears at ~~the~~ an altitude of 500 hPa, covering the latitude of 35-40°N. However, ~~in spite of~~despite the higher surface pressure (Figs. 6i and 9c) and stronger downward motion (Fig. 9d), the surface wind is also much stronger for Pattern 3 ~~as well~~ (Figs. 6g, 9a and 9c), which alleviates the problems of air pollution over the YRD compared to Pattern 1. ~~In all~~Overall, under the weather situation of Pattern 3, the strong northwest wind in the front of the high-pressure system usually leads to the transport of polluted air masses from the BTH to the YRD. Nevertheless, the strong surface wind is conducive to the mitigation of pollutants, which plays a significant role in the level of air pollution over the YRD.

Pattern 3

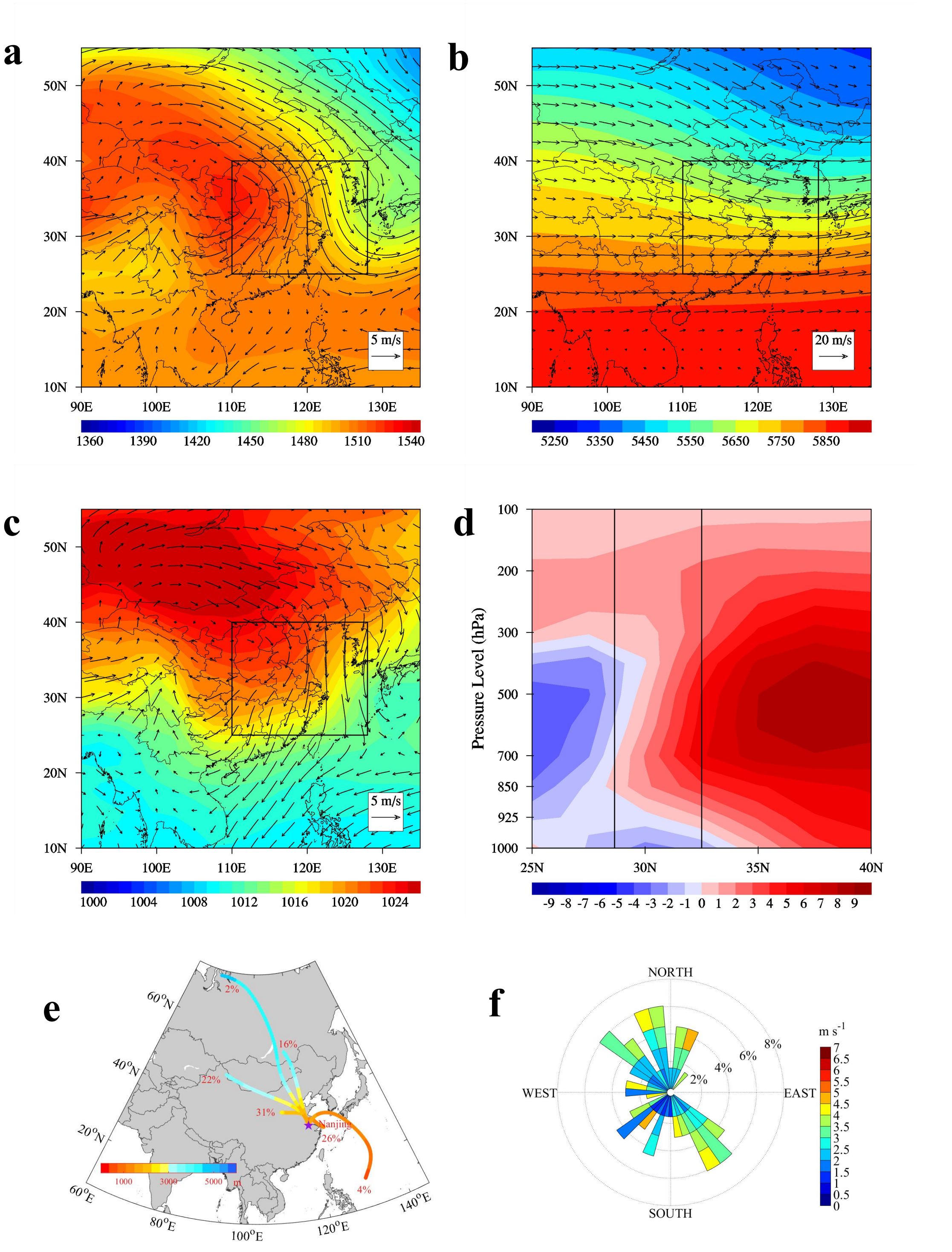

Figure 9. As in Fig. 7, but for Pattern 3.

~~With respect to~~In Pattern 4, on both the surface and at the 850 hPa level, the study ~~domain~~ area is under the control of a high-pressure system (Figs. 10a and 10c). The center of the high-pressure system is located ~~on~~ in the Sea of Japan, while a cyclonic circulation occurs over the

Philippine Sea. ~~The a~~Anti-cyclonic circulation prevails over the YRD and horizontally brings the clean marine air masses to the land. Meanwhile, the sparse isopleths represent a small geopotential height gradient in the middle troposphere, which is accompanied by a much weaker west wind compared to the other patterns (Fig. 10b). Accordingly, influenced by the high-pressure system, ~~the~~ downward atmospheric motion ~~dominates~~ is clearly dominant in the vertical direction ~~obviously~~ (Fig. 10d). The strongest downward motion (~6×10^{-2} Pa s^{-1}) appears between the altitudes of 300 hPa and 500 hPa ~~and~~ at ~~the~~ a latitude of 35°N. The weak updrafts near the surface may be related to the regional thermodynamic circulation. As shown in Fig. 10e, the cluster with the largest frequency of 32% ~~stands for~~represents the local transport of air masses from the southern adjacent areas in the YRD. Additionally, the air masses originating from northern China via the Bohai Bay (25%), from Japan via the Yellow Sea (23%), and from the Philippines via the East China Sea (5%) are also representative. In total, ~~These~~ the clusters ~~passing~~ that pass over the ocean areas ~~totally~~ account for more than 50% of all trajectories. Therefore, under this weather situation, ~~it is confirmed that~~ the dilution effects of clean marine air masses play ~~great~~ a large roles in the particle pollution over the YRD.

Pattern 5 features one of the most complex circulation situations at 850 hPa (Fig. 11a). The YRD is located between the bottom of the northern high-pressure system and the top of the southern weak low-pressure system. ~~For this reason~~Thus, the strong horizontal ~~strong~~ east wind prevails and easily carries clean marine air masses from the East China Sea to the YRD. The corresponding circulation structure at the surface layer is similar to that at the 850 hPa layer (Fig. 11c), while ~~the~~ east-northeast flows ~~prevails~~are prevalent over the study domain. In the upper troposphere, a ridge appears in the east due to the tropical cyclonic system, thus leading to the west-southwest flows over the region. ~~Owing~~ Due to the ~~above-mentioned~~abovementioned two opposite pressure systems (Fig. 11a), strong upward air flows are dominant ~~in~~ to the south of the latitude of 35 °N, while ~~the~~ downward motion is obvious in the north (Fig. 11d). The largest ascending velocity (~ -9×10^{-2} Pa s^{-1}) appears ~~in~~ at ~~the~~ a latitude of ~~around 2~~approximately 27.5 °N in the upper troposphere. ~~The~~ This strong upward motion facilitates the diffusion and removal of the accumulated pollutants from the surface layer. According to Fig. 11e, the cluster with the largest frequency of 45% consists of the wet air parcels originating from Japan via the Yellow Sea. Only 5% of the trajectories originates from the Philippines and pass over the East China Sea. ~~On~~

~~the whole~~Overall, under the weather situation ~~for~~ of Pattern 5, the transport of clean marine air masses and favorable diffusion conditions contribute to the good air quality over the YRD.

Pattern 4

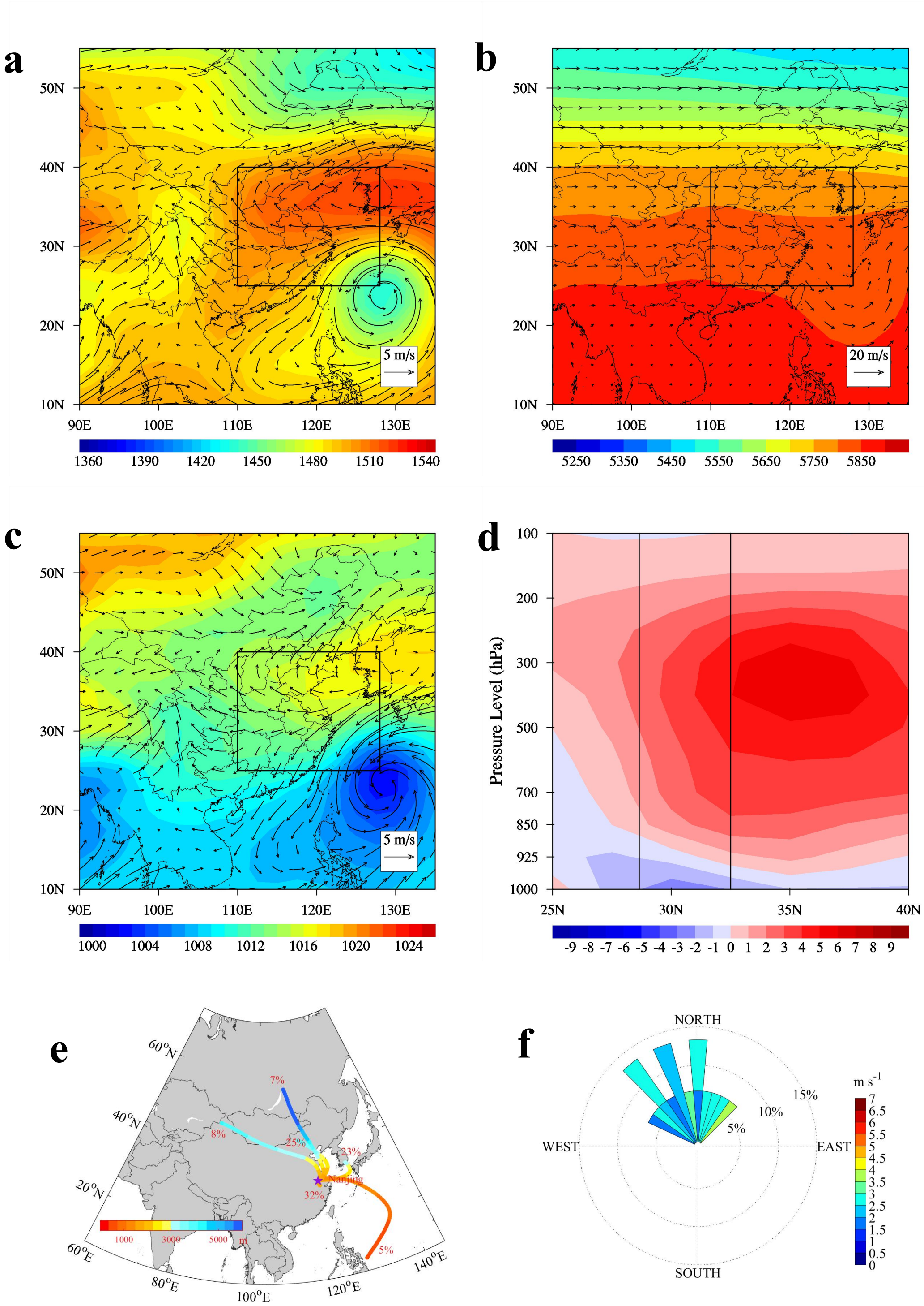

Figure 10. As in Fig. 7, but for Pattern 4.

Pattern 5

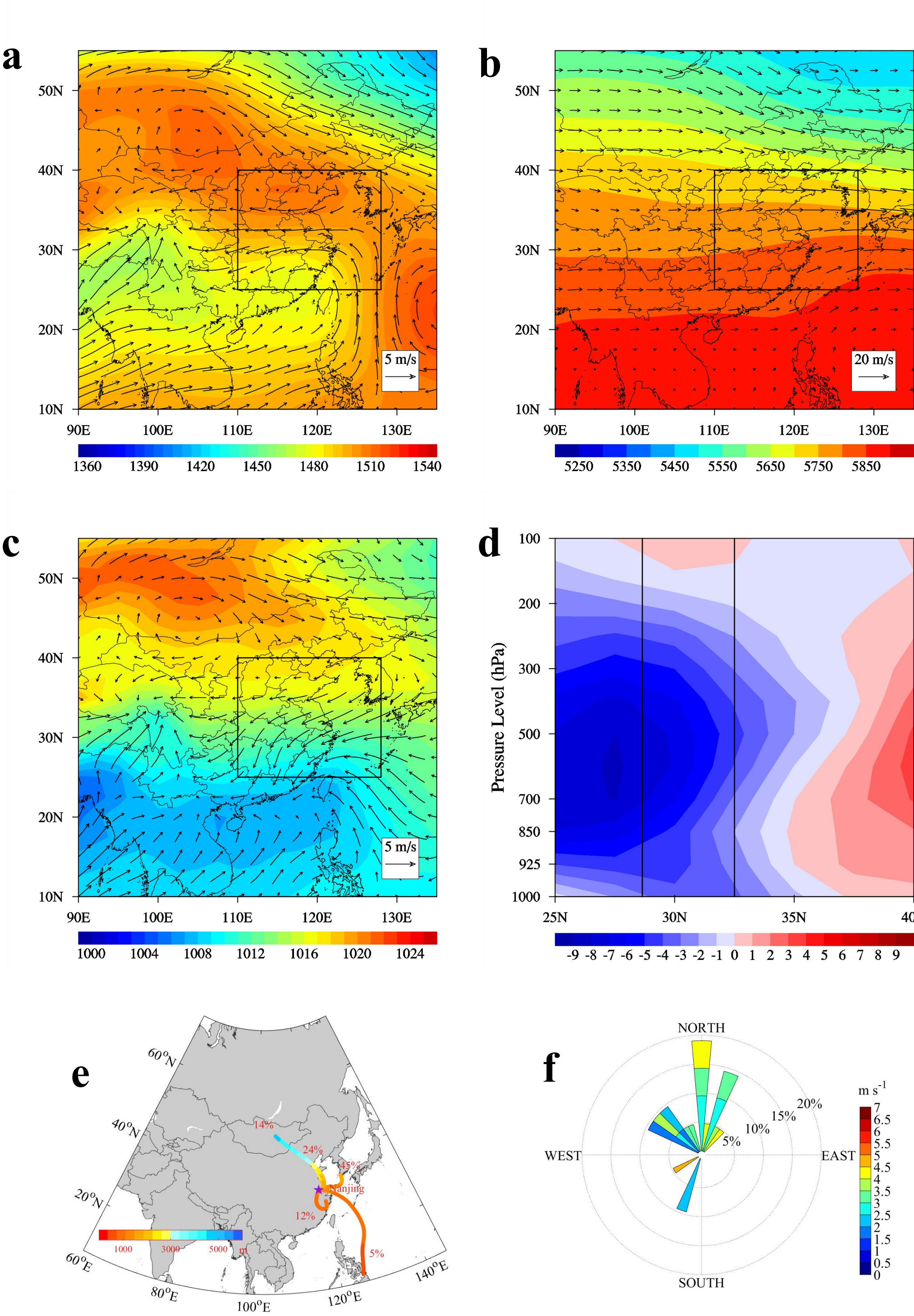

Figure 11. As in Fig. 7, but for Pattern 5.

To ~~sum up~~summarize, the weather situations for Patterns 1-5 are more or less affected by a high-pressure system. However, the relative positions of the study ~~domain~~ area to the anti-cyclonic circulation system ~~are~~ have ~~quite~~ significant ~~to~~ effects on the air quality of the YRD. These differences determine the wind speed and wind direction, and the latter further determines whether the YRD is influenced by the clean marine air masses. ~~For~~ In both Pattern 1 and Pattern 3, the YRD ~~are both~~is impacted by the northwest air flows at the rear of the East Asian major trough, which transport abundant air pollutants from other regions (such as the BTH and the SCB) to the YRD and cause severe particle pollution (as well as high AOD value~~s as well~~) in the YRD. In contrast, the weaker local surface wind ~~for~~ in Pattern 1 is extremely conducive to the local accumulation of pollutants. For this reason, Pattern 1 is ‘the most polluted pattern’, and it is responsible for ~~the~~ most of the large-scale particle pollution episodes over the YRD. ~~Owning~~ Due to ~~the~~ its stronger surface wind, Pattern 3 is ‘the second~~-~~most polluted pattern’. ~~As for~~ In Pattern 2, the polluted air masses mainly travel from the southern inland areas~~,~~ and synchronously meet with the clean marine air masses in the YRD. To some extent, this weather situation ~~is helpful to the mitigation of~~helps mitigate particle pollution in the YRD. ~~With respect to~~In Pattern 4 and Pattern 5, the YRD is directly influenced by ~~the~~ air flows traveling from the ocean areas, and it ~~has little chance of being~~is thus unlikely to be polluted. Thus, Pattern 4 and Pattern 5 can be identified as ‘the clean patterns’. ~~It~~ These data suggest~~s~~ that the clean marine air masses can ~~have great dilution impacts on~~substantially dilute the particle pollution over the YRD.

4. Conclusions

In this study, the spatial and temporal distributions of particle pollution in 16 YRD cities are characterized from December 2013 to November 2014. Meanwhile, ~~the~~ synoptic weather classification is conducted to identify the dominant weather patterns over the YRD. The meteorological fields and 72-h backward trajectories are analyzed to reveal the potential impacts of weather systems on ~~the~~ regional severe particle pollution episodes.

~~From the~~O~~o~~bservational records~~, it is shown~~ indicate that the concentrations of $PM_{2.5}$ and PM_{10} decrease progressively ~~along~~ in the northwest-southeast direction. The pollution levels are comparatively higher in ~~the~~ Jiangsu Province and much lower in the southeast coastal area (i.e., Ningbo, Taizhou and Zhoushan). The highest particle concentrations occur~~s~~ in Nanjing, ~~with~~ where the concentrations of $PM_{2.5}$ and PM_{10} ~~being~~ are 79 and 130 $\mu g \cdot m^{-3}$, respectively. The $PM_{2.5}/PM_{10}$ ratios are high in the YRD, especially in winter. The seasonal mean $PM_{2.5}/PM_{10}$ ratios are 0.73 (winter), 0.61 (spring), 0.67 (summer) and 0.63 (autumn)~~, respectively~~. These high

$PM_{2.5}/PM_{10}$ ratios suggest that the $PM_{2.5}$ fraction is extraordinarily dominant in the PM_{10} mass in the YRD. ~~Besides,~~ In addition, high AOD ~~is~~ values are also found in the YRD, with ~~the~~ an annual mean value of 0.71±0.57 and ~~the~~ a maximum seasonal mean value of 0.98±0.83 in summer. The diurnal cycles of the particle concentrations in most cities follow the same pattern, ~~with~~ reaching a morning peak from 8:00 to 12:00. There are three peaks in seasonal variations (December, March, and May or June). The wintertime peak is closely related to ~~the~~ enhanced emissions ~~in~~ during the heating season and poor meteorological conditions. Moreover, the YRD suffers from ~~the~~ $PM_{2.5}$ (PM_{10}) pollution ~~in~~ on nearly 28.0% (13.1%) of the days of the year. ~~The c~~Continuous large-scale regional $PM_{2.5}$ pollution episodes occur much more frequently than ~~the~~ PM_{10} pollution episodes.

Based on the sums-of-squares technique, five typical synoptic weather patterns are objectively identified in the YRD, including Pattern 1 (northwestly inland wind, which occurs on 47.7% of all days), Pattern 2 (southwestly, 20.0%), Pattern 3 (northly inland wind, 18.1%), Pattern 4 (cyclone-related, 4.1%) and Pattern 5 (oceanic circulation related, 5.8%).~~the East Asia major trough rear pattern (Pattern 1, occurs which occurs on 47.7% of all days), the depression inverted trough pattern (Pattern 2, 20.0%), the transversal trough pattern (Pattern 3, 18.1%), the high-pressure controlled pattern (Pattern 4, 4.1%) and the northeast cold vortex pattern (Pattern 5, 5.8%)~~. Each pattern differs from the other in respect to the relative position of the YRD to the main synoptic system (~~i.e.,~~ the anti-cyclonic circulation system). ~~The~~ This difference determines the wind speed and wind direction, which play ~~an~~ important roles in the air quality level of the YRD. ~~Especially~~In particular, the wind direction is closely associated with ~~the situation~~determining whether the YRD is influenced by clean marine air masses. ~~Under~~ In the patterns ~~when~~ in which the YRD is located at the rear of the East Asian major trough at 850 hPa (~~i.e.,~~ Pattern 1 and Pattern 3), ~~the~~ strong northwest wind can easily transport air pollutants from other polluted areas to the YRD, thus leading to serious particle pollution in the YRD. Due to the high-pressure system, significant vertical downward motion ~~dominates~~ is dominant above the YRD, resulting in relatively stable weather conditions at the surface. With weak local surface wind, the worst polluted weather pattern (Pattern 1) features the highest regional mean PM_{10} (116.5±66.9 $\mu g \cdot m^{-3}$), $PM_{2.5}$ (75.9±49.9 $\mu g \cdot m^{-3}$) and high AOD (0.74) values. Pattern 1 is also responsible for ~~the~~ most of the large-scale regional $PM_{2.5}$ (70.4%) and PM_{10} (78.3%) pollution episodes in the YRD. ~~As for~~ In Pattern 3, the strongest surface wind is conducive to the mitigation of pollution, thus resulting in the second~~-~~-highest PM_{10} (86.9±49.5 μg·m^{-3}) and $PM_{2.5}$ (59.1±37.3 μg·m^{-3}) values. In contrast, under the weather system of other synoptic patterns (especially Pattern 4 and Pattern 5), the clean marine air masses, which are transported via the east-southeast wind, play a crucial role in the mitigation of pollution over the YRD. Therefore, the YRD has a much ~~less~~ smaller chance of being polluted.

In summary, the above results reveal that ~~the~~ particle pollution in China is ~~no longer~~ a thorny issue not only over a single city~~,~~ but also ~~over~~ on a regional scale. This study can enhance ~~the~~ our understanding of the features of particle pollution in East Asia. Meanwhile, ~~it is~~these results also confirm~~ed~~ that large-scale synoptic weather systems ~~have~~ exert ~~great~~ large impacts on regional particle pollution. Therefore, ~~the establishment of the~~establishing potential links between different levels of particle pollution and predominant synoptic patterns can provide ~~an insightful view~~insight ~~on~~ into formulating pollution control and mitigation strategies.

5. Data availability

The air quality monitoring records are available at http://106.37.208.233:20035. The meteorological data are available at http://www.nmc.cn. The MODIS/AOD records are available at https://ladsweb.nascom.nasa.gov/search/index.html. The NCEP reanalysis data are available at https://www.esrl.noaa.gov/psd/data/gridded/data.ncep.reanalysis2.pressure.html an~~d~~ ~~h~~d http://ready.arl.noaa.gov/archives.php.

Acknowledgments

This work was supported by the National Natural Science Foundation of China (41475122, 91544230, 41621005~~41475122, 91544230, 91537102, 41621005~~), the National Key Research and Development Program of China (2016YFC0203303, 2016YFC0208504, 2017YFC0210106~~2016YFC0203303, 2016YFC0208504, 2016YFA0602104~~), and the open research fund of the Chongqing Meteorological Bureau (KFJJ-201607). The authors would ~~like to thank~~ like to thank the anonymous reviewers for their constructive and ~~precious~~ valuable comments on this manuscript.

References

Barry, R. G., Kiladis, G., and Bradley, R. S.: Synoptic climatology of the Western United States in relation to climatic fluctuations during the twentieth century, International Journal of Climatology, 1, 97-113, 1981.

Brook, R. D., Rajagopalan, S., Pope, C. A., Brook, J. R., Bhatnagar, A., Diez-Roux, A. V., Holguin, F., Hong, Y., Luepker, R. V., and Mittleman, M. A.: Particulate matter air pollution and cardiovascular disease, Circulation, 121, 2331-2378, 2010.

Buchanan, C., Beverland, I. J., and Heal, M. R.: The influence of weather-type and long-range transport on airborne particle concentrations in Edinburgh, UK, Atmospheric Environment, 36, 5343-5354, 2002.

Chan, C. K., and Yao, X.: Air pollution in mega cities in China, Atmospheric environment, 42, 1-42, 2008.

Chen, M. L., Mao, I. F., and Lin, I. K.: The PM 2.5 and PM 10 particles in urban areas of Taiwan, Science of the Total Environment, 226, 227-235, 1999.

Cheng, Z., Jiang, J., Fajardo, O., Wang, S., and Hao, J.: Characteristics and health impacts of particulate matter pollution in China (2001–2011), Atmospheric Environment, 65, 186-194, 2013.

Chuang, M.-T., Chiang, P.-C., Chan, C.-C., Wang, C.-F., Chang, E., and Lee, C.-T.: The effects of synoptical weather pattern and complex terrain on the formation of aerosol events in the Greater Taipei area, Science of the total environment, 399, 128-146, 2008.

Chu, D., Kaufman, Y., Ichoku, C., Remer, L., Tanré, D., and Holben, B.: Validation of MODIS aerosol optical depth retrieval over land, Geophysical research letters, 29, 2002.

Chu, D. A., Kaufman, Y., Zibordi, G., Chern, J., Mao, J., Li, C., and Holben, B.: Global monitoring of air pollution over land from the Earth Observing System‐Terra Moderate Resolution Imaging Spectroradiometer (MODIS), Journal of Geophysical Research: Atmospheres, 108, 2003.

Chu, D., Remer, L., Kaufman, Y., Schmid, B., Redemann, J., Knobelspiesse, K., Chern, J. D., Livingston, J., Russell, P., and Xiong, X.: Evaluation of aerosol properties over ocean from Moderate Resolution Imaging Spectroradiometer (MODIS) during ACE‐Asia, Journal of Geophysical Research: Atmospheres, 110, 2005.

Deng, J. J., Wang, T. J., Jiang, Z. Q., Xie, M., Zhang, R. J., Huang, X. X., Zhu, J. L.: Characterization of visibility and its affecting factors over Nanjing, China. Atmos Res, 101, 681-691, 2011.

Draxler, R., and Rolph, G.: HYSPLIT (HYbrid Single-Particle Lagrangian Integrated Trajectory), NOAA Air Resources Laboratory, College Park, MD, Model access via NOAA ARL READY Website, 2013.

El-Kadi, A. K. A., and Smithson, P. A.: Atmospheric classifications and synoptic climatology, Progress in Physical Geography, 16, 432-455, 1992.

Feng, J., Hu, J., Xu, B., Hu, X., Sun, P., Han, W., Gu, Z., Yu, X., and Wu, M.: Characteristics and seasonal variation of organic matter in PM 2.5 at a regional background site of the Yangtze River Delta region, China, Atmospheric Environment, 123, 288-297, 2015.

Flocas, H., Kelessis, A., Helmis, C., Petrakakis, M., Zoumakis, M., and Pappas, K.: Synoptic and local scale atmospheric circulation associated with air pollution episodes in an urban Mediterranean area, Theoretical and Applied Climatology, 95, 265-277, 2009.

Fu, Q., Zhuang, G., Wang, J., Xu, C., Huang, K., Li, J., Hou, B., Lu, T., and Streets, D. G.:

Mechanism of formation of the heaviest pollution episode ever recorded in the Yangtze River Delta, China, Atmospheric Environment, 42, 2023-2036, 2008.

Fu, Q., Zhuang, G., Li, J., Huang, K., Wang, Q., Zhang, R., Fu, J., Lu, T., Chen, M., and Wang, Q.: Source, long-range transport, and characteristics of a heavy dust pollution event in Shanghai, Journal of Geophysical Research Atmospheres, 115, 6128-6128, 2010.

Fu, X., Wang, S. X., Cheng, Z., Xing, J., Zhao, B., Wang, J. D., and Hao, J. M.: Source, transport and impacts of a heavy dust event in the Yangtze River Delta, China, in 2011, Atmospheric Chemistry & Physics, 14, 1239-1254, 2014.

Green, M. C., Chen, L. A., DuBois, D. W., and Molenar, J. V.: Fine particulate matter and visibility in the Lake Tahoe Basin: Chemical characterization, trends, and source apportionment, Journal of the Air & Waste Management Association, 62, 953-965, 2012.

Grundstrom, M., Tang, L., Hallquist, M., Nguyen, H., Chen, D., and Pleijel, H.: Influence of atmospheric circulation patterns on urban air quality during the winter, Atmospheric Pollution Research, 6, 278-285, 2015.

He, K., Yang, F., Ma, Y., Zhang, Q., Yao, X., Chan, C. K., Cadle, S., Chan, T., and Mulawa, P.: The characteristics of PM 2.5 in Beijing, China, Atmospheric Environment, 35, 4959-4970, 2001.

Ho, K. F., Lee, S. C., Chan, C. K., Yu, J. C., Chow, J. C., and Yao, X. H.: Characterization of chemical species in PM 2.5 and PM 10 aerosols in Hong Kong, Atmospheric Environment, 37, 31-39, 2003.

Hsu, N., Jeong, M. J., Bettenhausen, C., Sayer, A., Hansell, R., Seftor, C., Huang, J., and Tsay, S. C.: Enhanced Deep Blue aerosol retrieval algorithm: The second generation, Journal of Geophysical Research: Atmospheres, 118, 9296-9315, 2013.

Huang, K., Zhuang, G., Lin, Y., Fu, J. S., Wang, Q., Liu, T., Zhang, R., Jiang, Y., Deng, C., Fu, Q., Hsu, N. C., and Cao, B.: Typical types and formation mechanisms of haze in an Eastern Asia megacity, Shanghai, Atmos. Chem. Phys., 12, 105-124, 2012.

Huang, R. J., Zhang, Y., Bozzetti, C., Ho, K. F., Cao, J. J., Han, Y., Daellenbach, K. R., Slowik, J. G., Platt, S. M., and Canonaco, F.: High secondary aerosol contribution to particulate pollution during haze events in China, Nature, 514, 218-222, 2014.

Huang, X., Wang, T., Talbot, R., Xie, M., Mao, H., Li, S., Zhuang, B., Yang, X., Fu, C., and Zhu, J.: Temporal characteristics of atmospheric CO2 in urban Nanjing, China, Atmospheric Research, 153, 437-450, 2015.

Ji, D., Wang, Y., Wang, L., Chen, L., Hu, B., Tang, G., Xin, J., Song, T., Wen, T., and Sun, Y.: Analysis of heavy pollution episodes in selected cities of northern China, Atmospheric Environment, 50, 338–348, 2012.

Kanamitsu, M., Ebisuzaki, W., Woollen, J., Yang, S., Hnilo, J., Fiorino, M., and Potter, G.: NCEP-DOE AMIP-II reanalysis (R-2). Bulletin of the American Meteorological Society, Doibams, 2002.

Kang, H., Zhu, B., Su, J., Wang, H., Zhang, Q., and Wang, F.: Analysis of a long-lasting haze episode in Nanjing, China, Atmospheric Research, s 120–121, 78–87, 2013.

Kaufman, Y. J., Tanré, D., and Boucher, O.: A satellite view of aerosols in the climate system, Nature, 419, 215-223, 2002.

Kim, S.-W., Yoon, S.-C., Kim, J., and Kim, S.-Y.: Seasonal and monthly variations of columnar aerosol optical properties over east Asia determined from multi-year MODIS, LIDAR, and

AERONET Sun/sky radiometer measurements, Atmospheric Environment, 41, 1634-1651, 2007.

Kirchhofer, W,: Classification of European 500mb patterns, Arbeitsbericht der Schweizerischen Meteorologischen Zentralanstalt, Geneva, 43p, 1973.

Kappos, A. D., Bruckmann, P., Eikmann, T., Englert, N., Heinrich, U., Höppe, P., Koch, E., Krause, G. H., Kreyling, W. G., and Rauchfuss, K.: Health effects of particles in ambient air, International Journal of Hygiene & Environmental Health, 207, 399-407, 2004.

Kong, X., He, W., Qin, N., He, Q., Yang, B., Ouyang, H., Wang, Q., and Xu, F.: Comparison of transport pathways and potential sources of PM 10 in two cities around a large Chinese lake using the modified trajectory analysis, Atmospheric Research, 122, 284-297, 2013.

Kurokawa, J., Ohara, T., Morikawa, T., and Hanayama, S.: Emissions of air pollutants and greenhouse gases over Asian regions during 2000–2008: Regional Emission inventory in ASia (REAS) version 2, Atmospheric Chemistry & Physics, 13, 10049-10123, 2013.

Li, L., Chen, C. H., Fu, J. S., Huang, C., Streets, D. G., Huang, H. Y., Zhang, G. F., Wang, Y. J., Jang, C. J., and Wang, H. L.: Air quality and emissions in the Yangtze River Delta, China, Atmospheric Chemistry & Physics, 10, 1621-1639, 2011.

Li, Q., Zhang, R., and Wang, Y.: Interannual variation of the wintertime fog–haze days across central and eastern China and its relation with East Asian winter monsoon, International Journal of Climatology, 36, 346-354, 2016.

Mcgowan, H., and Clark, A.: Identification of dust transport pathways from Lake Eyre, Australia using Hysplit, Atmospheric Environment, 42, 6915-6925, 2008.

McGregor, G., and Bamzelis, D.: Synoptic typing and its application to the investigation of weather air pollution relationships, Birmingham, United Kingdom, Theoretical and Applied Climatology, 51, 223-236, 1995.

Malm, W. C., Sisler, J. F., Huffman, D., Eldred, R. A., and Cahill, T. A.: Spatial and seasonal trends in particle concentration and optical extinction in the United States, Journal of Geophysical Research: Atmospheres, 99, 1347-1370, 1994.

Ming, L., Ling, J., Li, J., Fu, P., Yang, W., Di, L., Gan, Z., Wang, Z., and Li, X.: PM 2.5 in the Yangtze River Delta, China: Chemical compositions, seasonal variations, and regional pollution events, Environmental Pollution, 223, 200, 2017.

Niu, F., Li, Z., Li, C., Lee, K. H., and Wang, M.: Increase of wintertime fog in China: Potential impacts of weakening of the Eastern Asian monsoon circulation and increasing aerosol loading, Journal of Geophysical Research: Atmospheres, 115, 2010.

Oanh N T K, Leelasakultum K.: Analysis of meteorology and emission in haze episode prevalence over mountain-bounded region for early warning, Science of the Total Environment, 409(11), 2261-2271, 2011.

Putaud, J.-P., Raes, F., Van Dingenen, R., Brüggemann, E., Facchini, M.-C., Decesari, S., Fuzzi, S., Gehrig, R., Hüglin, C., and Laj, P.: A European aerosol phenomenology—2: chemical characteristics of particulate matter at kerbside, urban, rural and background sites in Europe, Atmospheric environment, 38, 2579-2595, 2004.

Remer, L. A., Tanre, D., Kaufman, Y. J., Ichoku, C., Mattoo, S., Levy, R., Chu, D. A., Holben, B., Dubovik, O., and Smirnov, A.: Validation of MODIS aerosol retrieval over ocean, Geophysical research letters, 29, 2002.

Remer, L. A., Kaufman, Y., Tanré, D., Mattoo, S., Chu, D., Martins, J. V., Li, R.-R., Ichoku, C., Levy, R., and Kleidman, R.: The MODIS aerosol algorithm, products, and validation, Journal of the atmospheric sciences, 62, 947-973, 2005.

Rolph, G.: Real-time Environmental Applications and Display sYstem (READY) Website. Silver Spring, MD: NOAA Air Resources Laboratory, ready. arl. noaa. gov, 2013.

Russo, A., Trigo, R. M., Martins, H., and Mendes, M. T.: NO_2, PM_{10} and O_3 urban concentrations and its association with circulation weather types in Portugal, Atmospheric Environment, 89, 768-785, 2014.

Santurtún, A., González-Hidalgo, J. C., Sanchez-Lorenzo, A., and Zarrabeitia, M. T.: Surface ozone concentration trends and its relationship with weather types in Spain (2001–2010), Atmospheric Environment, 101, 10-22, 2015.

Singh, A., and Dey, S.: Influence of aerosol composition on visibility in megacity Delhi, Atmospheric Environment, 62, 367-373, 2012.

Shu, L., Xie, M., Wang, T., Chen, P., Han, Y., Li, S., Zhuang, B., Li, M., and Gao, D.: Integrated studies of a regional ozone pollution synthetically affected by subtropical high and typhoon system in the Yangtze River Delta region, China, 1-32, 2016.

State Environmental Protection Administration of China, 2006. China National Environmental Protection Standard: Automated Methods for Ambient Air Quality Monitoring. China Environmental Science Press, Beijing.

Stein, A. F., Draxler, R. R., Rolph, G. D., Stunder, B. J. B., Cohen, M. D., and Ngan, F.: NOAA's HYSPLIT Atmospheric Transport and Dispersion Modeling System, Bulletin of the American Meteorological Society, 96, 150504130527006, 2016.

Wang, Y., Stein, A. F., Draxler, R. R., Rosa, J. D. D. L., and Zhang, X.: Global sand and dust storms in 2008: Observation and HYSPLIT model verification, Atmospheric Environment, 45, 6368-6381, 2011.

Wang, J., Hu, Z., Chen, Y., Chen, Z., and Xu, S.: Contamination characteristics and possible sources of PM10 and PM2.5 in different functional areas of Shanghai, China, Atmospheric Environment, 68, 221-229, 2013.

Wang, Y., Li, L., Chen, C., Huang, C., Huang, H., Feng, J., Wang, S., Wang, H., Zhang, G., and Zhou, M.: Source apportionment of fine particulate matter during autumn haze episodes in Shanghai, China, Journal of Geophysical Research Atmospheres, 119, 1903–1914, 2014.

Wang, M., Cao, C., Li, G., and Singh, R. P.: Analysis of a severe prolonged regional haze episode in the Yangtze River Delta, China, Atmospheric Environment, 102, 112-121, 2015.

Xie, M., Zhu, K., Wang, T., Yang, H., Zhuang, B., Li, S., Li, M., Zhu, X., and Ouyang, Y.: Application of photochemical indicators to evaluate ozone nonlinear chemistry and pollution control countermeasure in China, Atmospheric Environment, 99, 466-473, 2014.

Xie, M., Liao, J., Wang, T., Zhu, K., Zhuang, B., Han, Y., Li, M., and Li, S.: Modeling of the anthropogenic heat flux and its effect on regional meteorology and air quality over the Yangtze River Delta region, China, Atmospheric Chemistry & Physics, 16, 6071-6089, 2016a.

Xie, M., Zhu, K., Wang, T., Chen, P., Han, Y., Li, S., Zhuang, B., and Shu, L.: Temporal characterization and regional contribution to O_3 and NO_x at an urban and a suburban site in Nanjing, China, Science of the Total Environment, 551, 533-545, 2016b.

Xie, M., Zhu, K., Wang, T., Feng, W., Li, M., Li, M., Han, Y., Li, S., Zhuang, B., and Shu, L.: Changes of regional meteorology induced by anthropogenic heat and their impacts on air quality in South China, Atmospheric Chemistry & Physics, 16, 15011-15031, 2016c.

Xie, M., Shu, L., Wang, T.-j., Liu, Q., Gao, D., Li, S., Zhuang, B.-l., Han, Y., Li, M.-m., and Chen, P.-l.: Natural emissions under future climate condition and their effects on surface ozone in the Yangtze River Delta region, China, Atmospheric Environment, 150, 162-180, 2017.

Xu, J. S., Xu, H. H., Xiao, H., Tong, L., Snape, C. E., Wang, C. J., and He, J.: Aerosol composition and sources during high and low pollution periods in Ningbo, China, Atmospheric Research, s 178–179, 559-569, 2016.

Yan, X. Y., Ohara, T., and Akimoto, H.: Bottom-up estimate of biomass burning in mainland China, Atmospheric Environment, 40, 5262-5273, 2006.

Yang, S., He, H., Lu, S., Chen, D., and Zhu, J.: Quantification of crop residue burning in the field and its influence on ambient air quality in Suqian, China, Atmospheric Environment, 42, 1961-1969, 2008.

Yarnal, B.: A procedure for the classification of synoptic weather maps from gridded atmospheric pressure surface data, Computers & Geosciences, 10, 397-410, 1984.

Young, D. E., Kim, H., Parworth, C., Zhou, S., Zhang, X., Cappa, C. D., Seco, R., Kim, S., Zhang, Q.: Influences of emission sources and meteorology on aerosol chemistry in a polluted urban environment: results from DISCOVER-AQ California, Atmospheric Chemistry and Physics, 16(8), 5427-5451, 2016.

Zhang, J. P., Zhu, T., Zhang, Q. H., Li, C. C., Shu, H. L., Ying, Y., Dai, Z. P., Wang, X., Liu, X. Y., and Liang, A. M.: The impact of circulation patterns on regional transport pathways and air quality over Beijing and its surroundings, Atmospheric Chemistry & Physics, 11, 33465-33509, 2012.

Zhang, Q., Quan, J., Tie, X., Li, X., Liu, Q., Gao, Y., and Zhao, D.: Effects of meteorology and secondary particle formation on visibility during heavy haze events in Beijing, China, Science of the Total Environment, 502C, 578-584, 2014.

Zhao, X. J., Zhao, P. S., Xu, J., and Meng, W.: Analysis of a winter regional haze event and its formation mechanism in the North China Plain, Atmospheric Chemistry & Physics, 13, 5685-5696, 2013.

Zheng, G., Duan, F., Su, H., Ma, Y., Cheng, Y., Zheng, B., Zhang, Q., Huang, T., Kimoto, T., and Chang, D.: Exploring the severe winter haze in Beijing: the impact of synoptic weather, regional transport and heterogeneous reactions, Atmospheric Chemistry and Physics, 15, 2969-2983, 2015a.

Zheng, X. Y., Fu, Y. F., Yang, Y. J., and Liu, G. S.: Impacts of atmospheric circulations on aerosol distributions in autumn over eastern China: observational evidences, Atmospheric Chemistry & Physics, 15, 3285-3325, 2015b.

Zhu, J., Wang, T., Deng, J., Jiang, A., and Liu, D.: An emission inventory of air pollutants from crop residue burning in Yangtze River Delta Region and its application in simulation of a heavy haze weather process, Acta Scientiae Circumstantiae, 32, 3045-3055, 2012.

Zhu, K., Xie, M., Wang, T., Cai, J., Li, S., and Feng, W.: A modeling study on the effect of urban land surface forcing to regional meteorology and air quality over South China, Atmospheric Environment, 152, 389-404, 2017.

Zhuang, G. S., Yuan, J. H., Yuan, H., Zhao, C. Y.: The compositions, sources, and size distribution of the dust storm from China in spring of 2000 and its impact on the global environment, Science Bulletin, 46, 895-901, 2001.

Regional severe particle pollution and its association with synoptic weather patterns in the Yangtze River Delta region, China

Lei Shu [1], Min Xie [1*], Da Gao [1], Tijian Wang [1*], Dexian Fang [2], Qian Liu [3], Anning Huang [1], Liwen Peng [1]

[1] School of Atmospheric Sciences, CMA-NJU Joint Laboratory for Climate Prediction Studies, Jiangsu Collaborative Innovation Center for Climate Change, Nanjing University, Nanjing 210023, China

[2] Chongqing Institute of Meteorology and Science, Chongqing 401147, China

[3] Jiangsu Provincial Academy of Environmental Science, Nanjing 210036, China

----

∗Corresponding to Min Xie (minxie@nju.edu.cn) and Tijian Wang (tjwang@nju.edu.cn)

Abstract: Regional air pollution is significantly associated with the dominant weather systems. In this study, the relationship between the particle pollution over the Yangtze River Delta (YRD) region and the weather patterns is investigated. Firstly, the pollution characteristics of particles ~~($PM_{2.5}$ and~~ , ~~PM_{10} and AOD)~~ in YRD are studied by using the in-~~-~~situ monitoring data ($PM_{2.5}$ and PM_{10}) in 16 cities ~~from December 2013 to November 2014~~, ~~as well as~~and Terra/MODIS AOD (aerosol optical depth)~~aerosol~~ products from December 2013 to November 2014. The results show that the regional mean value of AOD is high in YRD, with the annual mean value of 0.71±0.57. ~~t~~The annual mean~~average~~ particle concentrations in the cities of Jiangsu Province all exceed the national air quality standard. The pollution level is higher in the inland areas~~. Highest values can be found in Nanjing~~, with the highest concentrations of $PM_{2.5}$ and PM_{10} respectively being 79 ~~μg·m^{-3}~~ and 130 μg·m^{-3} in Nanjing~~, respectively~~. ~~The regional mean AOD is high with the annual mean value of 0.71±0.57, and peaks in summer (0.98±0.83).~~ The $PM_{2.5}$/PM_{10} ratios are usually high~~ in YRD~~, indicating that $PM_{2.5}$ is the overwhelmingly dominant particle pollutant in YRD. The wintertime peak of particle concentrations is tightly linked to the increased emissions in the heating season, as well as ~~and~~ the adverse~~poor~~ meteorological conditions. Secondly, based on NCEP reanalysis data, synoptic weather classification is conducted to reveal ~~that~~ the weather patterns that are easy to cause severe particle~~heavy~~ pollution in YRD. Five typical synoptic patterns are objectively identified, including the East Asian trough rear pattern, the depression inverted trough pattern, the transversal trough pattern, the high-pressure controlled pattern, and the northeast cold vortex pattern. Finally, synthetic analysis of meteorological fields and backward trajector~~y~~ies ~~calculation~~ are ~~used~~ applied to further clarify how these patterns impact particle concentrations. It is ~~clarified~~ demonstrated that ~~the weather situation of all patterns are~~air pollution is more or less influenced by ~~a~~ high-pressure systems. The relative positions of YRD to the anti-cyclonic circulations ~~system~~ are quite significant to the air quality of YRD. YRD is largely influenced by polluted air masses from the northern and the southern inland areas when it is at the rear of the East Asian major trough. Significant downward motion of air masses results in stable weather conditions~~In this case~~, and thereby ~~the strong northwest wind~~ hinders the ~~vertical outward transport of~~diffusion of air pollutants. Thus, the East Asian trough rear pattern is quite favorable for the accumulation of pollutants in YRD, and causes higher regional mean PM_{10} (116.5±66.9 μg·m-3), $PM_{2.5}$ (75.9±49.9 μg·m-3) and AOD (0.74). Moreover, this pattern is also resp~~ectively contributes 70.4% and 78.3% to the~~ onsible for the most occurrence of large-scale regional $PM_{2.5}$ (70.4%) and PM_{10} (78.3%) pollution episodes. High wind speed and the clean marine air masses may play important roles in the mitigation of the pollution in YRD. Especially when the clean marine air masses account for a large proportion of all trajectories~~While under the weather systems f~~ ~~or~~(YRD is controlled by the high-pressure controlled pattern and the northeast cold vortex pattern)~~other patterns~~, ~~the clean marine air masses may play great roles in the mitigation of particle pollution in YRD~~ the air in YRD has less chance of being polluted. The found correlation between weather patterns and particle pollution can provide valuable views in the decision-making on pollution control and mitigation strategies.

Keywords: $PM_{2.5}$; PM_{10}; air pollution meteorology; synoptic weather pattern; the Yangtze River Delta region

1. Introduction

The high occurrence of regional particle pollution is acquired worldwide attention in the scientific community (Malm et al., 1994; Putaud et al., 2004; Chan and Yao, 2008) due to its adverse impacts on visibility (Singh and Dey, 2012; Green et al., 2012) and public health (Kappos et al., 2004; Brook et al., 2010). Generally, t~~T~~he causes for this kind of pollution involve diverse aspects. Among them, the emission of pollutants and weather conditions are two major contributors (Oanh and Leelasakultum, 2011; Young et al., 2016). Particle pollution in urban agglomerations is primarily attributed to the huge amounts of anthropogenic emission of primary particles and ~~other~~ precursors (SO_2, NO_x, and VOCs, etc.). However, these emissions~~ source groups~~ are normally quasi-stable within a certain period of time (Kurokawa et al., 2013). Thus, the pollution level in a certain region generally depends on the regional weather conditions (namely weather patterns), which are strongly correlated with the synoptic-scale atmospheric circulation (Buchanan et al., 2002; Chuang et al., 2008; Flocas et al., 2009; Zhang et al., 2012; Zhao et al., 2013; Russo et al., 2014; Grundstrom et al., 2015; Zheng et al., 2015a; 2015b; Li et al., 2016).

Until now, researchers have gained improved knowledge of the relationship between weather patterns and particle pollution. For example, Buchanan et al. (2002) observed the significantly elevated concentrations of Black Smoke and PM_{10} under the anti-cyclonic, southerly and southeasterly weather types in the city of Edinburgh in UK between 1981 and 1996. Russo et al. (2014) showed an objective classification scheme of the atmospheric circulation affecting Portugal between 2002 and 2010, and revealed that higher concentrations of PM_{10}, O_3 and NO_2 are predominantly associated with synoptic circulation characterized by an eastern component and advection of dry air masses. Previous studies have confirmed that the levels of air pollution have close relations with weather patterns, and also showed great spatial variability ascribed to that the dominant weather pattern differs among different regions (Flocas et al., 2009; Grundstrom et al., 2015).

In recent decades, the air pollution caused by PM_{10} and $PM_{2.5}$ has become the extremely prominent air quality problem in urban areas of China (Deng et al., 2011; Huang et al., 2012; Ji et al., 2012; Cheng et al., 2013; Kang et al., 2013; Huang et., 2014; Zhang et al., 2014; Xie et al., 2016a; 2016c; Zhu et al., 2017). Many studies have tried to reveal the contribution of meteorology to the severe particle pollution episodes~~ as well~~. Chuang et al. (2008) identified seven weather patterns for aerosol events from March 2002 to February 2005 in the Taipei basin, and suggested that weather systems and the associated terrain blocking played important roles in the $PM_{2.5}$ accumulation during events days. Niu et al. (2010) revealed the potential impacts of weakening of the East~~ern~~ Asian monsoon circulation and increased~~ing~~ aerosol loading on the increase of wintertime fog in China. Zhao et al. (2013) analyzed a regional haze episode in the North China Plain from 16 to 19 January 2010, and pointed out that the strong temperature inversion, weak surface wind speed and descending air motions in the boundary layer were responsible for the accumulation of pollutants in a shallow layer and produced high pollutant concentrations within the source region. Zheng et al. (2015a) found that the favorable atmospheric circulation conditions are responsible for the severe winter haze over northeastern China. Li et al. (2016) pointed out that the fog-haze days over central and eastern China shows a clear feature of inter-annul variation, and the strong (weak) East Asian winter monsoon may result in less (more) fog-haze days across the region.

Located in the southeast coastal area of East China, the Yangtze River Delta (YRD) region is one of the most developed urban economic circles in the world, generally includes Shanghai, Jiangsu Province and Zhejiang Province, and occupies over 20% of China's total gross domestic product (GDP) (Shu et al., 2016; Xie et al., 2016a; 2017). In recent years, like other megacity clusters in China, such as the Beijing-Tianjin-Hebei (BTH) region (He et al., 2001; Chan and Yao, 2008; Ji et al., 2012; Zhang et al., 2012; 2014; Zhao et al., 2013; Zheng et al., 2015a) and the Pearl River Delta (PRD) region (Ho et al., 2003; Chan and Yao, 2008; Xie et al., 2016c; Zhu et al., 2017), YRD ~~also~~ has also been suffering severe air pollution problems brought by accelerated population, urban expansion, and industrialization (Chan and Yao, 2008; Fu et al., 2008; 2010; 2014; Deng et al., 2011; Li et al., 2011; Huang et al., 2012; Kang et al., 2013; Wang et al., 2013; 2014; 2015; Xie et al., 2014; 2016a, 2016b, 2017; Feng et al., 2015; Zheng et al., 2015b; Shu et al., 2016; Xu et al., 2016; Ming et al., 2017). Especially, the severe particle pollution episodes are widely recognized as one of the major air pollution issues in YRD (Fu et al., 2008; 2010; Deng et al., 2011; Huang et al., 2012; Kang et al., 2013; Kong et al., 2013; Wang et al., 2013; 2014; 2015; Fu et al., 2014; Feng et al., 2015; Zheng et al., 2015b; Xu et al., 2016; Ming et al., 2017). Thus, a ~~great deal~~lot of researches have been conducted to figure out the contamination status (Fu et al., 2010; Kang et al., 2013; Wang et al., 2013; 2015; Feng et al., 2015; Ming et al., 2017), possible source (Fu et al., 2010; 2014; Kong et al., 2013; Wang et al., 2013; 2014; Xu et al., 2016), or causes and features (Fu et al., 2008; 2010; Huang et al., 2012; Wang et al., 2015; Zheng et al., 2015a) of these episodes. However, among these studies, the work trying to figure out how particle pollution in YRD is associated with synoptic weather patterns is still quite limited. Zheng et al. (2015b) once summarized the synoptic-scale atmospheric circulations influencing the distribution of particles over eastern China in autumn from 2001 to 2010. They found that there are six polluted weather types and three clean ones, and revealed that heavy pollution events particularly occur when the study areas are at the rear of the anticyclone. This study considers the influence in a region larger than YRD, only focuses on the pollution in October, and is mainly on basis of satellite aerosol optical depth (AOD) data. Ground-based monitoring particle concentration data can better represent the status of particle pollution in the urban atmosphere of YRD. Thus, to better understand the relationship between the pollution in planetary boundary layer and the synoptic weather patterns over YRD, further study should be conducted based on the data at least over a year from the surface monitoring in YRD.

This work attempts to enhance the understanding of particle pollution in YRD, and provides the scientific knowledge for the association of regional severe particle pollution and synoptic weather patterns. Firstly, we analyze the spatial and temporal distribution of PM_{10}~~,~~ ~~and~~ $PM_{2.5}$ and AOD in YRD from December 2013 to November 2014, aimed to illustrate the characteristics of particle pollution over the region. Secondly, synoptic weather classification is conducted to reveal the weather patterns related ~~with~~to heavy pollution. Finally, synthetic analysis of meteorological fields and backward trajectorie~~y~~s ~~calculation~~ are used to further clarify the impact mechanism. In this paper, Section 2 describes the observed data, synoptic weather classification method and the trajectory model. Section 3 presents our main findings, including the detailed analysis of the characteristics of particle pollution in YRD, the synoptic weather patterns affecting the pollution, and the mechanism how weather systems impact the pollution. In the end, a brief summary is addressed in Section 4.

2. Data and methods

2.1 Observed data

The observed air quality data ~~($PM_{2.5}$ and PM_{10})~~ used in this study are from the National Environmental Monitoring Center (NEMC) of China. The in situ monitoring data for the hourly concentrations of ~~AQI,~~ $PM_{2.5}$, PM_{10}, CO, NO_2, SO_2 and O_3 can be acquired from the national air quality real-time publishing platform (http://106.37.208.233:20035). ~~Besides In addition, monitored meteorological parameters hourly data are applied as well, including temperature (T),~~

~~relative humidity (RH), wind speed (WS), wind direction (WD) and surfaceair pressure (P). The data are collected from the National Meteorological Center (www.nmc.cn).~~ Sixteen cities are selected as the representative research objects to better reflect the status of particle pollution over the YRD region. They are Shanghai, Changzhou, Nanjing, Nantong, Suzhou, Taizhoushi, Wuxi, Yangzhou, Zhenjiang, Hangzhou, Huzhou, Jiaxing, Ningbo, Shaoxing, Taizhou, and Zhoushan~~.~~ ~~Here we rename~~ (Taizhou in Jiangsu Province is renamed as Taizhoushi to distinguish ~~it~~ from the city Taizhou in Zhejiang Province). Fig. 1 shows the location of the 16 cities ~~over~~in YRD. The hourly pollutant concentration for a city is calculated as the average of the pollutant concentrations from several national monitoring sites in that city, which can better characterize the pollution levels of the city. The sampling methods and the quality assurance and quality control (QA/QC) procedures at each site act in accordance with the Chinese national standard HJ/T193-2005 (State Environmental Protection Administration of China, 2006; Xie et al., 2016b). Furthermore, manual inspection is conducted in data processing, including the removal of the absent and the abnormal values (such as $PM_{2.5}$ higher than PM_{10}). The period of this study starts from December 2013 to November 2014. In the following analysis, winter refers to the period from December 2013 to February 2014. Accordingly, spring, summer and fall represent the period from March to May, June to August, and September to November in 2014, respectively.

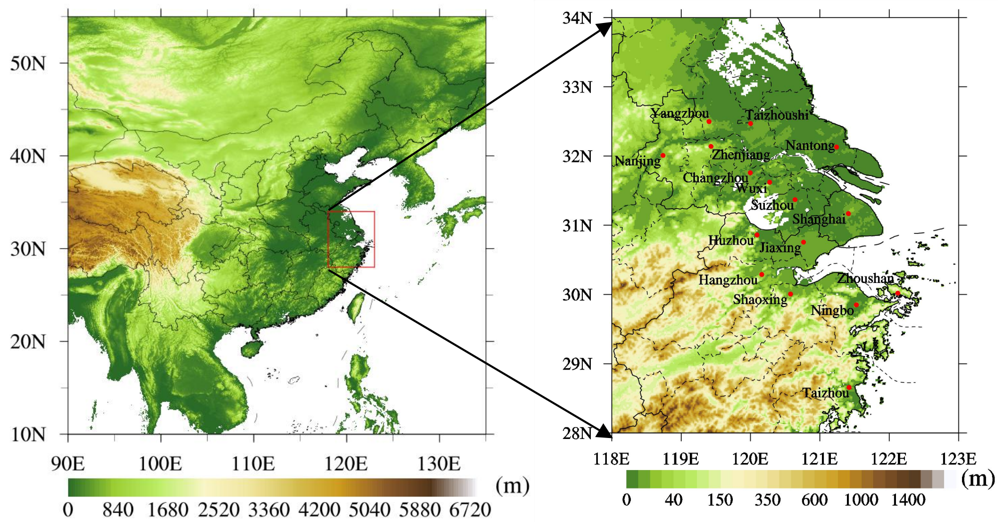

Figure 1. The location of YRD in China (a) and ~~the~~ 16 typical cities ~~over the~~ in YRD (b) ~~region~~, with the terrain elevations data. The terrain elevations data are obtained from the website (https://www.ngdc.noaa.gov/mgg/global/relief/ETOPO1/data/bedrock/cell_registered/).

The Moderate Resolution Imaging Spectroradiometer (MODIS) aerosol products can help to comprehensively analyze the spatial and temporal variations of aerosol loading over China. In this study, we ~~employ~~use the aerosol optical depth (AOD) data at 550 nm wavelength in ~~MODIS/~~Terra-/MODIS daily global Level 3 products (MOD08_D3)~~ of aerosol optical depth (AOD) at 550 nm wavelength~~. The~~ data~~y can be obtained from MODIS collection 6 (C6) dataset (~~available at~~ https://ladsweb.nascom.nasa.gov/search/index.html). MODIS aerosol products are derived by two entirely independent retrieval algorithms, one for deriving aerosols over land (Chu et al, 2002; 2003) and another for aerosols over the ocean (Remer et al, 2002; 2005; Chu et al., 2005). Here, we use the C6 Deep Blue (DB) products for deriving aerosols over land with the spatial resolution of 1° × 1° during the period from December 2013 to November 2014. The detailed descriptions of the retrieval algorithms, accuracy and validation can further refer to the work of Hsu et al. (2013).

In order to illustrate the real weather situation, the hourly monitored meteorological parameter records in each of 16 typical cities are applied as well. The data include 2 m temperature (T), 2 m relative humidity (RH), 10 m wind speed (WS), 10 m wind direction (WD) and surface air pressure (P). They are collected from the National Meteorological Center (http://www.nmc.cn).

2.2 Synoptic weather classification

Synoptic weather classification refers to the analysis of historical weather charts and characterization of weather systems. It ~~has widespread applications in the weather forecast, and~~ is more effective for the disastrous weather forecast due to its ~~intense~~ ability to reveal the atmospheric circulation situation. With the gradual popularization of computer and greater sharing of data, synoptic weather classification has great practical value in many other research fields~~;~~. ~~f~~For example, it has widespread applications in the field of analyzing the weather patterns related ~~with~~to air pollution (Mcgregor and Bamzelis, 1995; Zhang et al., 2012; Santurtún et al., 2015).

Methods of synoptic weather classification can be generally divided into the objective and the subjective methods (El-Kadi and Simithson, 1992). In this study, we apply the sums-of-squares technique, which is one of the objective classification methods and established in 1973 by Kirchhofer (Kirchhofer, 1973). The sums-of-squares technique can effectively categorize more than 90% of the analyzed weather maps, which is an improvement over the correlation techniques

(Yarnal, 1984). The steps of applying this technique are threefold. Firstly, the daily pressure data at grid points are normalized as follows:

$$Z_i = \frac{(X_i - \overline{X})}{s} \tag{1}$$

where Z_i is the normalized value of the grid point i, X_i is the value at grid point i, $\overline{X}$ is the mean of the study domain, and s is the standard deviation. Data normalization removes the effects of pressure magnitude and improves the seasonal comparability of weather types. Secondly, each normalized grid is compared to all other grids on the basis of the Kirchhofer score (S) for each grid:

$$S = \sum_{i=1}^{N} (Z_{ai} - Z_{bi}) \tag{2}$$

where Z_{ai} is the normalized value in grid i on the day a, Z_{bi} is the normalized value in grid i on the day b, and N is the number of grid points. The Kirchhofer score (S) is calculated for each row (denoted as S_R), each column (S_C) and the entire study domain (S_T) to ensure the pattern similarity between any pair of patterns for all grid points. Finally, all days are separated into one of the identified synoptic weather patterns according to the three values and empirically derived thresholds. Thereinto, the values of S_R, S_C and S_T must be lower than their respective threshold values so that the patterns can be accepted as similar (Barry et al., 1981). For each daily grid, the lowest significant Kirchhofer score (S) is recorded with the associated key day denoting the synoptic type of the day. Remaining days are considered as ‘unclassified’.

The dataset of meteorological field used in the sums-of-squares technique is from NCEP–DOE AMIP-II Reanalysis 2 data (Kanamitsu et al., 2002), which are collected at 00:00, 06:00, 12:00, and 18:00 UTC (universal time coordinated) (https://www.esrl.noaa.gov/psd/data/gridded/data.ncep.reanalysis2.pressure.html). The data have horizontal grids of 144×73, with a grid spacing of 2.5°. From the ground level to 10 hPa, there are 17 pressure levels in the vertical direction. The classification of synoptic weather maps is conducted by using the gridded data at the geopotential height of 850 hPa during the same time period when the air quality data are recorded. The domain of interest is centered over the YRD region, covering an area of 25-40° N in latitude and 110-128°E in longitude.

2.3 HYSPLIT model

Backward trajectories can be adopted to help understand transport paths and identify source regions of air masses~~ (Shan et al., 2009)~~. The Hybrid Single-Particle Lagrangian Integrated Trajectory (HYSPLIT) Model (Version 4) is developed by National Oceanic and Atmospheric Administration (NOAA) Air Resources Laboratory (ARL). It is one of the most extensively used atmospheric transport and dispersion models for the study of air parcel trajectories (Draxler and Rolph, 2013; Rolph, 2013; Stein et al., 2016), and has been well applied in complex transport, diffusion, chemical transformation and deposition processes simulations of atmospheric pollutants (Mcgowan and Clark, 2008; Wang et al., 2011; Huang et al., 2015; Xie et al., 2016b).

In this study, HYSPLIT is used to compute the air parcel backward trajectories, ~~determine~~reveal the possible source region of air masses, and establish the source-receptor relationships for each synoptic weather pattern. For each synoptic weather pattern, the terminus of the trajectories is considered to be located at the observation site in Nanjing (32°N, 118.8°E). The 72-h backward trajectories are calculated and clustered. The ending point is set at 1500 m above sea level. The NCEP reanalysis data (http://ready.arl.noaa.gov/archives.php) are used to drive the backward trajectory calculation. The NCEP data contain 6-hourly basic meteorological fields on pressure surfaces with the spatial resolution of 2.5°. In this study, the data are also converted to hemispheric 144 by 73 polar stereographic grids, which is the same grid configuration as the dataset applied in synoptic weather classification.~~ For each synoptic weather pattern, the terminus of the trajectories is considered to be located at the observation site in Nanjing (32°N, 118.8°E).~~

3. Results and discussion

3.1 Characteristics of particle pollution in ~~the~~ YRD~~ region~~

3.1.1 Spatial distributions of particle pollution

~~With the development of modern industrialization and urbanization, the contrasts of atmospheric pollution levels among urbanbetween each citiesy decrease gradually, and the heavysevere air pollution episodes tend to exhibit significant regional pollution characteristics. Figs. 2a and Fig. 2.b respectively shows the spatial distributions of the annual mean concentrations of $PM_{2.5}$ (Fig. 2a) and PM_{10} (Fig. 2b) in the 16 typical cities over YRD from~~

~~December 2013 to November 2014. The spatial distributions present the a similar pattern as a whole. GenerallyTaken together, the annual mean $PM_{2.5}$ and PM_{10} concentrations decrease progressively along the northwest-southeast direction, which means particle concentrations are comparatively high in the northwest inland areas and low in the southeast coastal areas. The pollution levels in most cities have a positive correlation with the proximity from the city to the sea. The farther the city is from the sea, the higher the concentrations are. Thereinto, the maximum concentrations of $PM_{2.5}$ and PM_{10} occur in Nanjing, with the value of 79 and 130 μg·m^{-3}, respectively. Given the previous researches on major climatic features in YRD, the southeast coastal area is dramatically affected by the land-sea breeze and marine air masses. The clean marine air masses are advantageous to the dilution and the diffusion of atmospheric pollutants, thus leading to lighter air pollution. DifferentlyHowever, in the inland region, the clustered cities and the industrial districts tend to emit more pollutants and thereby result in more accumulated air pollutants around cities. Furthermore,~~ Fig. 2ea displays the annual mean values of AOD at 550 nm wavelength ~~over the eastern~~in most areas of –China. The high values ~~AOD~~ (larger than 0.6) ~~mainly~~generally occur in ~~large megacity clusters, such as~~ BTH, YRD ~~and~~, the Sichuan Basin (SCB) ~~region~~, and some~~as well as~~~~and~~ central and southern provinces in China (Hubei, Hunan and Guangxi provinces). ~~Since~~ AOD is mainly governed by fine particles in industrialized urban conditions (Kim et al., 2006), thus ~~it indicates that~~ these abovementioned –areas should be ~~are~~ suffering high columnar aerosol loading. In YRD, with the development of modern industrialization and urbanization, the contrasts of atmospheric pollution levels among the cities decrease gradually, and severe air pollution episodes tend to exhibit significant regional pollution characteristics.

–Fig. 2db shows the temporal variation of regional ~~mean~~averaged value of AOD in YRD (covering 16 cities within the area of 25-40°N and 110-128°N)~~This domain can be used to represent the maximum effect of pollution aerosols resulting from anthropogenic activities in YRD~~. The annual mean ~~MODIS-derived~~value ~~–AOD spatially averaged for YRD~~ is 0.71±0.57~~,~~. ~~with an AOD~~The maximum seasonal value is 0.98±0.83 in summer, followed by ~~(0.98±0.83)~~ 0.81±0.57 in winter, 0.59±0.24 in spring, and ~~and an AOD minimum~~ 0.48±0.35 in autumn ~~(0.48±0.35). The regional seasonal mean AOD values for winter and spring are 0.81±0.57 and 0.59±0.24, respectively. The~~Though the peak of particle concentrations occurs ~~peak~~ in winter (as Fig. 3 and 5 shows~~s~~), the above results demonstrate that the ~~highest~~maximum regional mean AOD value occurs in summer, with the highest value of 1.60 in June.~~ June (1.60), distinctly higher than that in winter.~~ The result is similar to that found by Kim et al. (2006). I~~Thus, i~~It is ~~suggested~~reported that the value of AOD is not only associated with the pollution levels of fine particles, but also strongly affected by other factors ~~in terms of the seasonal mean condition~~ (such as solar radiation, water vapor and etc.)~~ in terms of the seasonal mean condition~~.~~ The work of Kim et al. (2006) also found a peak of monthly mean AOD averaged for industrialized coastal region of China appeared in June.~~ ~~They explained that t~~The maximum AOD value in hot seasons ~~June maximum~~ should be ascribed to the combined effects of an increase of fine aerosol production (secondary aerosol formation by gas-to-particle conversion, hygroscopic growth of hydrophilic aerosols and biomass burning emissions) and humid weather~~stagnant synoptic meteorological system~~ (Kim et al., 2006). Consequently, the aerosol optical depth data from satellite observation can reveal the spatial distribution of aerosols to some extent, but they cannot exactly reflect the pollution level and replace the concentration data.

Figs. 2c and 2d show the spatial distributions of annual mean particle concentrations in 16 typical cities over YRD from December 2013 to November 2014. Generally, the spatial distributions of $PM_{2.5}$ (Fig. 2c) and PM_{10} (Fig. 2d) present a similar pattern as a whole. The annual mean $PM_{2.5}$ and PM_{10} decrease progressively along the northwest-southeast direction, which means particle concentrations are comparatively high in the northwest inland areas and low in the southeast coastal areas. The pollution levels in most cities have a positive correlation with the proximity from the city to the sea. The farther the city is from the sea, the higher the concentrations are. The maximum particle concentrations occur in Nanjing, with the values of 79μg·m^{-3} for $PM_{2.5}$ and 130 μg·m^{-3} for PM_{10}. Given the previous researches on major climatic features in YRD, the southeast coastal area is dramatically affected by the land-sea breeze and marine air masses. The clean marine air masses are advantageous to the dilution and the diffusion of atmospheric pollutants, thus leading to lighter air pollution. However, in the inland region, the clustered cities and the industrial districts tend to emit more pollutants, and thereby result in more accumulated air pollutants around these cities.

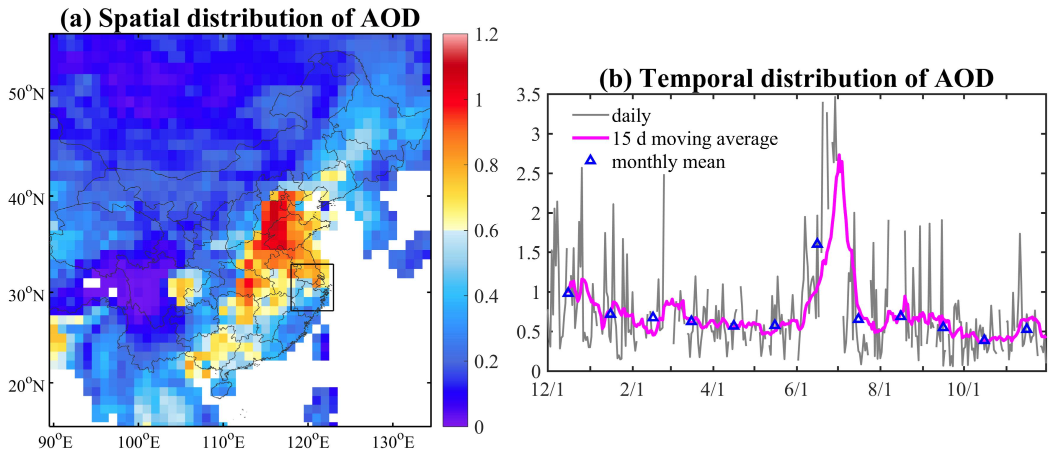

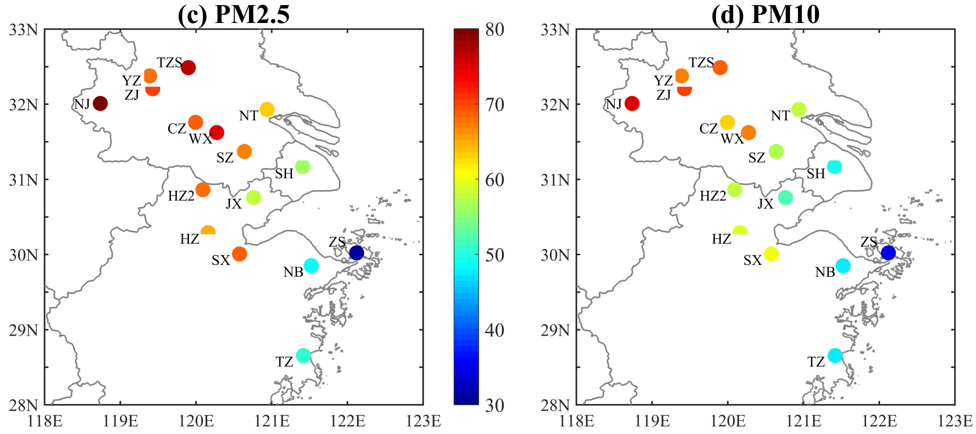

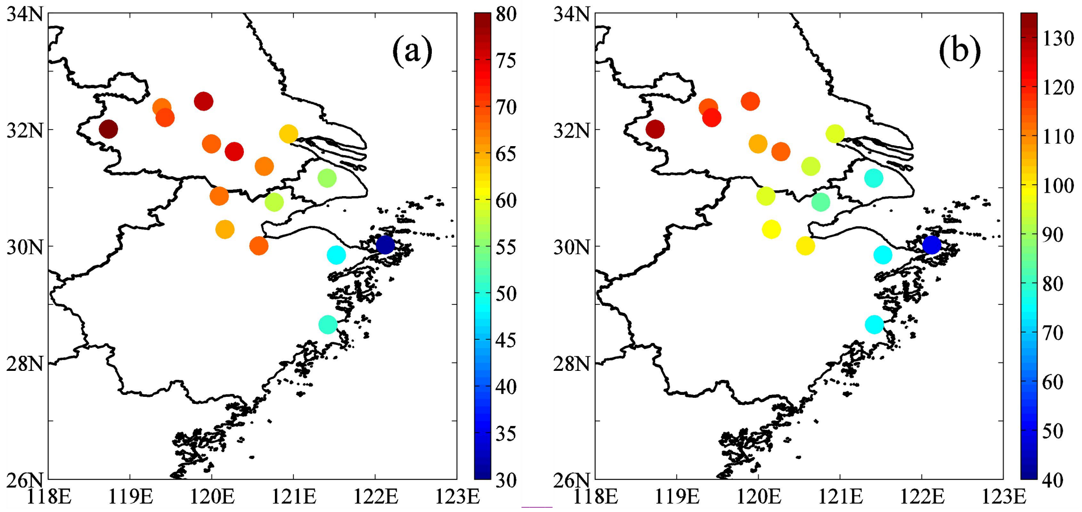

Figure 2. The ~~(a-e) The s~~Sspatial distributions of ~~the~~ annual mean AOD (at 550 nm wavelength) values – ~~concentrations of $PM_{2.5}$ (a) , and PM_{10} ,(b) and AOD at 550 nm wavelength (unit: μg·m-3)~~ over ~~the~~ YRD (a) ~~region from December 2013 to November 2014.~~

~~. (d),~~ ~~T~~the temporal variation ~~(daily: gray line; monthly mean: blue markers) and; 15 days moving average : (magenta line)~~ of regional averaged AOD value ~~–mean AOD~~ over (28-33°N, 118-123°N) (b), the spatial distribution of annual mean $PM_{2.5}$ concentrations (c), and the spatial distribution of annual mean PM_{10} concentrations (d). In (b), the gray line represents the daily value, the blue markers represent the

monthly mean values, and the magenta line represents the 15 days moving average value. In (c) and (d), ~~T~~the acronyms of each city ~~names~~ are marked, including ~~the top figures (~~Shanghai-SH, Changzhou-CZ, Nanjing-NJ, Nantong-NT, Suzhou-SZ, Taizhoushi-TZS, Wuxi-WX, Yangzhou-YZ, Zhenjiang-ZJ, Hangzhou-HZ, Huzhou-HZ2, Jiaxing-JX, Ningbo-NB, Shaoxing-SX, Taizhou-TZ, and Zhoushan-ZS~~)~~.

Fig. 3 illustrates the spatial distribution of ~~the~~ seasonal mean ~~concentrations of~~ $PM_{2.5}$ in 16 cities over ~~the~~ YRD ~~region~~. The pattern in each season is similar to the annual mean pattern (Fig. 2c~~a~~). The $PM_{2.5}$ pollution levels are much higher in inland cities, and decrease along the northwest-southeast direction. ~~From~~ For the ~~perspective of~~ seasonal variation, $PM_{2.5}$ concentrations are highest in winter with the maximum value being up to 120 μg·m^{-3}, decrease through the spring, and show the lowest values in summer and autumn. The difference between the $PM_{2.5}$ concentration in summer and that in autumn is relatively small, both with the maximum value lower than 60 μg·m^{-3} in Nanjing and the minimum close to 20 μg·m^{-3} in Zhoushan.

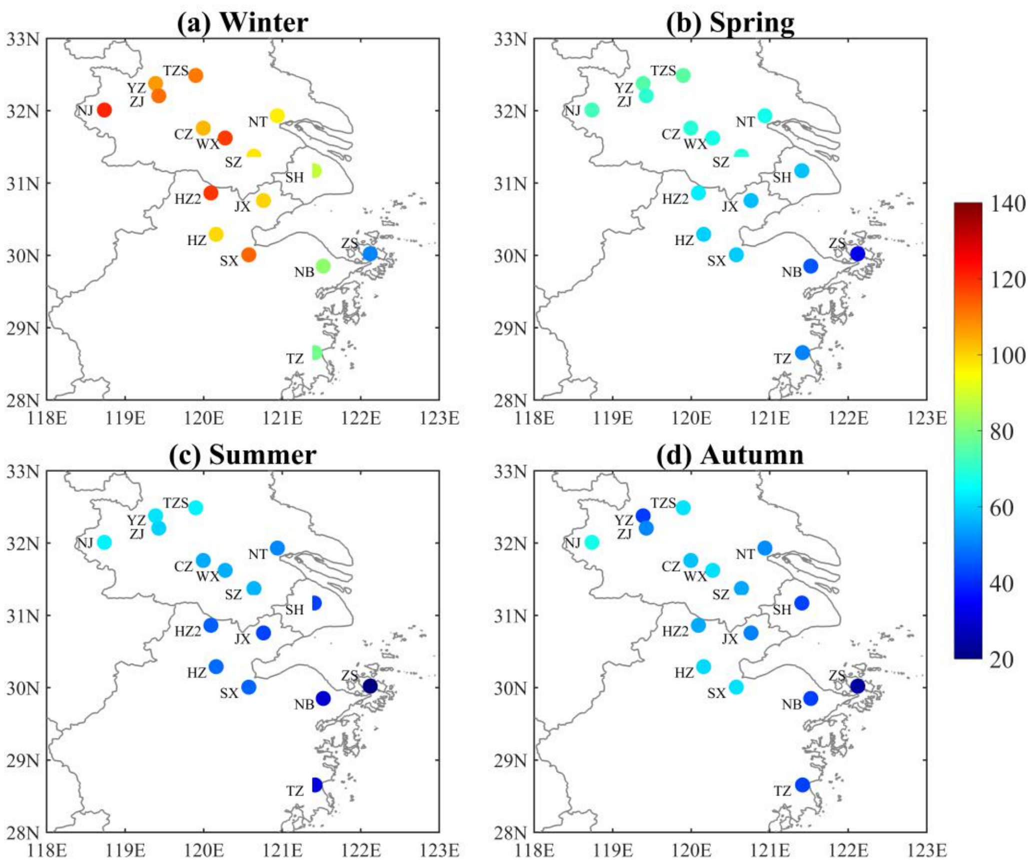

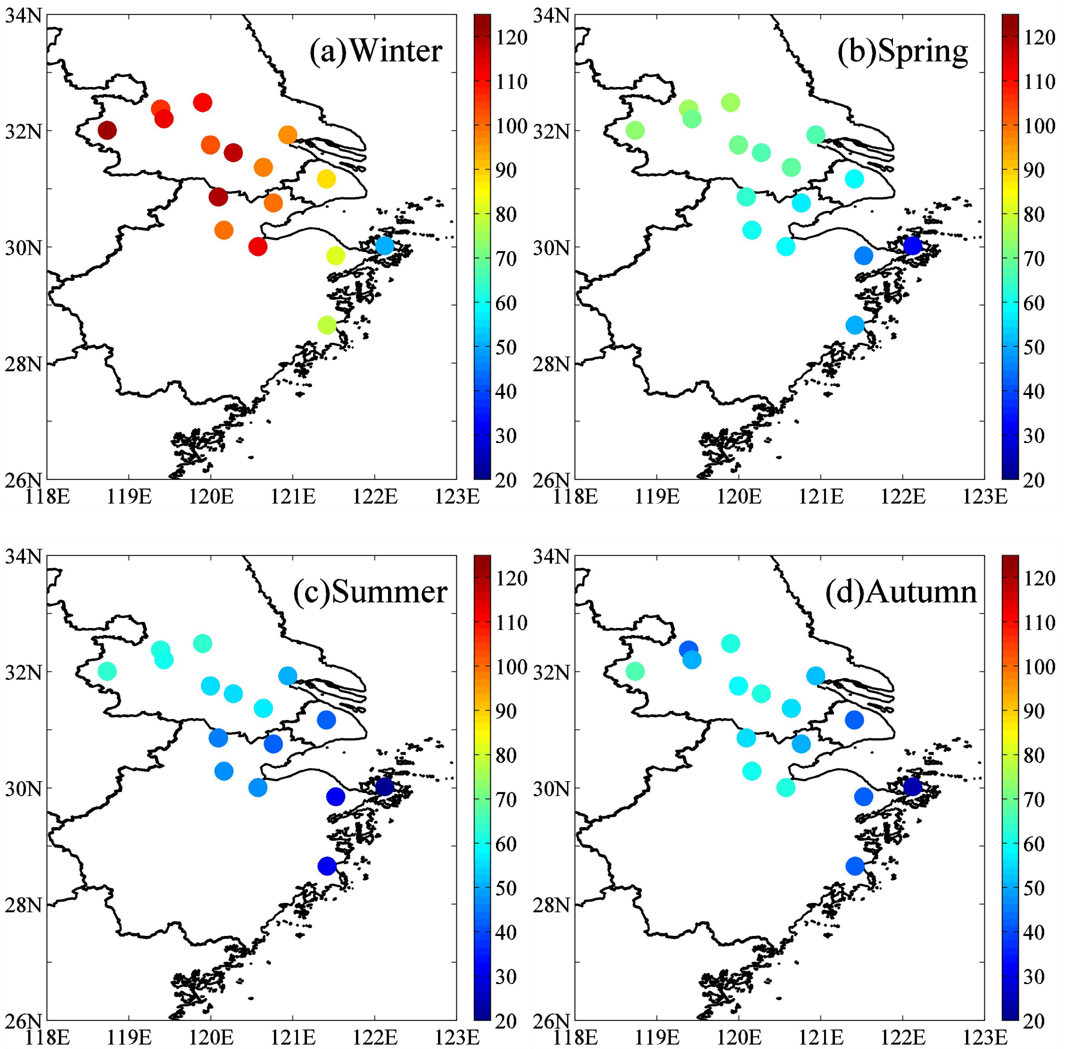

Figure 3. The The sSspatial distribution of the _seasonal mean $PM_{2.5}$ concentrations (unit: μg·m^{-3}) over the YRD region in: (a) winter, (b) spring, (c) summer, and (d) autumn. The acronyms for each citycity names are the same as those in Figure 42.

Table 1 quantitatively demonstrates the annual mean concentrations of $PM_{2.5}$ and PM_{10} in 16 cities over the YRD region. It also shows that the concentrationsparticle pollution levels in inland cities are relatively higher. The concentrations of $PM_{2.5}$ and PM_{10} in 8 cities of Jiangsu province are all higher than 60 μg·m^{-3} ($PM_{2.5}$) and 80 μg·m^{-3} (PM_{10}), respectively. However, the concentrations in the cities located in the coastal area (such as Ningbo, Taizhou and Zhoushan) are comparatively lower. Only the air quality of Zhoushan meets the national standard, which may be attributed to the fact that it is located on the island where the air is more likely influenced by the clean marine air masses.

To reveal the important role of $PM_{2.5}$ in particle pollution, the ratios of $PM_{2.5}$ concentration to

PM_{10} concentration ($PM_{2.5}/PM_{10}$) are calculated over YRD. As listed in Table 1, the maximum annual mean value of the $PM_{2.5}/PM_{10}$ ratio is 0.72 in Shanghai, followed by Huzhou and Suzhou (~~with the value of~~ 0.71), implying that $PM_{2.5}$ fraction is overwhelmingly dominant of the PM_{10} mass in these cities. The $PM_{2.5}/PM_{10}$ ratios in other cities are between 0.60 and 0.69, with the minimum value of 0.58 in Zhenjiang. These values are comparable to those in other cities like Beijing (He et al., 2001), Shanghai (Wang et al., 2013), Tai~~wan~~bei (Chen et al., 1999), and Hong Kong (Ho et al., 2003), suggesting that the formation of $PM_{2.5}$ from gases is the most importan~~ce~~t source of particles in the cities of China. Table 1 also presents that the $PM_{2.5}/PM_{10}$ ratios in all cities show a distinct seasonal variation. It is remarkable that the values of $PM_{2.5}/PM_{10}$ ~~in winter~~ are much higher in winter than in ~~those in~~ other seasons, with the maximum value reaching 0.85 in Shanghai and followed by 0.82 in Suzhou. The highest concentrations of $PM_{2.5}$ usually occur in winter (Fig. 3a) and high values of $PM_{2.5}/PM_{10}$ ratio also appear in the same season (Table 1), ~~suggesting~~ indicating that $PM_{2.5}$ poses a greater threat to human health in cold seasons that may be related to the heating activities. In summer, the values of $PM_{2.5}/PM_{10}$ in 16 cities ~~the ratios~~ are medium, with the mean value of 0.67. The lowest ratios usually occur in spring and autumn, with the mean ratios of all cities being 0.61 (spring) and 0.63 (autumn). The minimum value occurs in the autumn of Yangzhou with the value of 0.51, followed by 0.52 in the spring of Nanjing and the autumn of Zhenjiang. The above discussion ~~about~~ on the spatial and temporal variations of $PM_{2.5}/PM_{10}$ ratios also implies that particles originate from various kinds of sources and are variedly emitted.

Table 1. Annual mean concentrations of $PM_{2.5}$ and PM_{10}, and the annual and seasonal mean values of $PM_{2.5}/PM_{10}$ ratio in 16 cities over ~~the of~~ YRD ~~region~~.

Cities		$PM_{2.5}$ ($\mu g \cdot m^{-3}$)	PM_{10} ($\mu g \cdot m^{-3}$)	$PM_{2.5}/PM_{10}$				
				Annual	Winter	Spring	Summer	Autumn
Shanghai		56	78	0.72	0.85	0.68	0.72	0.66
Jiangsu Province	Nanjing	79	130	0.61	0.64	0.52	0.70	0.60
	Changzhou	69	106	0.65	0.73	0.60	0.67	0.62
	Nantong	63	95	0.66	0.72	0.62	0.71	0.64
	Suzhou	67	94	0.71	0.82	0.68	0.71	0.67
	Taizhoushi	76	117	0.65	0.66	0.58	0.72	0.66
	Wuxi	75	114	0.66	0.73	0.59	0.67	0.62
	Yangzhou	68	114	0.60	0.69	0.58	0.59	0.51

	Zhenjiang	70	121	0.58	0.71	0.54	0.58	0.52
Zhejiang Province	Hangzhou	65	99	0.66	0.74	0.59	0.63	0.66
	Huzhou	68	96	0.71	0.78	0.66	0.68	0.69
	Jiaxing	58	84	0.69	0.75	0.65	0.68	0.69
	Ningbo	48	75	0.64	0.69	0.62	0.63	0.62
	Shaoxing	68	100	0.68	0.72	0.62	0.71	0.68
	Taizhou	50	75	0.67	0.69	0.66	0.66	0.65
	Zhoushan	31	50	0.63	0.66	0.62	0.66	0.55

3.1.2 Temporal variations of particle pollution

Fig. 4 shows the annual mean diurnal variation of $PM_{2.5}$ (Fig. 4a) and PM_{10} (Fig. 4b) in 16 cities over YRD. Obviously, the diurnal cycles of particle concentrations in most cities follow the similar pattern. The $PM_{2.5}$ concentrations maintain comparably high values from 0:00 to 8:00 ~~(local time)~~. From then on, coinciding with more vehicle emission in rush hours, the concentrations go up rapidly from 8:00 to 12:00. After reaching the peak, $PM_{2.5}$ concentrations decrease and keep the low values until the sunset. During the nighttime, the pollutants get accumulated until the midnight, which ~~might~~ should be attributed to the more stable atmospheric stratification in the boundary layer. In comparison, there are two peaks in the diurnal cycles of PM_{10} concentrations in several cities. The broad morning peak of PM_{10} concentrations is more evident from 8:00 to 12:00, and the evening one occurs around 20:00. Besides, the diurnal change of particle concentrations in the southeast coastal area like Zhoushan is much smaller. As discussed in Section 3.1.1, the difference might be related to its special geographic location, ~~low pollution level and~~ less emission of precursors and low pollution level.

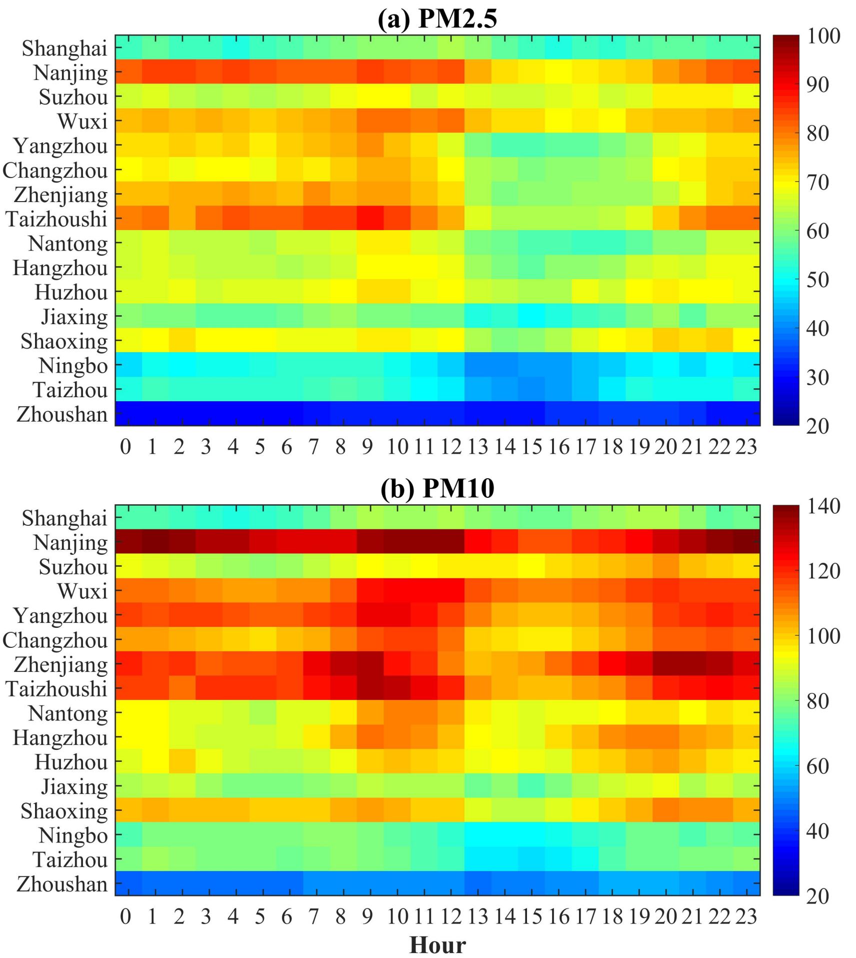

(a) PM2.5
Shanghai
Nanjing
Suzhou
Wuxi
Yangzhou
Changzhou
Zhenjiang
Taizhoushi
Nantong
Hangzhou
Huzhou
Jiaxing
Shaoxing
Ningbo
Taizhou
Zhoushan
0 1 2 3 4 5 6 7 8 9 10 11 12 13 14 15 16 17 18 19 20 21 22 23
100
90
80
70
60
50
40
30
20
(b) PM10
Shanghai
Nanjing
Suzhou
Wuxi
Yangzhou
Changzhou
Zhenjiang
Taizhoushi
Nantong
Hangzhou
Huzhou
Jiaxing
Shaoxing
Ningbo
Taizhou
Zhoushan
0 1 2 3 4 5 6 7 8 9 10 11 12 13 14 15 16 17 18 19 20 21 22 23
Hour
140
120
100
80
60
40
20

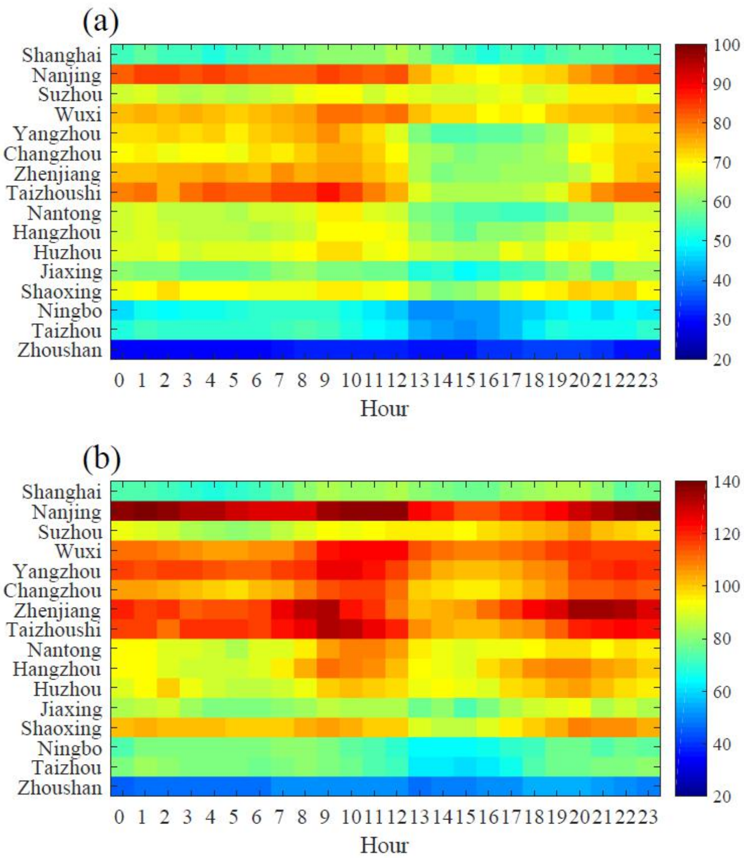

Figure 4. Diurnal variationss of ~~(a)~~ PM$_{2.5}$ (a) and ~~(b)~~ PM$_{10}$ (b) concentrations ~~(unit: μg·m^{-3})~~ in 16 cities of ~~the~~ YRD ~~region~~ (unit: μg·m^{-3}).

Fig. 5 demonstrates the monthly mean concentrations of PM$_{2.5}$ ~~(Fig. 5a)~~ and PM$_{10}$ ~~(Fig. 5b)~~ in 16 cities of ~~the~~ YRD ~~region~~. As illustrated in the figure, there are three peaks in the seasonal variations of particles ~~over YRD~~. The three peaks occur in December, March, and May/June~~,~~. ~~which~~ This monthly variation pattern is more obvious ~~in the monthly variation of~~for PM$_{10}$. The causes resulting in the wintertime peak of particle concentrations can be explained by two factors. One is the enhanced pollutants emissions from residential heating. The other is the stable and poor meteorological conditions that limit the ~~dilution and~~ diffusion of atmospheric pollutants. For the peak appearing in March, the drivers may be associated with dust storms events in spring (Zhuang et al., 2001; Fu et al., 2010; 2014). As discussed in Section 3.1.1, the values of PM$_{2.5}$/PM$_{10}$ ratio in 16 cities are lowest in spring with the mean ratios of 0.61. High PM$_{10}$ concentrations during this period further prove that dust storms can bring more coarse dust particles to YRD. For the peak in May ~~or~~ /June, it is probably caused by field burning of crop residue in rural areas of China, which is regarded as an important source of biomass burning (Yan et al., 2006; Yang et al., 2007; Zhu et al., 2012).

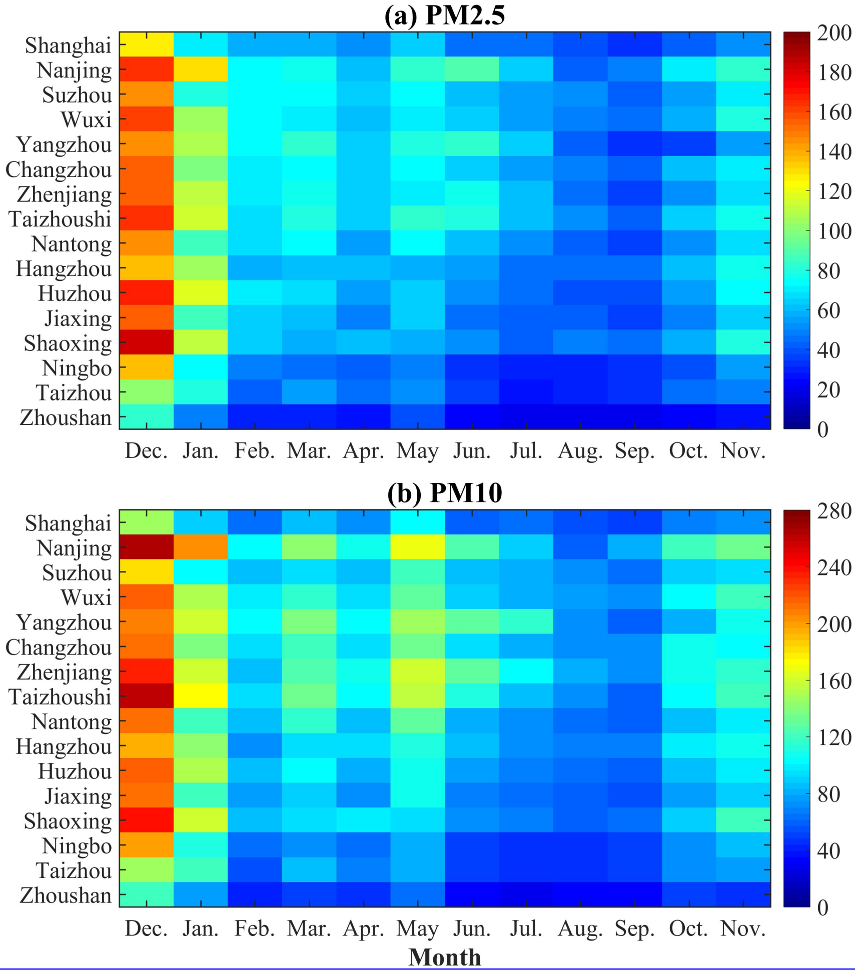
(a) PM2.5
Shanghai
Nanjing
Suzhou
Wuxi
Yangzhou
Changzhou
Zhenjiang
Taizhoushi
Nantong
Hangzhou
Huzhou
Jiaxing
Shaoxing
Ningbo
Taizhou
Zhoushan
Dec. Jan. Feb. Mar. Apr. May Jun. Jul. Aug. Sep. Oct. Nov.
200
180
160
140
120
100
80
60
40
20
0
(b) PM10
Shanghai
Nanjing
Suzhou
Wuxi
Yangzhou
Changzhou
Zhenjiang
Taizhoushi
Nantong
Hangzhou
Huzhou
Jiaxing
Shaoxing
Ningbo
Taizhou
Zhoushan
Dec. Jan. Feb. Mar. Apr. May Jun. Jul. Aug. Sep. Oct. Nov.
Month
280
240
200
160
120
80
40
0

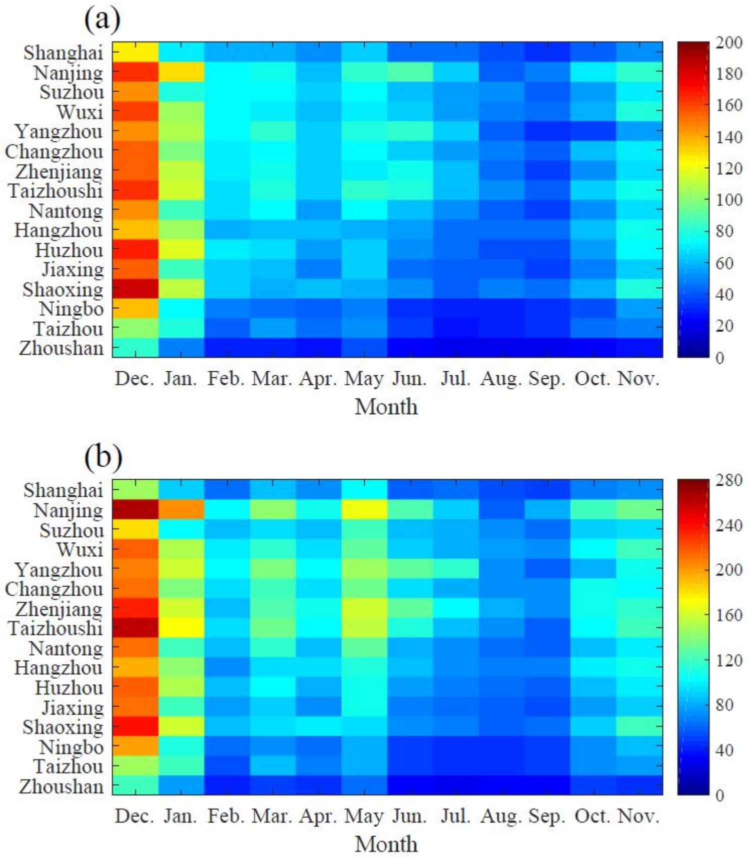

Figure 5. Monthly variations of ~~(a)~~ _$PM_{2.5}$ (a) and ~~(b)~~ PM_{10} (b) concentrations ~~(unit: μg·m^{-3})~~ in 16 cities of ~~the~~ YRD ~~region~~ (unit: μg·m^{-3}).

3.1.3 Regional severe particle pollution in YRD

According to the National Ambient Air Quality Standard (NAAQS) of China, the urban air quality needs to meet the second standard with the ~~annual~~ daily mean concentrations of $PM_{2.5}$ and PM_{10} lower than ~~35~~ 75 μg·m^{-3} and ~~70~~ 150 μg·m^{-3}, respectively. In this study, when the daily mean $PM_{2.5}$ (PM_{10}) concentrations exceed the national air quality standard in most (8 or more) of the 16 ~~YRD~~ cities, we define that there is a large-scale regional $PM_{2.5}$ (PM_{10}) pollution. Consequently, from December 2013 to November 2014, 98 (46) days when the large-scale regional $PM_{2.5}$ (PM_{10}) pollution episode occurred are identified. That is, YRD suffered from the regional $PM_{2.5}$ (PM_{10}) pollution in nearly 28.0% (13.1%) days of the year.

Table 2 shows the typical regional severe particle pollution episodes (no less than 3 days) in YRD from December 2013 to November 2014. As illustrated in the table, there are dozens of continuous large-scale particle pollution episodes. For example, $PM_{2.5}$ concentrations exceeded the national standard in all 16 cities from December 1 to 5 in 2013, and there were more than 14 cities facing ~~the~~ heavy PM_{10} pollution at the same time. From May 26 to 30 in 2014, serious $PM_{2.5}$

and PM_{10} pollution were found in more than 10 cities. It seems that high $PM_{2.5}$ ~~level~~ pollution episodes are remarkably associated with high PM_{10} ~~level~~ pollution episodes. Moreover, ~~the~~ regional $PM_{2.5}$ pollution episodes occurred much more frequently than ~~the~~ PM_{10} pollution episodes. It might be owing to the fact that fine particles dominate the composition of particles in YRD (as discussed in Section 3.1.2).

Table 2. The typical regional severe particle pollution episodes (no less than 3 days) in YRD from December 2013 to November 2014.

Episodes of $PM_{2.5}$ pollution	Episodes of PM_{10} pollution
1-6 Dec.	1-6 Dec.
11-15 Dec.	12-15 Dec.
24-26 Dec.	24-26 Dec.
28 Dec. - 6 Jan.	29 Dec. - 5 Jan.
15-20 Jan.	17-20 Dec.
30 Jan. - 2 Feb.	26-30 May
20-24 Feb.	
16-18 Mar.	
8-10 Apr.	
20-22 May	
26-30 May	
5-7 Jun.	
28 Jun. - 1 Jul.	
10-12 Nov.	

3.2 Synoptic weather classification

To examine the relationship between ~~the~~ regional severe particle pollution in YRD and ~~the~~ weather situations, ~~the~~ synoptic weather classification is carried out from December 2013 to November 2014 in this work. Following the method described in Section 2.2, we conduct the classification of synoptic weather pattern by using the dataset of geopotential height at 850 hPa collected from NCEP ~~gridded~~ reanalysis data. As shown in Table 3, five weather patterns are finally identified, including the East Asian trough rear pattern (Pattern 1), the depression inverted trough pattern (Pattern 2), the transversal trough pattern (Pattern 3), the high-pressure controlled pattern (Pattern 4), and the northeast cold vortex pattern (Pattern 5). The unknown type is defined as 'the unclassified pattern'. During the study period, weather situation on 95.6% of the days is classified as one of the five typical synoptic weather patterns.

Table 3 lists the typical date, the number of days, and seasonal occurrence frequencies of each synoptic weather pattern. As demonstrated in the table, Pattern 1 is the dominant weather pattern in YRD, which accounts for 47.6% of all days of the year (from December 2013 to November 2014). The occurrence frequencies of Pattern 2 and 3 are 20.0% and 18.1%, respectively. Pattern 4 and 5 are identified on the fewest number of days, with the occurrence frequencies of 4.1% and 5.8%, respectively.

Table 3 also shows the seasonal occurrence frequencies of each pattern from December 2013 to November 2014. Obviously, they are distinctly different. Pattern 1 tends to occur in winter with the frequency of 30.5%, followed by spring (25.9%), summer (21.8%) and autumn (21.8%). Pattern 2 is the most popular weather pattern in summer with the occurrence frequency of 37.0%, followed by spring (30.1%), autumn (21.9%) and winter (11.0%). As for Pattern 3, the seasonal frequencies are in the order of winter (36.4%), spring (27.3%), autumn (19.7%) and summer (16.7%). For Pattern 4 and Pattern 5, they are both most likely to take place in autumn, with the occurrence frequencies being 53.3% and 42.9%, respectively. The occurrence frequencies of Pattern 4 and Pattern 5 in other seasons account for nearly 50%.

Table 3. The typical date, the number of days, and the seasonal occurrence frequencies of each synoptic weather pattern.

~~Synoptic weather patterns~~Type	Typical date	Number of days	Occurrence frequency (%)			
			Spring	Summer	Autumn	Winter
East Asian trough rear pattern (Pattern 1)	2014-05-12	174 (47.7%)	25.9	21.8	21.8	30.5
Depression inverted trough pattern (Pattern 2)	2014-05-09	73 (20.0%)	30.1	37.0	21.9	11.0
Transversal trough pattern (Pattern 3)	2014-02-18	66 (18.1%)	27.3	16.7	19.7	36.4
High-pressure controlled pattern (Pattern 4)	2014-10-07	15 (4.1%)	13.3	26.7	53.3	6.7
Northeast cold vortex pattern (Pattern 5)	2014-09-14	21 (5.8%)	19.0	23.8	42.9	14.3
Unclassified pattern	—	16 (4.4%)	—	—	—	—

3.3 Effects of synoptic weather patterns on particle pollution

3.3.1 Relationship between synoptic weather pattern and particle pollution

To figure out the relationship between synoptic weather pattern and particle pollution, the occurrence frequencies of the five typical synoptic patterns during the regional severe particle pollution episodes are calculated. As shown in Table 4, during the regional $PM_{2.5}$ (PM_{10}) pollution episode days, Pattern 1 is the dominant synoptic weather pattern, with the occurrence frequency of 70.4% (78.3%). For $PM_{2.5}$ pollution, Pattern 2 and Pattern 3 both occur ~~for~~in 14.3% of the days. For PM_{10} pollution, Pattern 2 (6.5%) appears less frequently than Pattern 3 (15.2%). The occurrence frequencies of Pattern 4 and Pattern 5 are less than 1%, and can almost be ignored on that account.

According to Table 3 and Table 4, the occurrence frequency of Pattern 1 during the regional particle pollution episodes is obviously higher than its occurrence in the whole year. In contrast, the occurrences of Pattern 2 and Pattern 3 during the~~ regional particle pollution~~ episodes are less frequent~~ly~~ than those throughout the year. Moreover, Pattern 4 and Pattern 5 appear far less frequently during the regional particle pollution episodes than their appearance within a year. To sum up, it suggests that the weather situation of Pattern 1 is more beneficial for the formation of large-scale regional particle pollution in YRD.

Table 4. The occurrence frequencies of synoptic weather patterns during the regional severe $PM_{2.5}$ and PM_{10} pollution episodes

~~Synoptic weather patterns~~Type	$PM_{2.5}$		PM_{10}	
	Number of days	Frequency (%)	Number of days	Frequency (%)
Pattern 1	69	70.4	36	78.3
Pattern 2	14	14.3	3	6.5
Pattern 3	14	14.3	7	15.2
Pattern 4	0	0%	0	0
Pattern 5	1	1.0	0	0

Fig. 6 show the whisker-box plot of mean air pollutants (PM_{10}, $PM_{2.5}$, O_3, NO_2, SO_2 and CO) concentrations and ~~meterological~~meteorological parameters (~~wind speed~~ WS, ~~temperature~~ T, P~~pressure~~ and ~~relative humidity~~ RH) of 16 cities ~~in YRD under~~under –the five synoptic weather patterns, as well as the corresponding spatial distribution of AOD over eastern China. The statistical results are listed in Table 5 as well.

As shown in Figs. 6a~~ to ~~-6f and Table 5, the highest concentrations of main air pollutants (except O_3) averaged for 16 cities in YRD are observed to be associated with Pattern 1~~, with the greatest variability of all six air pollutants~~. Since aerosols can reflect and absorb solar radiation-

~~(Kaufman et al, 2002), thus causing~~ and thereby cause the decrease of the photochemical production of O_3 (Kaufman et al, 2002), the O_3 concentration is lowest for Pattern 1 (Fig. 6c). As above mentioned, Pattern 1 is most likely to occur in winter (30.5%) and spring (25.9%). Therefore, the weather situation of this pattern ~~generally~~ features the weakest surface wind, the lowest humidity, the second highest surface pressure, and low temperature ~~and relatively high surface pressure (only second to that for Pattern 3)~~. All ~~T~~these ~~synoptic conditions~~weather characteristics are conducive to an accumulation of particles and their precursors (SO_2, NO_2 and CO). For Pattern 3, the concentrations of PM_{10}, $PM_{2.5}$ NO_2 and SO_2 are the second highest compared to other patterns~~, as well as the variability of all six air pollutants~~. This pattern features the highest surface pressure and much stronger surface wind. The temperature is lowest as Pattern 3 also tends to take place in winter (37.0%) and spring (30.1%). Under the weather situation of Pattern 1 and Pattern 3, YRD is ~~usually~~both under the control of high-pressure ~~system~~, and ~~most~~ likely to suffer ~~heavy~~serious particle pollution. ~~However, t~~The strength of surface wind for different weather patterns plays a key role in the occurrence frequency of regional severe particle pollution episodes. With the weakest surface wind, ~~making~~ Pattern 1 is regarded as ~~be~~'~~"~~the most polluted~~"~~ pattern'~~"~~. As for Pattern 2, the pollution levels of main pollutants are in the middle and slightly lower than those for Pattern 3. Due to the high occurrence frequency in summer (37.0%) and spring (30.1), the weather condition of Pattern 2 is characterized as ~~RH was found to be lowest, with~~ relatively high temperature ~~and~~, low pressure, ~~with~~and the lowest RH. In contrast, Pattern 4 and Pattern 5 are ~~"~~'the clean ~~least polluted"~~ pattern'~~"~~, with the concentrations of all pollutants ~~concentrations being closely approximated and obvious~~distinctly lower than other three patterns. The relatively high humidity, high temperature, strong wind ~~speed~~ (especially for Pattern 5) and much low surface pressure are favorable to the mitigation~~diffusion~~ of pollutants.

~~Furthermore,~~ Figs. 6k to 6o display the spatial distribution of AOD over eastern China under different synoptic weather patterns. ~~Thereinto, t~~The regional mean values of AOD in YRD (28-33°N, 118-123°N) ~~corresponding to Pattern 1 to 5~~ are 0.74 for Pattern 1, 0.64 for Pattern 2, 0.81 for Pattern 3, 0.47 for Pattern 4 and 0.49 for Pattern 5 ~~corresponding to Pattern 1 to 5~~, respectively. It can also be ~~seen~~found ~~from Fig. 6~~ that AOD over YRD is high~~est~~er for Pattern 3, ~~followed by~~ Pattern 1 and Pattern 2. For these three patterns, high AOD usually ~~is observed covering~~occurs in ~~large areas of China (~~BTH, YRD, SCB, ~~an~~as well as~~d~~ the provinces of Shanxi, Shandong, Hubei, Hunan, Anhui and Guangxi). Worthy of noteEspecially., TThereinto, the highest AOD values isare mainly found in northeastern China. For Pattern 4 and Pattern 5, However, hhigh AOD for Pattern 4 and 5 areis most concentrated in BTH and Shandong province, while relatively low AOD is observedfound in YRD. Since AOD is mainly upclosely related to fine particles concentrations and then other factors (as discussed in Section 3.1.2), it can be concluded that YRD is most heavily polluted under the weather situations of Pattern 1 and Pattern 3.

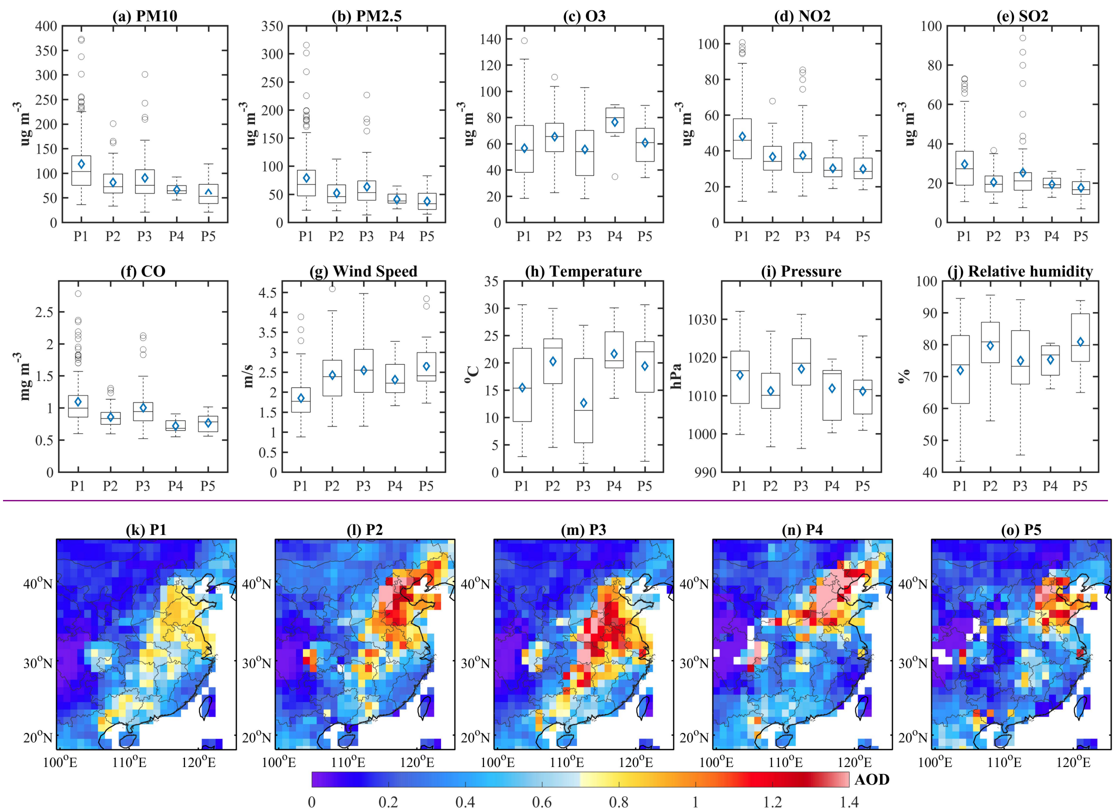

Figure 6. (a-j) Whisker-box plots ofor mean values of air pollutants concentrations and meteorological parameters of 16 typical YRD cities in YRD, (k-p) the spatial distribution of AOD for the five synoptic weather patterns. The bottom and topedges of eachthe box in (a-j) are the first 25th and third 75th percentilesquartiles, and the band inside the box is the median and , the diamond is the average, and .the whiskers extend to the most extreme data. (k-p) Spatial distributions of AOD for the five synoptic weather patterns. P1, P2, P3, P4, and P5 represent Pattern 1, Pattern2, Pattern 3, Pattern 4, and Pattern 5, respectively.

Table 5. The average values of air pollutionant concentrations and meteorological conditionsfactors averaged for 16 typical YRD cities in YRD forunder –the fivedifferent synoptic weather patterns.

Type	PM_{10}	$PM_{2.5}$	O_3	NO_2	SO_2	CO	SO_2	WS	T	P	RH
Pattern 1	116.5±66.9	75.9±49.9	57.7±27.3	46.9±19.2	29.3±17.1	1.08±0.41	29.3±17.1	1.84±0.67	15.8±7.8	1015.0±8.5	72.3±14.4
Pattern 2	81.5±38.4	52.3±27.4	65.5±23.6	36.1±13.4	20.6±9.9	0.86±0.24	20.6±9.9	2.38±0.88	20.3±6.3	1011.2±6.7	79.8±10.2

Pattern 3	86.9±49.5	59.1±37.3	58.5±25.5	35.1±15.5	23.3±15.9	0.96±0.35	23.3±15.9	2.59±0.87	13.4±8.2	1016.1±9.6	76.0±11.6
Pattern 4	66.1±18.8	40.7±15.9	76.8±19.6	29.4±9.8	19.4±6.4	0.72±0.17	19.4±6.4	2.29±0.64	21.7±4.9	1011.8±7.0	75.4±5.8
Pattern 5	58.7±31.3	37.4±22.5	61.1±20.6	29.1±11.1	17.8±8.4	0.77±0.22	17.8±8.4	2.63±0.93	19.4±8.0	1011.1±6.9	81.0±9.8

3.3.2 The impact mechanism of synoptic weather patterns on heavy severe particle pollution

Figs. 67 to -110 present the meteorological fields and the backward trajectories under the weather situations of the the five synoptic weather patterns. The first two graphs of Figs. 76- to 1110 , which are identified as a, illustrate the 850 hPa and 500 hPa geopotential height field and wind field, respectively. The third graphs display the sea level pressure field and 1000 hPa wind field on the typical date of each pattern. . The highlighted red boxes point out the essential area (YRD) that we focus on. The fourthsecond graphs identified as b demonstrate the height-latitude cross-sections of vertical velocity in the latitude (25-40°N), which is averaged from 110-128°E in the longitude. The bold black lines show the latitude range of 16 cities (28.6-32.5°N) over YRD. The positive wind speeds (10^2 Pa s^{-1}) indicate that there are vertical downward atmospheric motions, while the negative wind speeds represent the upward motion. Besides, it is well known that the atmospheric pollutant transport trajectories are deeply affected by synoptic systems. As shown in the thirdlastfifth graphs marked with c in Figs. 67- to 1101, to reveal how the typical synoptic weather patterns influence the distribution of particles in YRD, the 72-h backward trajectories are calculated and then clustered. Given that Nanjing is the most polluted among the 16 citiescity in YRD as described in Section 3.1, the observational site in Nanjing (32°N, 118.8°E) is chosen for the terminus of the trajectories for each synoptic weather pattern.

As illustrated in Fig. 6a7a, Pattern 1 usually occurs when YRD is located at the rear of the East Asian major trough and under the control of a high-pressure ridge at 850 hPpa. The center of the high-pressure system is on the northwestern Pacific Ocean. the northeastern China is entirestrongly affected by a low-pressure system at 850 hpa, namely the Aleutian Low.the Siberian high. Meanwhile, northeastern China is strongly affected by a low-pressure system, namely the Aleutian Low. East Asian major trough appears along the eastern coastline of China, and it is nearly close and parallel to the right edge of the study domain (shown by the red box). At this time, the YRD region is located at the rear of the East Asian major trough and under the control of a high-pressure the front edge of the ridge. The center of the high-pressure system is on the northwestern Pacific Ocean. The strong horizontal northwest wind inat the frontrear of the East Asian major trough can transport the pollutants from the Beijing-Tianjin-Hebei (BTH (high AOD as shown in Fig. 6k)) region to YRD. At the same time, a weak low-pressure center appears in central China. In the south of the low-pressure center, the west and southwest wind at the rear of the high-pressure ridge can also transport the pollutants from central and southwestern China (such as SCB and the Sichuan BasinGuangxi province) to YRD. The confluence of air flows may contribute tocause an the accumulation of pollutants in YRD. Accordingly, the atmospheric circulation at 500 hPa features a shallow through with west-northwest flow (Fig. 67b). The sea level pressure pattern is almost dominated by uniform pressure field, with relatively weak anti-cyclonic circulation over YRD (Fig. 76c). The above discussion can be further provedexplained by the 72-h backward trajectories displayed in Fig. 76ce. When YRD is under the control of Pattern 1, the air masses are mainly from the north ofnorthern China (44%), followed by central regionthe Sichuan Basin (36%) and the northeast of YRD (19%). It suggests that the particle pollution is remarkably affected by the polluted air masses from BTH and Cheng-Yucentral city clusters agglomeration. It isSurface meteorological observation records also shown (Fig. S1a) that west-northwest, southwest and west surface winds dominate in Nanjing (Fig. 7f), and high $PM_{2.5}$ is closely associated with the transport of polluted air masses in these wind direction.

In the vertical section (Fig. 76bd), the relatively weak upward air flows dominate in the south of 320°N, while the clear downward air flows prevail in the north of 320°N. The largest ascending velocity (< -15×10^{-2} Pa s^{-1}) and subsiddescending velocity (> ~248×10^{-2} Pa s^{-1}) both appears at the altitude of 500 hPa, . They respectively occurring and in the latitude of 27.5°N and 37.5°N. Downward motion dominates above YRD, which is in accordance with the 850 hPa circulation pattern represented by a high-pressure ridge. For this reason, the weather conditions are relatively stable near the surface and beneficial to the local accumulation of pollutants. It is convinced that there is a large-scale vertical atmospheric circulation above the YRD cities. Particularly, weak upward motion dominates below the altitude of 925 hPa. That means that local pollutants are transported upward and then back to the YRD cities by the strong outward downdrafts in the higher latitude. The strong horizontal northwest wind hinders the vertical transport. Overall, the above resultsPattern 1 –represents a stable synoptic weather pattern, and this weather situation is extremely conductive to the built-up~~disadvantageous to the diffusion~~ of atmospheric pollutants over YRD. This result is consistent with the finding of Zheng et al (2015b).

Pattern 1

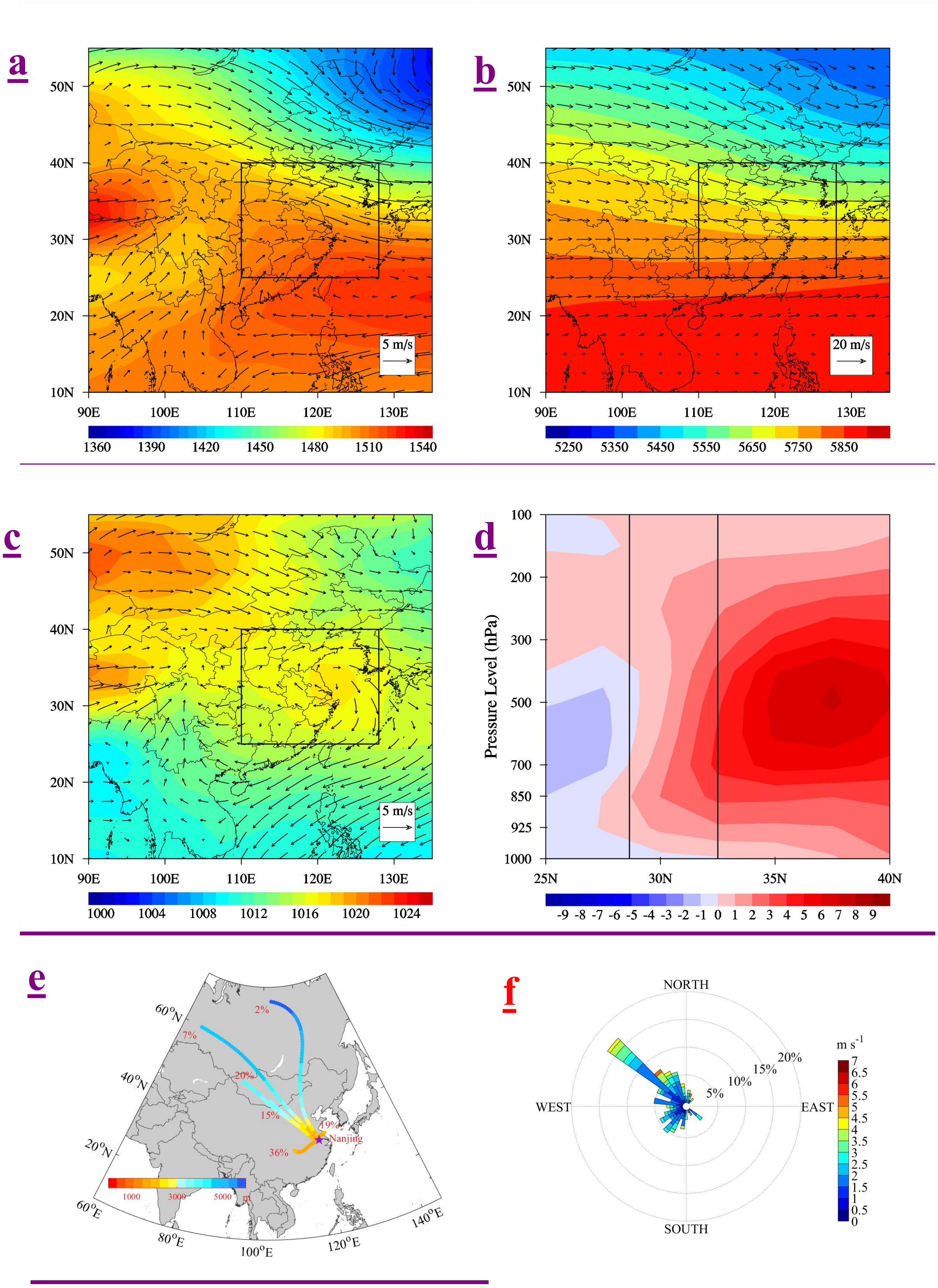

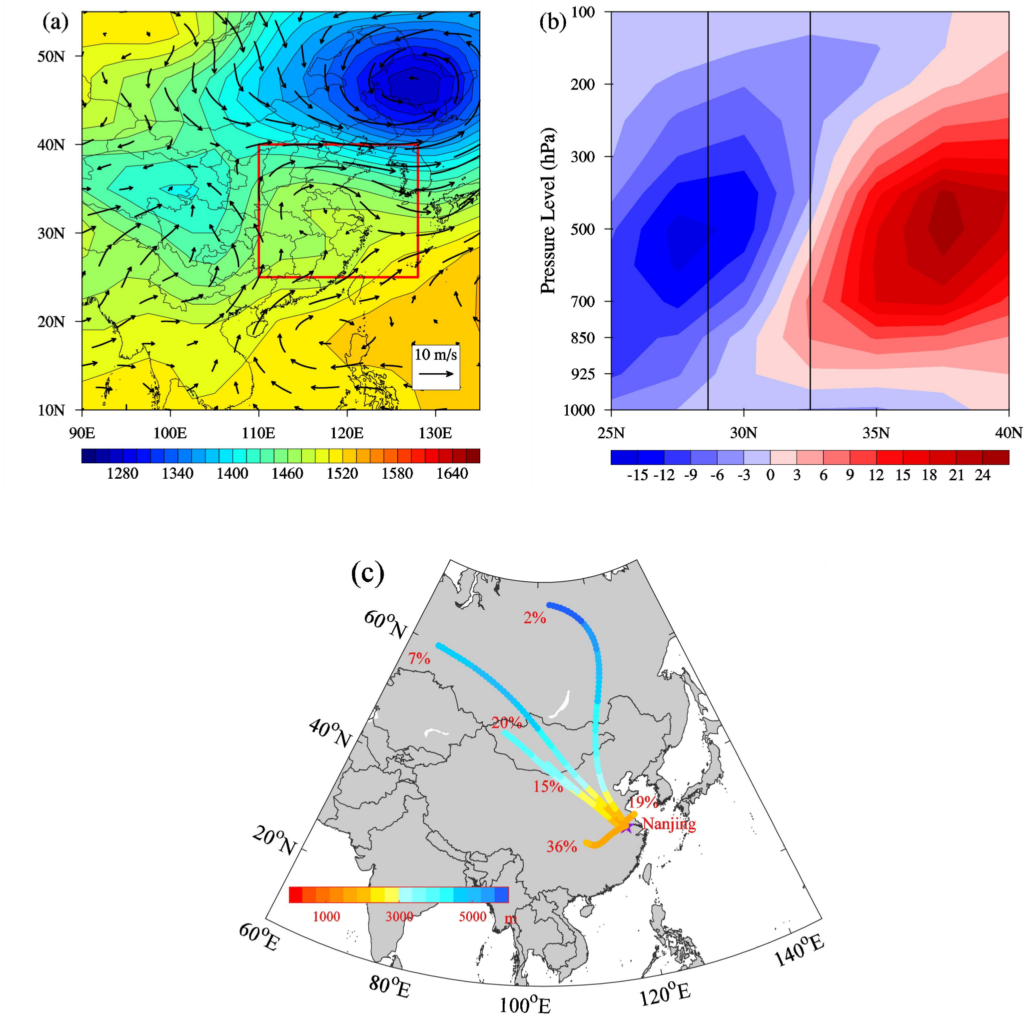

Figure 7~~6~~. Weather condition in ~~East Asia major trough rear pattern (~~Pattern 1~~)~~. (a) 850 hPa geopotential height field and wind field, (b) 500 hPa geopotential height field and wind field, (c) sea level pressure field and 1000 hPa wind field, (~~b~~d) height-latitude cross-sections of vertical velocity (unit: 10^{-2} Pa/s) averaged from longitude of 110-128°E~~. The black rectangular region represents the 16 cities in YRD (28.6-32.5°N)~~, ~~and~~ (~~c~~e) 72-h backward trajectory ending at the height of 1500 m, and (f) observation wind rose plots in Nanjing. In (a)-(c), the highlighted boxes point out the essential area (YRD) that we focus on. In (d), the black rectangular region represents the 16 cities in YRD (28.6-32.5°N). In (e), ~~T~~the purple marker indicates the location of Nanjing (32°N, 118.8°E). The data is averaged for all days corresponding to Pattern 1.

As for Pattern 2, a~~two~~ low-pressure center (the Southeast Vortex)~~s~~ ~~are~~is centered in ~~the central China and the north of Inner Mongolia region~~SCB, the East China Sea is influenced by a high-pressure system, and a depression inverted trough extends and covers the YRD region in latitude at 850 hPa (Fig. 8~~7~~a). Consequently, in YRD, the strong southwest air flows from southern China meet with the southeast air flows from the East China Sea. After the convergence of air masses, they jointly transport pollutants northwestward. While at surface (Fig. 8~~7~~c), the study domain is located at the bottom of a high-pressure system~~ also~~ and impacted by strong southeast wind at the bottom of a high-pressure system. In the middle troposphere (Fig. 87b), the sparse isopleths indicate small geopotential height gradient, while the shallow ridge causesthe wind field at 500 hPa features wester-southwestly flows. Fig. 87ee also illustrates these air pollutant transport paths. For the days when Pattern 2 dominates, about 42% of the air masses are from the southwest and the south of China, and 15% are from the East China Sea. Besides, there are nearly 43% originating from the local sources of YRD, which may be related withto the short-range air masses transport. The air masses from the East China Sea are very important, because the clean marine air masses may dilute the particle concentrations in YRD. Besides, there are nearly 43% air masses originating from the local sources of YRD, which may be related to the short-range transport in the northwest direction. This is also in accordance with the dominant northwest surface wind in Nanjing (Fig. S18bf). When it comes toFor the vertical structure (Fig. 87ed), Pattern 2 is obviously different from Pattern 1, as the upward air flows dominate in the south of 347.5°N. except for weak downward motion between 30-33°N below the 850 hPa layer. The largest updrafts zone (~< -157$\times 10^{-2}$ Pa s^{-1}) appears above YRDin the north of 28°N - and between the altitude of 700 hPa and 500 hPa. The vertical velocity close to surface is relatively weaker compared to that at higher levels over YRD. Meantime, there is stronger upward motion near surface in the latitude of 37.5°N, with weak downward motion above the 700 hPa layer. Different from Pattern 1, there is weaker descending motion above the 500 hPa layer and stronger ascending motion below that level. The above discussionis difference - suggests that atmospheric pollutants in YRD are horizontally transported northwestward to higher latitude, and vertically transport upward to higher atmospheric levels.layers-. Therefore, despite the transport of abundant pollutants to YRD via southwest air flows and short-range northwest transport of polluted air masses, the strong surface southeast wind and upward motion under the weather situation of Pattern 2 determine that there is much slighter particle pollution over YRD compared in contrast to Pattern 1.Thus, though Pattern 2 may cause the regional particle pollution in YRD, it can also benefit the diffusion of pollutants to some extent.

Pattern 2

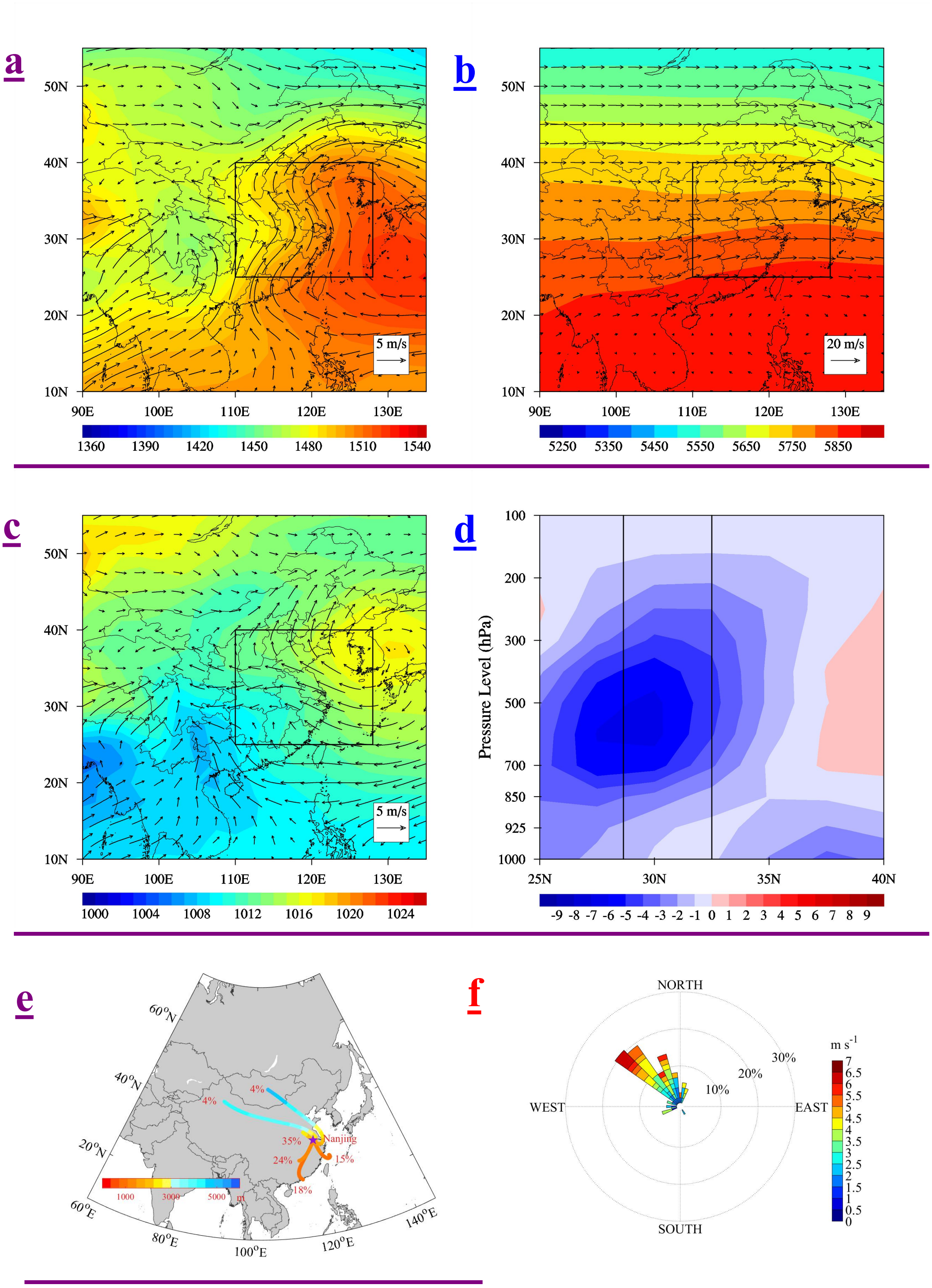
a
b
c
d
e
f
50N
40N
30N
20N
10N
90E
100E
110E
120E
130E
5 m/s
20 m/s
1360 1390 1420 1450 1480 1510 1540
5250 5350 5450 5550 5650 5750 5850
1000 1004 1008 1012 1016 1020 1024
Pressure Level (hPa)
100
200
300
500
700
850
925
1000
25N
30N
35N
40N
-9 -8 -7 -6 -5 -4 -3 -2 -1 0 1 2 3 4 5 6 7 8 9
60°N
40°N
20°N
60°E
80°E
100°E
120°E
140°E
Nanjing
4%
4%
35%
24%
15%
18%
1000
3000
5000
m
NORTH
SOUTH
WEST
EAST
10%
20%
30%
m s-1

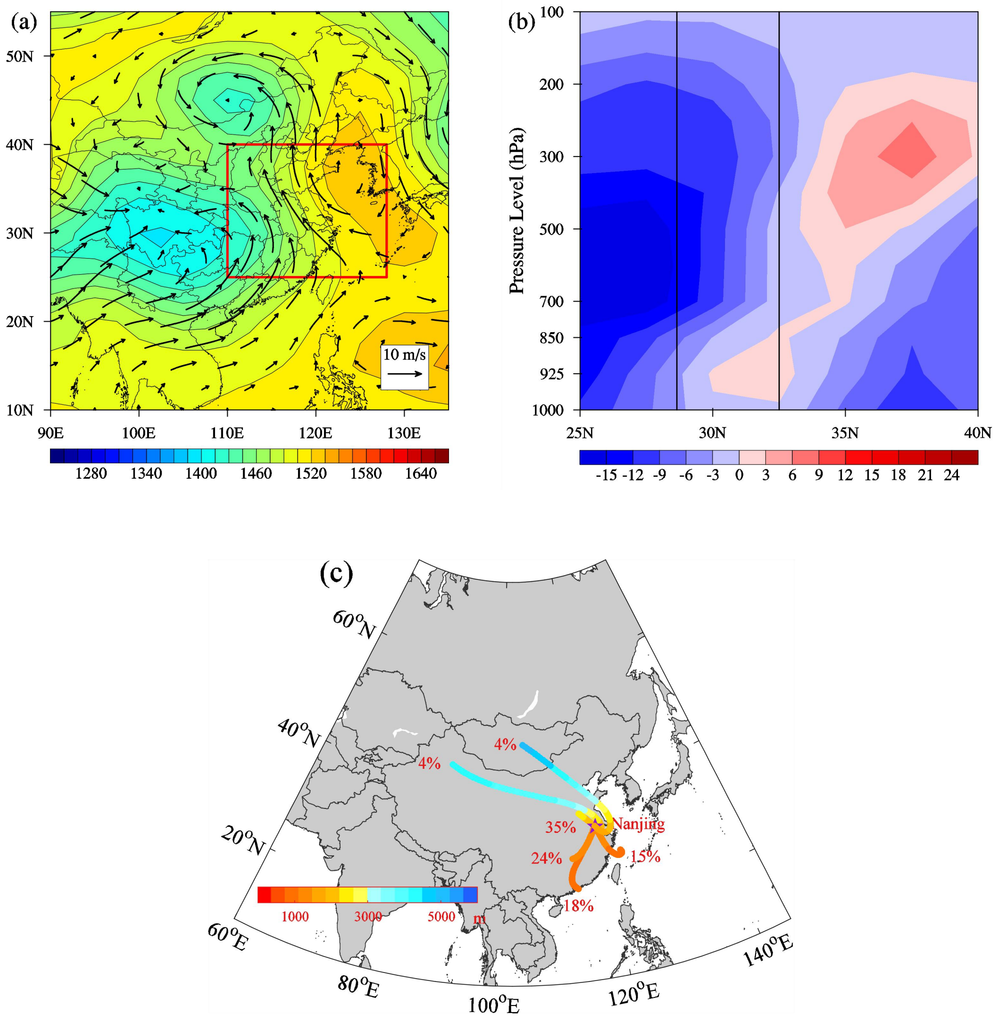

Figure 87.– As in Fig. 76 but for depression inverted trough pattern (Pattern 2).

For Pattern 3, it tends to occur in winter (36.4%, as displayed in Table 3). Under this circumstance, YRD is mainly controlled by a high-pressure system centered in cCentral China (Fig. 98a). Meanwhile, the Qinghai-Tibet Plateau is usually regarded as a cold source. A strong cold high-pressure system is formed in the lower layer of the plateau, accompanied by an anti-cyclonic circulation (Fig. 8a). Meanwhile, the northeastern China is under the steering influence of the high-pressure ridgethe northwest air flows at the rear of the East Asian major trough, with . A transversal troughthe its trough axis appearing along the eastern coastline of China. covers the YRD region, and its axis orienting from the northeastern sea areas to southwest inland areas. Affected by the strong northerlwesty winds coming from the east wind from the Yellow SeaNorthnorthern China, the polluted northwest air masses from BTH are easily transported to YRDflows. At the higher layer of 500 hPa (Fig. 98b), the geopotential height field

~~and wind field~~circulation structure pattern are similar to those for ~~–of~~ Pattern 1. A trough appears in the upper atmosphere, resulting in relatively strong west-northwest flows. The dense isopleths indicate large geopotential height gradient and strong downward flows. While at the surface layer (Fig. 9~~8~~c), the strong northerly wind is also evident, and YRD is located at the bottom of a high-pressure system centered in the remote Mongolian region. ~~–in the north of transversal trough are slowed down.~~ The above discussion is further proved by the results from back trajectory calculations. As suggested in Fig. ~~8e~~9~~8~~e, most air masses in clusters are from the Loess Plateau, with the percentage of 31%. The transport path of this cluster is relatively short, which might be attributed to the ~~weakened~~ strong anti-cyclonic circulation~~northwest wind~~. Due to the strong northerly wind~~For this reason~~, t~~T~~he long-range transport of air masses from remote Mongolia and northern~~north~~ China ~~also~~ accounts for 22% and 18% of all trajectories, respectively. Besides, the local transport of air masses from the southeast coastal area in YRD accounts for 26%~~, which is associated with the northeast air flows~~. The marine air masses cluster originates from western Pacific via the Yellow Sea accounts for 4%. ~~They both bring the clean marine air masses to YRD, which is somewhat beneficial to the mitigation of particle pollution in YRD.~~? For the vertical structure (Fig. ~~8b~~9~~8~~d), the distribution of vertical ~~velocit~~flow field~~y below the altitude of 300 hPa~~ is similar to that of Pattern 1, whereas the vertical wind is slightly ~~slower~~ stronger for the weather systems in Pattern 3. ~~Unde~~Due to~~r~~ the ~~steering~~ influence of the high-pressure system, it is observed that ~~The~~ evident downward air flows dominate in the north of around 28°N (including YRD) below the altitude of 300 hPa. The largest descending velocity (~9×10^{-2} Pa s^{-1}) also appears at the altitude of 500 hPa, covering the latitude of 35-40°N.~~Thus, influenced by the downdrafts in higher latitudes and horizontal northeast air flows, more clean marine air masses may be transported to YRD.~~ ~~Due to the fact that YRD is under the steering influence of the high-pressure system, downward motion dominates above YRD as well, the same to that of Pattern 1.~~ However, in ~~de~~spite of –the higher surface pressure (Figs. 6i and 9~~8~~c) and stronger downward motion (Fig. 9~~8~~d), the surface wind is much stronger for Pattern 3 as well (~~as displayed in~~ Figs. 6g, 9~~8~~a and 9~~8~~c), which alleviat~~ing~~es the problems of air pollution ~~resulting in much slighter air pollution~~ over YRD compared to~~than that of~~ Pattern 1. In all, under the weather situation of –Pattern 3, the strong northwest~~erly~~ wind in the front of the high-pressure system usually lead to the transport of polluted air masses from BTH to YRD~~–may cause particle pollution in YRD when the north~~

~~polluted air masses are transported in, but~~. Nevertheless, the strong surface wind is conducive to the ~~diffusion and dilution~~mitigation of pollutants ~~plays a significant role in the level of air pollution over YRD~~, which plays a significant role in the level of air pollution over YRD~~is it is also conducive to the diffusion~~ and dilution ~~of pollutants because of the clean marine air masses.~~.

Pattern 3

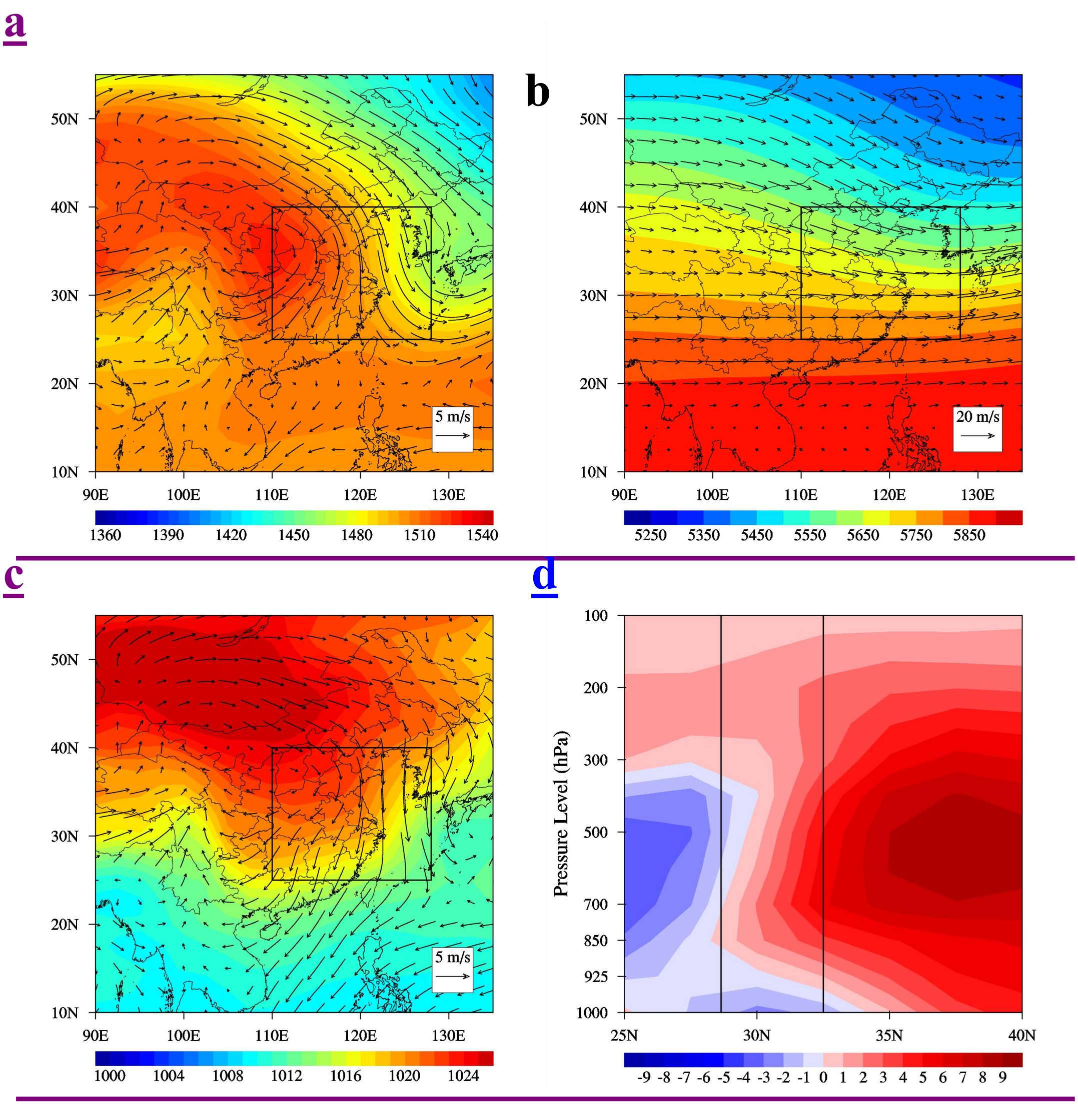

e

fe

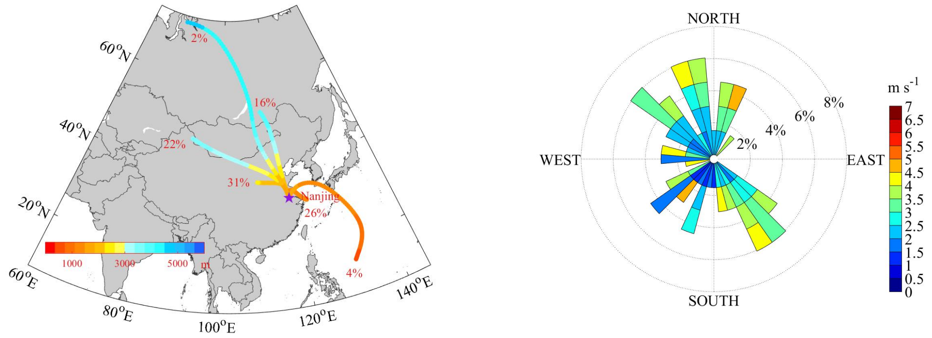

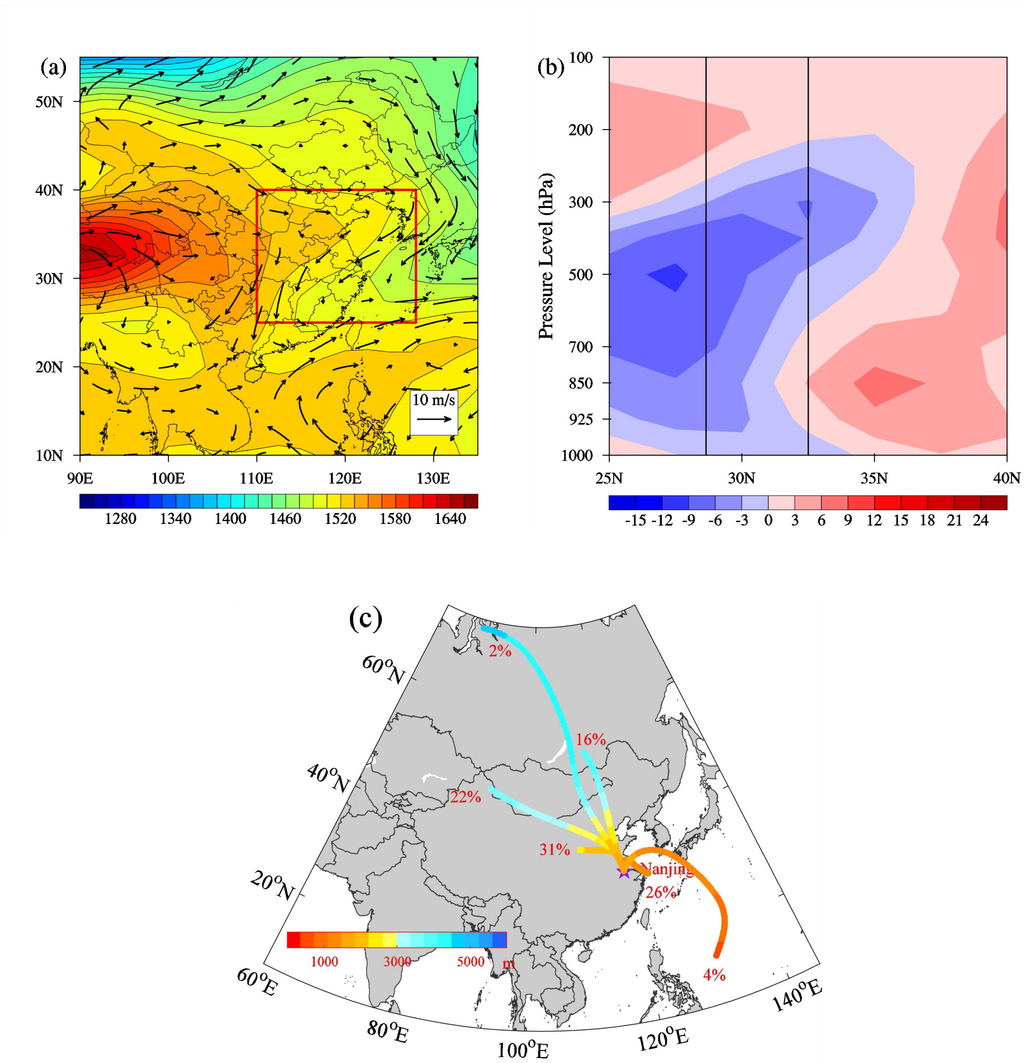

Figure 9~~8~~. As in Fig. 7~~6~~ but for ~~transversal trough pattern (~~Pattern 3~~)~~.

With respect to Pattern 4, on both~~ the~~ surface and 850 hPa level, the study domain is ~~totally~~ under the control of a high-pressure system ~~as well~~ (Figs. 10~~9~~a and 10~~9~~c). The center of the high-pressure system is located on the Sea of Japan, while a cyclonic circulation occurs over the Philippine Sea. The anti-cyclonic circulation prevails over YRD and horizontally brings the clean marine air masses to the land. Meanwhile, the sparse isopleths represent ~~ing~~ small~~weak~~ geopotential height gradient in the middle troposphere, accompanied by much~~rather~~ weaker west wind compared to ~~that of~~ other patterns (Fig. 10~~9~~b). Accordingly, influenced by the high-pressure system, the downward atmospheric motion dominates in the vertical direction obviously (Fig. ~~9b~~10~~9~~d). The strongest downward motion (~6×10^{-2} Pa s^{-1}) appears between the altitude of 300 hPa and 500 hPa and at the latitude of 35°N. The weak updrafts near the surface may be related to the regional thermodynamic circulation. As shown in Fig. 10~~9~~e~~e~~, the cluster with the largest frequency of 32% stands for the local transport of air masses from southern adjacent areas in YRD. Additionally, the air masses from ~~North~~northern China via Bohai Bay (25%), from Japan via the Yellow Sea (23%), and from the Philippines via the East China Sea (5%) are also representative. These clusters passing over the ocean areas totally account for more than 50% of all trajectories. Therefore, under this weather situation, it is confirmed that the dilution effects of clean marine air masses play great roles in the particle pollution over YRD.

Pattern 5 features one of the most complex circulation situation at 850 hPa (Fig. 11a). YRD is located between the bottom of the northern high-pressure system and the top of the southern weak low-pressure system. For this reason, the horizontal strong east wind prevails and easily carries clean marine air masses from the East China Sea to YRD. The corresponding circulation structure at the surface layer is similar to that at 850 hPa layer (Fig. 11c), while the east-northeast flows prevails over the study domain. In the upper troposphere, a ridge appears in the east due to the tropical cyclonic system, thus leading to the west-southwest flows over the region. Owing to the above-mentioned two opposite pressure systems (Fig. 11a), strong upward air flows are dominant in the south of the latitude of 35 °N, while the downward motion is obvious in the north (Fig. 11d). The largest ascending velocity (~ -9×10^{-2} Pa s^{-1}) appears in the latitude of around 27.5 °N in the upper troposphere. The strong upward motion facilitates the diffusion and removal of the accumulated pollutants from the surface layer. According to Fig. 11e, the cluster with the largest frequency of 45% consists of the wet air parcels from Japan via the Yellow Sea. Only 5% of the trajectories originates from the Philippines and pass over the East China Sea. On the whole, under the weather situation for Pattern 5, the transport of clean marine air masses and favorable diffusion condition contribute to the good air quality over YRD.

Pattern 4

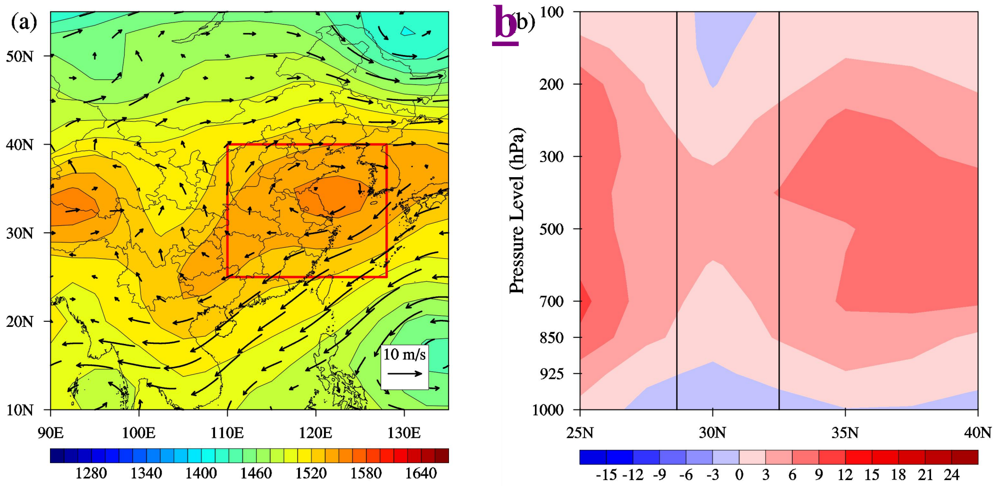

c

d

a

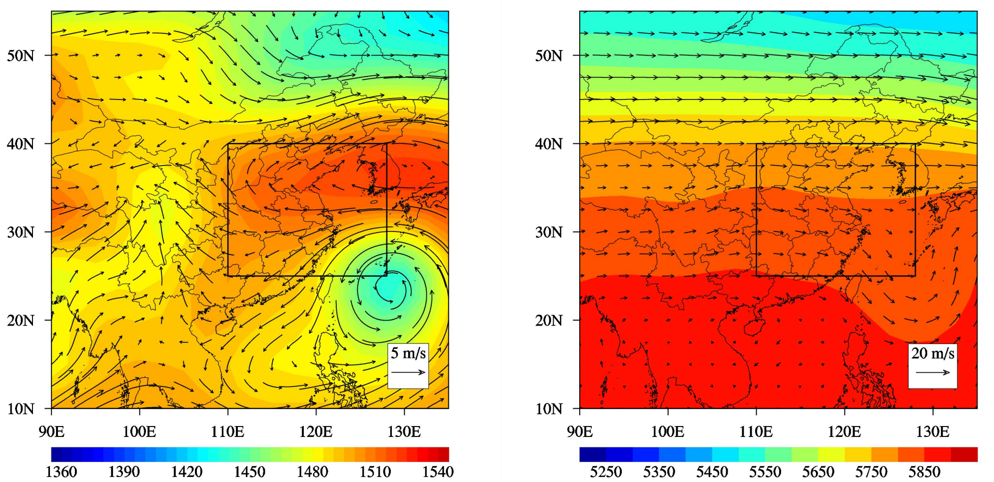

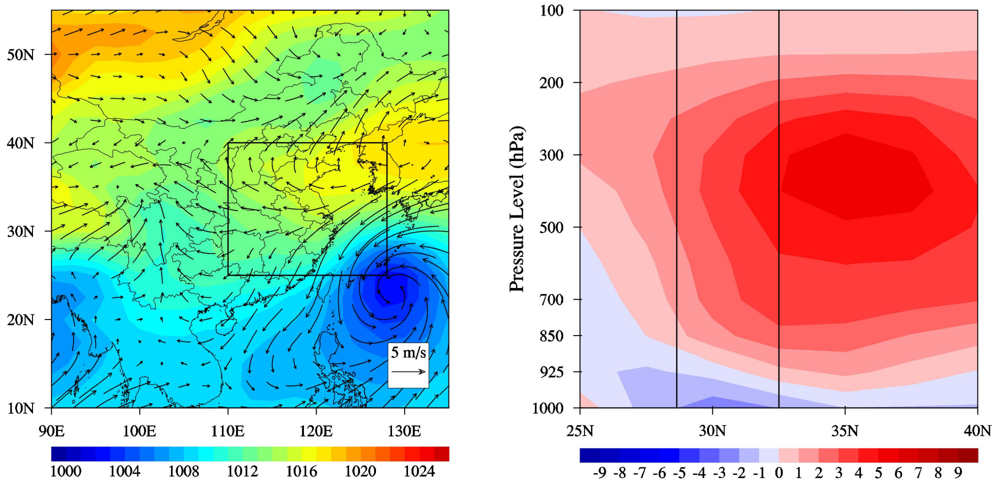

e

f

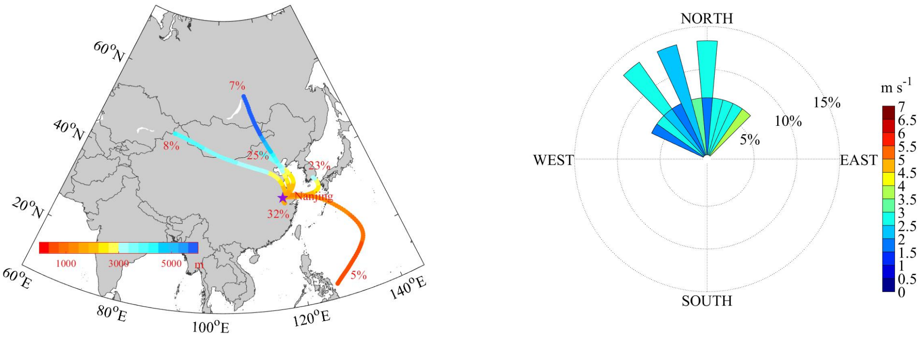

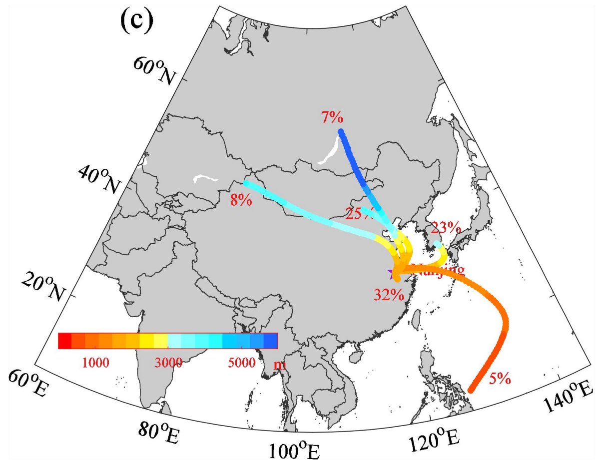

Figure 109. As in Fig. 76 but for high-pressure controlled pattern (Pattern 4).

Finally, Pattern 5 features one of the most complex circulation situation at 850 hPa level (Fig. 110a). At 850 hPa, The northeastern China is controlled by a cold eddy system. The central China is impacted by a high-pressure ridge. A strong tropical low-pressure system is located around Luzon. At this time, YRD is located in between the south bottom of the northerncentral high-pressure system and the north top of the southern strong weaktropical low-pressure system. For this reason, tThe horizontal strong southeast wind prevails and easily carries clean marine air masses from the East China Sea to YRD. The corresponding circulation structure at the surface layer is similar to that at 850 hPa layer (Fig. 119c), andwhile the east-northeast flows prevails over the study domain. In the upper troposphere, a shallow ridge appears in the east due to the tropical cyclonic system, thus causingleading to the west-southwest flows over the region. Owing to the above-mentioned two opposite pressure systems (Fig. 11a), strong At the same time, upward air flows are dominant in the south of the latitude of 35 °N, while the downward motion is obvious in the north and comparatively weak (>-3×10^{-2} Pa s^{-1}) in the lower troposphere (Fig. 110db). The largest ascending velocity (~ -9×10^{-2} Pa s^{-1}) appears in the latitude of around 27.5 °N in the upper troposphere. The strong upward motion facilitates the diffusion and removal of the accumulated pollutants from the surface layer. According to Fig. 110ec, the cluster with the largest frequency of 45% consists of the wet air parcels from Japan via the Yellow Sea. Only 5% of the trajectories originates from the Philippines and pass over the East China Sea. On the whole, under the weather situationsystems in for Pattern 45, and 5 are both mainly influenced by the transport of clean marine air masses and favorable diffusion condition contribute to the good air quality over YRD., and largely beneficial to the diffusion of the pollutants.

Pattern 5

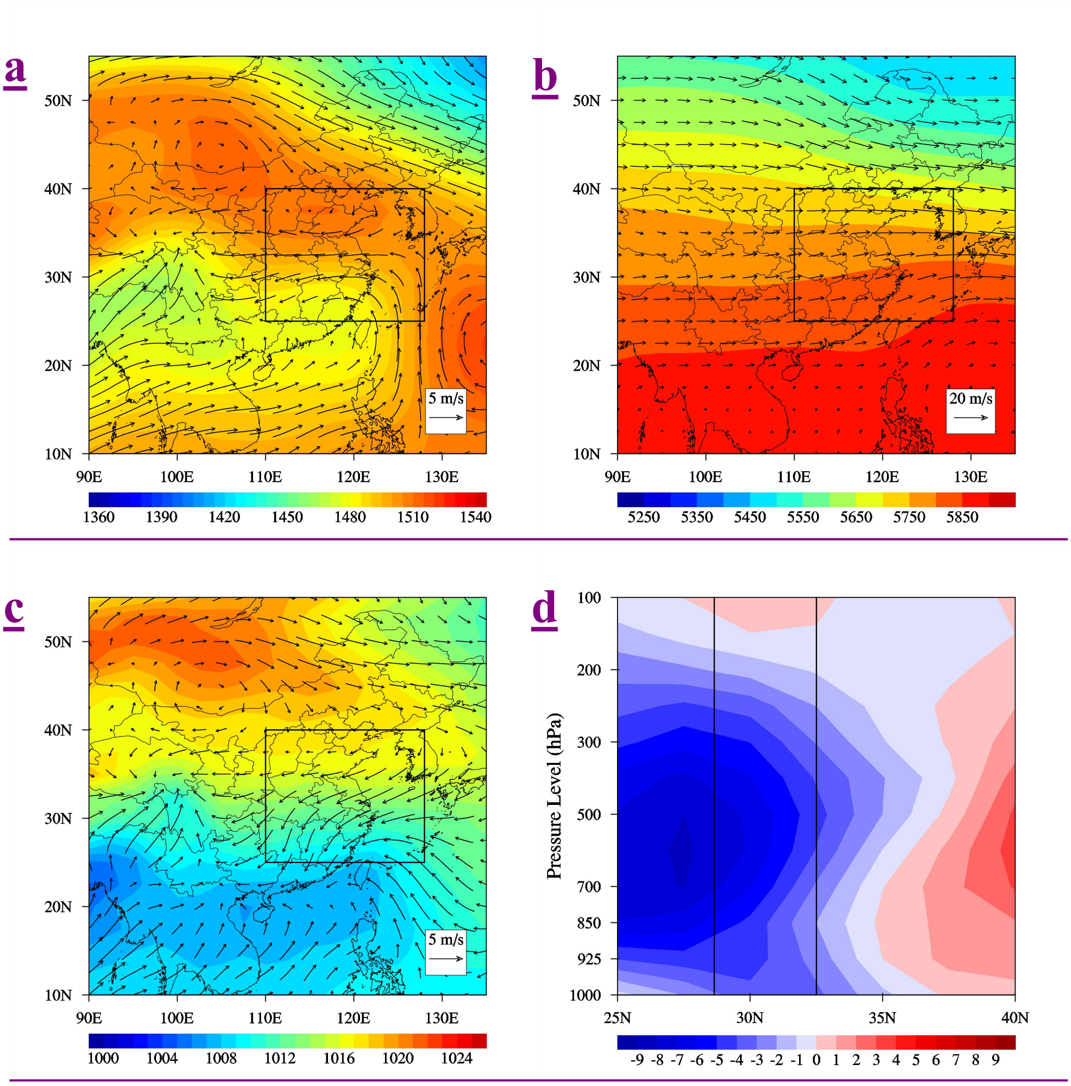

e **f**

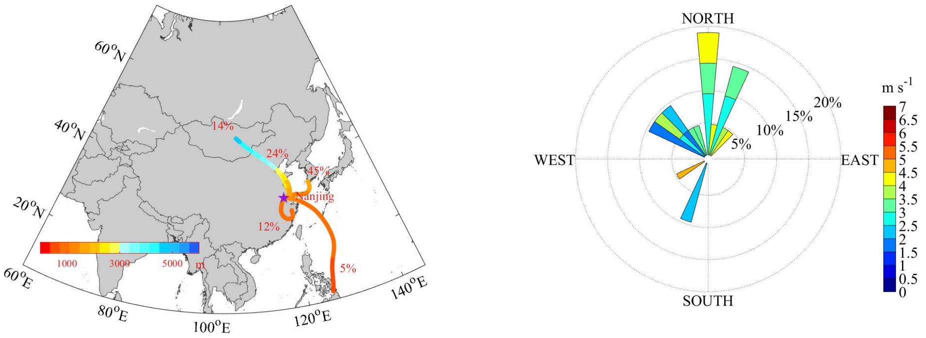

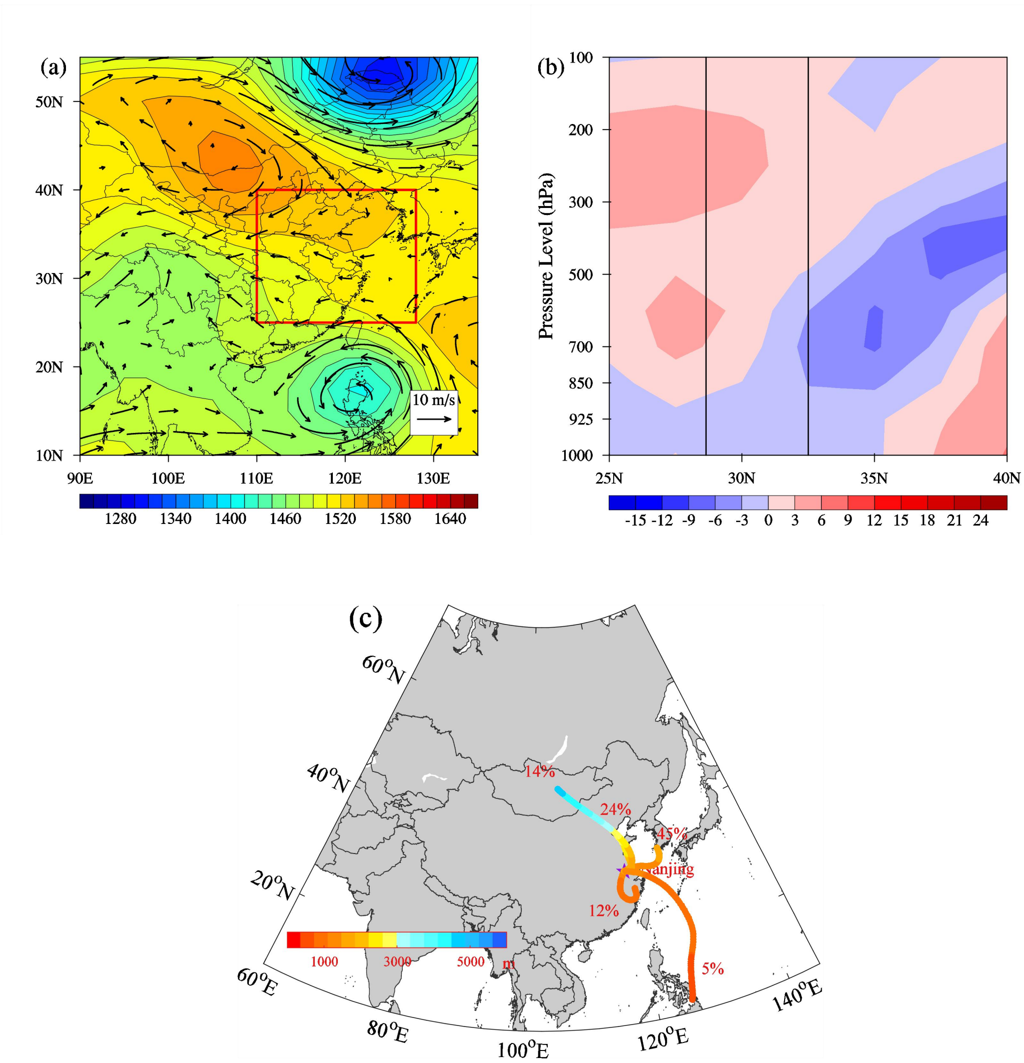

Figure 11~~0~~. As in Fig. 7~~6~~ but for ~~northeast cold vortex pattern (~~ Pattern 5~~)~~.

To sum up, the weather situation for Pattern 1-5 are more or less affected by a high-pressure system. However, the relative positions of the study domain to the anti-cyclonic circulation system are quite significant to the air quality of YRD. The differences determine the wind speed and wind direction, and the latter further determine whether YRD is influenced by the clean marine air masses. For Patten 1 and Pattern 3, –YRD are both impacted by the northwest air flows at the rear of the East Asian major trough, which transport abundant air pollutants from ~~BTH~~other regions (such as BTH and SCB) to YRD and cause ~~heavy~~severe particle pollution (high AOD value as well) in YRD. In contrast, the weaker local surface wind for Pattern 1 is extremely conducive to the local accumulation of pollutants.~~under the influence of weather system of Pattern 1, the particle pollution in YRD is largely affected by the transport of pollutants from the south and north inland regions of China. This weather situation is extremely not favorable to the diffusion of air pollutants,~~ For this reason, Pattern 1 is 'the most polluted pattern', and responsible for the most large-scale particle pollution episodes over YRD. Owning to the stronger surface wind, Pattern 3 is 'the second most polluted pattern'. As for Pattern 2~~ and Pattern 3~~, the polluted air masses mainly travel from southern inland areas, and synchronously meet with the clean marine air masses in YRD. To some extent~~.~~, ~~T~~this weather situation is helpful to the mitigation of particle pollution in YRD~~ to some extent, and this pattern can also be regarded as 'the polluted pattern'~~. With respect to Pattern 4 and Pattern ~~, and Pattern ~~5, YRD is directly influenced by the air flows traveling from the ocean areas, and has little chance of being polluted. Thus, Pattern 4 and Pattern -5 can be identified as 'the clean pattern'. It suggests that the clean marine air masses have great dilution impacts on the particle pollution over YRD.

4. Conclusions

In this study, the spatial and temporal distributions of particle pollution in 16 YRD cities are characterized from December 2013 to November 2014. Meanwhile, the synoptic weather classification is conducted to identify the dominant weather patterns over YRD. The meteorological fields and 72-h backward trajectories are analyzed to reveal the potential impacts of weather systems on the regional severe particle pollution.

From the observational records, it is shown that the concentrations of $PM_{2.5}$ and PM_{10} decrease progressively along the northwest-southeast direction. The pollution levels are comparatively high in the Jiangsu Province and much lower in the southeast coastal area (Ningbo, Taizhou and Zhoushan). The highest particle concentration occurs in Nanjing, with the concentrations of $PM_{2.5}$ and PM_{10} being 79 ~~μg·m^{-3}~~ and 130 μg·m^{-3}, respectively. The $PM_{2.5}/PM_{10}$ ratios are high in YRD, especially in winter. The seasonal mean $PM_{2.5}/PM_{10}$ ratios are 0.73

(winter), 0.61 (spring), 0.67 (summer) and 0.63 (autumn), respectively. These high $PM_{2.5}/PM_{10}$ ratios suggest that the $PM_{2.5}$ fraction is extraordinarily dominant in the PM_{10} mass in YRD. Besides, high AOD is also found in YRD, with the annual mean value of 0.71±0.57 and ~~thea~~the maximum ~~of~~ seasonal mean ~~AOD~~value ~~occurring~~ of 0.98±0.83 in summer ~~(0.98±0.83)~~. The diurnal cycles of particle concentrations in most cities follow the same pattern, with a morning peak from 8:00 to 12:00. There are three peaks in seasonal variations (December, March, and May or June). The wintertime peak is closely related to the enhanced emissions in the heating season and poor meteorological conditions. Moreover, YRD ~~suffered~~ suffers from the $PM_{2.5}$ (PM_{10}) pollution in nearly 28.0% (13.1%) days of the year. The continuous large-scale regional $PM_{2.5}$ pollution episodes occur much more frequently than the PM_{10} pollution episodes.

Based on the sums-of-squares technique, five typical synoptic weather patterns are objectively ~~classified~~ identified in YRD, including the East Asia major trough rear pattern (Pattern 1, occurs 47.7% of all days), the depression inverted trough pattern (Pattern 2, 20.0%), the transversal trough pattern (Pattern 3, 18.1%), the high-pressure controlled pattern (Pattern 4, 4.1%) and the northeast cold vortex pattern (Pattern 5, 5.8%). Each pattern differs from the other in respect to the relative position of YRD to the main synoptic system (anti-cyclonic circulation system). The difference determines the ~~The weather conditions (~~wind speed and wind direction, which play an important role in the air quality level of YRD. Especially, the wind direction is closely associated with the situation whether YRD is influenced by clean marine air masses.~~) play an important role in the air quality level of YRD.~~ Under the patterns when YRD is at the rear of the East Asian major trough at 850 hPa (Pattern 1 and Pattern 3), the strong northwest wind can easily transport air pollutants from other polluted areas~~BTH~~ to YRD, leading to serious particle pollution in YRD. Due to the high-pressure system, significant vertical downward motion dominates above YRD, resulting in relatively stable weather conditions at the surface. With ~~fair~~ weak local surface wind, the worst polluted weather pattern (Pattern 1) features the highest regional mean PM_{10} (116.5±66.9 $\mu g \cdot m^{-3}$), $PM_{2.5}$ (75.9±49.9 $\mu g \cdot m^{-3}$) and high AOD (0.74). Pattern 1 is also responsible for~~For the When YRD is located at the rear of the East Asian major trough at 850 hPa (Pattern 1), it is primarily strikingly influenced by the polluted air masses traveling from southern and northern inland regions. Significant downward motion dominates above YRD, resulting in stable weather conditions at the surface (high pressure, the weakest wind, low~~

humidity and temperature). The analysis of meteorological field also indicates that the strong horizontal northwest wind hinders the vertical outward transport of pollutants. Thus, this weather situation is extremely unfavorable for the diffusion of the pollutants, leading to the highest PM_{10} (116.5±66.9 μg·m^{-3}), $PM_{2.5}$ (75.9±49.9 μg·m^{-3}) and high AOD (0.74). For this reason, Pattern 1 can be regarded as 'the most polluted pattern', and responsible for the most large-scale and contributes most to the occurrence of large-scale regional $PM_{2.5}$ (70.4%) and PM_{10} (78.3%) pollution episodes in YRD. As for Pattern 3, the the strong northerly wind usually leads to the transport of polluted air masses from BTH to YRD, while the high-pressure system causes dominant downward motion over the region. hHighest AOD (0.81) is observed in YRD under this pattern. However, the strongest surface wind is conducive to the mitigation of pollution,. Thus, Pattern 3 is supposed to be "the polluted pattern", withresulting in –the second highest PM_{10} (86.9±49.5 μg·m^{-3}) and $PM_{2.5}$ (59.1±37.3μg·m^{-3}). –the —In contrast, under the weather system of other synoptic patterns (, especially Pattern 4 and Pattern 5), the clean marine air masses via east-southeast wind play a crucial roles in the mitigation of pollution over YRD. Under these weather patternTherefore,s, YRD has much less chance of being polluted.

In summary, the above results reveal that the particle pollution in China is no longer a thorny issue over a single city, but over a regional scale. This study can enhance the understanding of features of particle pollution in East Asia. Meanwhile, it wasis also confirmed that large-scale synoptic weather systems have great impacts on regional particle pollution episodes. Therefore, the establishment of the potential links between different levels of particle pollution and predominant synoptic patterns can provide an insightful view on formulating pollution control and mitigation strategies.

5. Data availability

The air quality monitoring records are available at http://106.37.208.233:20035. The meteorological data are available at http://www.nmc.cn. The MODIS/AOD records are available at https://ladsweb.nascom.nasa.gov/search/index.html. The NCEP reanalysis data are available at https://www.esrl.noaa.gov/psd/data/gridded/data.ncep.reanalysis2.pressure.html and http://ready.arl.noaa.gov/archives.php.

Acknowledgments

This work was supported by the National Natural Science Foundation of China (41475122, 91544230, 91537102, 41621005), the National Key Research and Development Program of China (2016YFC0203303, 2016YFC0208504, 2016YFA0602104), and open research fund of Chongqing Meteorological Bureau (KFJJ-201607). The authors would like to thank the anonymous reviewers for their constructive and precious comments on this manuscript.

References

Barry, R. G., Kiladis, G., and Bradley, R. S.: Synoptic climatology of the Western United States in relation to climatic fluctuations during the twentieth century, International Journal of Climatology, 1, 97-113, 1981.

Brook, R. D., Rajagopalan, S., Pope, C. A., Brook, J. R., Bhatnagar, A., Diez-Roux, A. V., Holguin, F., Hong, Y., Luepker, R. V., and Mittleman, M. A.: Particulate matter air pollution and cardiovascular disease, Circulation, 121, 2331-2378, 2010.

Buchanan, C., Beverland, I. J., and Heal, M. R.: The influence of weather-type and long-range transport on airborne particle concentrations in Edinburgh, UK, Atmospheric Environment, 36, 5343-5354, 2002.

Chan, C. K., and Yao, X.: Air pollution in mega cities in China, Atmospheric environment, 42, 1-42, 2008.

Chen, M. L., Mao, I. F., and Lin, I. K.: The PM 2.5 and PM 10 particles in urban areas of Taiwan, Science of the Total Environment, 226, 227-235, 1999.

Cheng, Z., Jiang, J., Fajardo, O., Wang, S., and Hao, J.: Characteristics and health impacts of particulate matter pollution in China (2001–2011), Atmospheric Environment, 65, 186-194, 2013.

Chuang, M.-T., Chiang, P.-C., Chan, C.-C., Wang, C.-F., Chang, E., and Lee, C.-T.: The effects of synoptical weather pattern and complex terrain on the formation of aerosol events in the Greater Taipei area, Science of the total environment, 399, 128-146, 2008.

Chu, D., Kaufman, Y., Ichoku, C., Remer, L., Tanré, D., and Holben, B.: Validation of MODIS aerosol optical depth retrieval over land, Geophysical research letters, 29, 2002.

Chu, D. A., Kaufman, Y., Zibordi, G., Chern, J., Mao, J., Li, C., and Holben, B.: Global monitoring of air pollution over land from the Earth Observing System ‐ Terra Moderate Resolution Imaging Spectroradiometer (MODIS), Journal of Geophysical Research: Atmospheres, 108, 2003.

Chu, D., Remer, L., Kaufman, Y., Schmid, B., Redemann, J., Knobelspiesse, K., Chern, J. D., Livingston, J., Russell, P., and Xiong, X.: Evaluation of aerosol properties over ocean from Moderate Resolution Imaging Spectroradiometer (MODIS) during ACE ‐ Asia, Journal of Geophysical Research: Atmospheres, 110, 2005.

Deng, J. J., Wang, T. J., Jiang, Z. Q., Xie, M., Zhang, R. J., Huang, X. X., Zhu, J. L.: Characterization of visibility and its affecting factors over Nanjing, China. Atmos Res, 101, 681-691, 2011.

Draxler, R., and Rolph, G.: HYSPLIT (HYbrid Single-Particle Lagrangian Integrated Trajectory),

NOAA Air Resources Laboratory, College Park, MD, Model access via NOAA ARL READY Website, 2013.
El-Kadi, A. K. A., and Smithson, P. A.: Atmospheric classifications and synoptic climatology, Progress in Physical Geography, 16, 432-455, 1992.
Feng, J., Hu, J., Xu, B., Hu, X., Sun, P., Han, W., Gu, Z., Yu, X., and Wu, M.: Characteristics and seasonal variation of organic matter in PM 2.5 at a regional background site of the Yangtze River Delta region, China, Atmospheric Environment, 123, 288-297, 2015.
Flocas, H., Kelessis, A., Helmis, C., Petrakakis, M., Zoumakis, M., and Pappas, K.: Synoptic and local scale atmospheric circulation associated with air pollution episodes in an urban Mediterranean area, Theoretical and Applied Climatology, 95, 265-277, 2009.
Fu, Q., Zhuang, G., Wang, J., Xu, C., Huang, K., Li, J., Hou, B., Lu, T., and Streets, D. G.: Mechanism of formation of the heaviest pollution episode ever recorded in the Yangtze River Delta, China, Atmospheric Environment, 42, 2023-2036, 2008.
Fu, Q., Zhuang, G., Li, J., Huang, K., Wang, Q., Zhang, R., Fu, J., Lu, T., Chen, M., and Wang, Q.: Source, long-range transport, and characteristics of a heavy dust pollution event in Shanghai, Journal of Geophysical Research Atmospheres, 115, 6128-6128, 2010.
Fu, X., Wang, S. X., Cheng, Z., Xing, J., Zhao, B., Wang, J. D., and Hao, J. M.: Source, transport and impacts of a heavy dust event in the Yangtze River Delta, China, in 2011, Atmospheric Chemistry & Physics, 14, 1239-1254, 2014.
Green, M. C., Chen, L. A., DuBois, D. W., and Molenar, J. V.: Fine particulate matter and visibility in the Lake Tahoe Basin: Chemical characterization, trends, and source apportionment, Journal of the Air & Waste Management Association, 62, 953-965, 2012.
Grundstrom, M., Tang, L., Hallquist, M., Nguyen, H., Chen, D., and Pleijel, H.: Influence of atmospheric circulation patterns on urban air quality during the winter, Atmospheric Pollution Research, 6, 278-285, 2015.
He, K., Yang, F., Ma, Y., Zhang, Q., Yao, X., Chan, C. K., Cadle, S., Chan, T., and Mulawa, P.: The characteristics of PM 2.5 in Beijing, China, Atmospheric Environment, 35, 4959-4970, 2001.
Ho, K. F., Lee, S. C., Chan, C. K., Yu, J. C., Chow, J. C., and Yao, X. H.: Characterization of chemical species in PM 2.5 and PM 10 aerosols in Hong Kong, Atmospheric Environment, 37, 31-39, 2003.
Hsu, N., Jeong, M. J., Bettenhausen, C., Sayer, A., Hansell, R., Seftor, C., Huang, J., and Tsay, S. C.: Enhanced Deep Blue aerosol retrieval algorithm: The second generation, Journal of Geophysical Research: Atmospheres, 118, 9296-9315, 2013.
Huang, K., Zhuang, G., Lin, Y., Fu, J. S., Wang, Q., Liu, T., Zhang, R., Jiang, Y., Deng, C., Fu, Q., Hsu, N. C., and Cao, B.: Typical types and formation mechanisms of haze in an Eastern Asia megacity, Shanghai, Atmos. Chem. Phys., 12, 105-124, 2012.
Huang, R. J., Zhang, Y., Bozzetti, C., Ho, K. F., Cao, J. J., Han, Y., Daellenbach, K. R., Slowik, J. G., Platt, S. M., and Canonaco, F.: High secondary aerosol contribution to particulate pollution during haze events in China, Nature, 514, 218-222, 2014.
Huang, X., Wang, T., Talbot, R., Xie, M., Mao, H., Li, S., Zhuang, B., Yang, X., Fu, C., and Zhu, J.: Temporal characteristics of atmospheric CO2 in urban Nanjing, China, Atmospheric Research, 153, 437-450, 2015.
Ji, D., Wang, Y., Wang, L., Chen, L., Hu, B., Tang, G., Xin, J., Song, T., Wen, T., and Sun, Y.:

Analysis of heavy pollution episodes in selected cities of northern China, Atmospheric Environment, 50, 338–348, 2012.

Kanamitsu, M., Ebisuzaki, W., Woollen, J., Yang, S., Hnilo, J., Fiorino, M., and Potter, G.: NCEP-DOE AMIP-II reanalysis (R-2). Bulletin of the American Meteorological Society, Doibams, 2002.

Kang, H., Zhu, B., Su, J., Wang, H., Zhang, Q., and Wang, F.: Analysis of a long-lasting haze episode in Nanjing, China, Atmospheric Research, s 120–121, 78–87, 2013.

Kaufman, Y. J., Tanré, D., and Boucher, O.: A satellite view of aerosols in the climate system, Nature, 419, 215-223, 2002.

Kim, S.-W., Yoon, S.-C., Kim, J., and Kim, S.-Y.: Seasonal and monthly variations of columnar aerosol optical properties over east Asia determined from multi-year MODIS, LIDAR, and AERONET Sun/sky radiometer measurements, Atmospheric Environment, 41, 1634-1651, 2007.

Kirchhofer, W,: Classification of European 500mb patterns, Arbeitsbericht der Schweizerischen Meteorologischen Zentralanstalt, Geneva, 43p, 1973.

Kappos, A. D., Bruckmann, P., Eikmann, T., Englert, N., Heinrich, U., Höppe, P., Koch, E., Krause, G. H., Kreyling, W. G., and Rauchfuss, K.: Health effects of particles in ambient air, International Journal of Hygiene & Environmental Health, 207, 399-407, 2004.

Kong, X., He, W., Qin, N., He, Q., Yang, B., Ouyang, H., Wang, Q., and Xu, F.: Comparison of transport pathways and potential sources of PM 10 in two cities around a large Chinese lake using the modified trajectory analysis, Atmospheric Research, 122, 284-297, 2013.

Kurokawa, J., Ohara, T., Morikawa, T., and Hanayama, S.: Emissions of air pollutants and greenhouse gases over Asian regions during 2000–2008: Regional Emission inventory in ASia (REAS) version 2, Atmospheric Chemistry & Physics, 13, 10049-10123, 2013.

Li, L., Chen, C. H., Fu, J. S., Huang, C., Streets, D. G., Huang, H. Y., Zhang, G. F., Wang, Y. J., Jang, C. J., and Wang, H. L.: Air quality and emissions in the Yangtze River Delta, China, Atmospheric Chemistry & Physics, 10, 1621-1639, 2011.

Li, Q., Zhang, R., and Wang, Y.: Interannual variation of the wintertime fog–haze days across central and eastern China and its relation with East Asian winter monsoon, International Journal of Climatology, 36, 346-354, 2016.

Mcgowan, H., and Clark, A.: Identification of dust transport pathways from Lake Eyre, Australia using Hysplit, Atmospheric Environment, 42, 6915-6925, 2008.

McGregor, G., and Bamzelis, D.: Synoptic typing and its application to the investigation of weather air pollution relationships, Birmingham, United Kingdom, Theoretical and Applied Climatology, 51, 223-236, 1995.

Malm, W. C., Sisler, J. F., Huffman, D., Eldred, R. A., and Cahill, T. A.: Spatial and seasonal trends in particle concentration and optical extinction in the United States, Journal of Geophysical Research: Atmospheres, 99, 1347-1370, 1994.

Ming, L., Ling, J., Li, J., Fu, P., Yang, W., Di, L., Gan, Z., Wang, Z., and Li, X.: PM 2.5 in the Yangtze River Delta, China: Chemical compositions, seasonal variations, and regional pollution events, Environmental Pollution, 223, 200, 2017.

Niu, F., Li, Z., Li, C., Lee, K. H., and Wang, M.: Increase of wintertime fog in China: Potential impacts of weakening of the Eastern Asian monsoon circulation and increasing aerosol loading, Journal of Geophysical Research: Atmospheres, 115, 2010.

Oanh N T K, Leelasakultum K.: Analysis of meteorology and emission in haze episode prevalence over mountain-bounded region for early warning, Science of the Total Environment, 409(11), 2261-2271, 2011.

Putaud, J.-P., Raes, F., Van Dingenen, R., Brüggemann, E., Facchini, M.-C., Decesari, S., Fuzzi, S., Gehrig, R., Hüglin, C., and Laj, P.: A European aerosol phenomenology—2: chemical characteristics of particulate matter at kerbside, urban, rural and background sites in Europe, Atmospheric environment, 38, 2579-2595, 2004.

Remer, L. A., Tanre, D., Kaufman, Y. J., Ichoku, C., Mattoo, S., Levy, R., Chu, D. A., Holben, B., Dubovik, O., and Smirnov, A.: Validation of MODIS aerosol retrieval over ocean, Geophysical research letters, 29, 2002.

Remer, L. A., Kaufman, Y., Tanré, D., Mattoo, S., Chu, D., Martins, J. V., Li, R.-R., Ichoku, C., Levy, R., and Kleidman, R.: The MODIS aerosol algorithm, products, and validation, Journal of the atmospheric sciences, 62, 947-973, 2005.

Rolph, G.: Real-time Environmental Applications and Display sYstem (READY) Website. Silver Spring, MD: NOAA Air Resources Laboratory, ready. arl. noaa. gov, 2013.

Russo, A., Trigo, R. M., Martins, H., and Mendes, M. T.: NO_2, PM_{10} and O_3 urban concentrations and its association with circulation weather types in Portugal, Atmospheric Environment, 89, 768-785, 2014.

Santurtún, A., González-Hidalgo, J. C., Sanchez-Lorenzo, A., and Zarrabeitia, M. T.: Surface ozone concentration trends and its relationship with weather types in Spain (2001–2010), Atmospheric Environment, 101, 10-22, 2015.

~~Shan, W., Yin, Y., Lu, H., and Liang, S.: A meteorological analysis of ozone episodes using HYSPLIT model and surface data, Atmospheric Research, 93, 767-776, 2009.~~

Singh, A., and Dey, S.: Influence of aerosol composition on visibility in megacity Delhi, Atmospheric Environment, 62, 367-373, 2012.

Shu, L., Xie, M., Wang, T., Chen, P., Han, Y., Li, S., Zhuang, B., Li, M., and Gao, D.: Integrated studies of a regional ozone pollution synthetically affected by subtropical high and typhoon system in the Yangtze River Delta region, China, 1-32, 2016.

State Environmental Protection Administration of China, 2006. China National Environmental Protection Standard: Automated Methods for Ambient Air Quality Monitoring. China Environmental Science Press, Beijing.

Stein, A. F., Draxler, R. R., Rolph, G. D., Stunder, B. J. B., Cohen, M. D., and Ngan, F.: NOAA's HYSPLIT Atmospheric Transport and Dispersion Modeling System, Bulletin of the American Meteorological Society, 96, 150504130527006, 2016.

Wang, Y., Stein, A. F., Draxler, R. R., Rosa, J. D. D. L., and Zhang, X.: Global sand and dust storms in 2008: Observation and HYSPLIT model verification, Atmospheric Environment, 45, 6368-6381, 2011.

Wang, J., Hu, Z., Chen, Y., Chen, Z., and Xu, S.: Contamination characteristics and possible sources of PM10 and PM2.5 in different functional areas of Shanghai, China, Atmospheric Environment, 68, 221-229, 2013.

Wang, Y., Li, L., Chen, C., Huang, C., Huang, H., Feng, J., Wang, S., Wang, H., Zhang, G., and Zhou, M.: Source apportionment of fine particulate matter during autumn haze episodes in Shanghai, China, Journal of Geophysical Research Atmospheres, 119, 1903–1914, 2014.

Wang, M., Cao, C., Li, G., and Singh, R. P.: Analysis of a severe prolonged regional haze episode in the Yangtze River Delta, China, Atmospheric Environment, 102, 112-121, 2015.

Xie, M., Zhu, K., Wang, T., Yang, H., Zhuang, B., Li, S., Li, M., Zhu, X., and Ouyang, Y.: Application of photochemical indicators to evaluate ozone nonlinear chemistry and pollution control countermeasure in China, Atmospheric Environment, 99, 466-473, 2014.

Xie, M., Liao, J., Wang, T., Zhu, K., Zhuang, B., Han, Y., Li, M., and Li, S.: Modeling of the anthropogenic heat flux and its effect on regional meteorology and air quality over the Yangtze River Delta region, China, Atmospheric Chemistry & Physics, 16, 6071-6089, 2016a.

Xie, M., Zhu, K., Wang, T., Chen, P., Han, Y., Li, S., Zhuang, B., and Shu, L.: Temporal characterization and regional contribution to O_3 and NO_x at an urban and a suburban site in Nanjing, China, Science of the Total Environment, 551, 533-545, 2016b.

Xie, M., Zhu, K., Wang, T., Feng, W., Li, M., Li, M., Han, Y., Li, S., Zhuang, B., and Shu, L.: Changes of regional meteorology induced by anthropogenic heat and their impacts on air quality in South China, Atmospheric Chemistry & Physics, 16, 15011-15031, 2016c.

Xie, M., Shu, L., Wang, T.-j., Liu, Q., Gao, D., Li, S., Zhuang, B.-l., Han, Y., Li, M.-m., and Chen, P.-l.: Natural emissions under future climate condition and their effects on surface ozone in the Yangtze River Delta region, China, Atmospheric Environment, 150, 162-180, 2017.

Xu, J. S., Xu, H. H., Xiao, H., Tong, L., Snape, C. E., Wang, C. J., and He, J.: Aerosol composition and sources during high and low pollution periods in Ningbo, China, Atmospheric Research, s 178–179, 559-569, 2016.

Yan, X. Y., Ohara, T., and Akimoto, H.: Bottom-up estimate of biomass burning in mainland China, Atmospheric Environment, 40, 5262-5273, 2006.

Yang, S., He, H., Lu, S., Chen, D., and Zhu, J.: Quantification of crop residue burning in the field and its influence on ambient air quality in Suqian, China, Atmospheric Environment, 42, 1961-1969, 2008.

Yarnal, B.: A procedure for the classification of synoptic weather maps from gridded atmospheric pressure surface data, Computers & Geosciences, 10, 397-410, 1984.

Young, D. E., Kim, H., Parworth, C., Zhou, S., Zhang, X., Cappa, C. D., Seco, R., Kim, S., Zhang, Q.: Influences of emission sources and meteorology on aerosol chemistry in a polluted urban environment: results from DISCOVER-AQ California, Atmospheric Chemistry and Physics, 16(8), 5427-5451, 2016.

Zhang, J. P., Zhu, T., Zhang, Q. H., Li, C. C., Shu, H. L., Ying, Y., Dai, Z. P., Wang, X., Liu, X. Y., and Liang, A. M.: The impact of circulation patterns on regional transport pathways and air quality over Beijing and its surroundings, Atmospheric Chemistry & Physics, 11, 33465-33509, 2012.

Zhang, Q., Quan, J., Tie, X., Li, X., Liu, Q., Gao, Y., and Zhao, D.: Effects of meteorology and secondary particle formation on visibility during heavy haze events in Beijing, China, Science of the Total Environment, 502C, 578-584, 2014.

Zhao, X. J., Zhao, P. S., Xu, J., and Meng, W.: Analysis of a winter regional haze event and its formation mechanism in the North China Plain, Atmospheric Chemistry & Physics, 13, 5685-5696, 2013.

Zheng, G., Duan, F., Su, H., Ma, Y., Cheng, Y., Zheng, B., Zhang, Q., Huang, T., Kimoto, T., and Chang, D.: Exploring the severe winter haze in Beijing: the impact of synoptic weather, regional transport and heterogeneous reactions, Atmospheric Chemistry and Physics, 15, 2969-2983, 2015a.

Zheng, X. Y., Fu, Y. F., Yang, Y. J., and Liu, G. S.: Impacts of atmospheric circulations on aerosol distributions in autumn over eastern China: observational evidences, Atmospheric Chemistry & Physics, 15, 3285-3325, 2015b.

Zhu, J., Wang, T., Deng, J., Jiang, A., and Liu, D.: An emission inventory of air pollutants from crop residue burning in Yangtze River Delta Region and its application in simulation of a heavy haze weather process, Acta Scientiae Circumstantiae, 32, 3045-3055, 2012.

Zhu, K., Xie, M., Wang, T., Cai, J., Li, S., and Feng, W.: A modeling study on the effect of urban land surface forcing to regional meteorology and air quality over South China, Atmospheric Environment, 152, 389-404, 2017.

Zhuang, G. S., Yuan, J. H., Yuan, H., Zhao, C. Y.: The compositions, sources, and size distribution of the dust storm from China in spring of 2000 and its impact on the global environment, Science Bulletin, 46, 895-901, 2001.

Regional severe particle pollution and its association with synoptic weather patterns in the Yangtze River Delta region, China

Lei Shu [1], Min Xie [1*], Da Gao [1], Tijian Wang [1*], Dexian Fang [2], Qian Liu [3], Anning Huang [1], Liwen Peng [1]

[1] School of Atmospheric Sciences, CMA-NJU Joint Laboratory for Climate Prediction Studies, Jiangsu Collaborative Innovation Center for Climate Change, Nanjing University, Nanjing 210023, China

[2] Chongqing Institute of Meteorology and Science, Chongqing 401147, China

[3] Jiangsu Provincial Academy of Environmental Science, Nanjing 210036, China

----

*Corresponding to Min Xie (minxie@nju.edu.cn) and Tijian Wang (tjwang@nju.edu.cn)

Abstract: Regional air pollution is significantly associated with ~~the~~ dominant weather systems. In this study, the relationship between the particle pollution over the Yangtze River Delta (YRD) region and ~~the~~ weather patterns is investigated. ~~Firstly,~~ First, the pollution characteristics of particles in the YRD are studied ~~by~~ using ~~the in-situ~~in situ monitoring data ($PM_{2.5}$ and PM_{10}) in 16 cities and Terra/MODIS AOD (aerosol optical depth) products collected from December 2013 to November 2014. The results show that the regional mean value of AOD is high in the YRD, with ~~the~~ an annual mean value of 0.71±0.57. The annual mean particle concentrations in the cities of Jiangsu Province all exceed the national air quality standard. The pollution level is higher in ~~the~~ inland areas, ~~with~~ and the highest concentrations of $PM_{2.5}$ and PM_{10} ~~respectively being~~are 79 and 130 $\mu g \cdot m^{-3}$~~–~~, respectively, in Nanjing. The $PM_{2.5}/PM_{10}$ ratios are ~~usually~~ typically high, thus indicating that $PM_{2.5}$ is the overwhelmingly dominant particle pollutant in the YRD. The wintertime peak of particle concentrations is tightly linked to the increased emissions ~~in~~ during the heating season, as well as ~~the~~ adverse meteorological conditions. ~~Secondly,~~ Second, based on NCEP reanalysis data, synoptic weather classification is conducted to reveal the weather patterns that ~~are easy to~~can easily cause severe particle pollution in the YRD. Five typical synoptic patterns are objectively identified, including the East Asian trough rear pattern, the

depression inverted trough pattern, the transversal trough pattern, the high-pressure controlled pattern, and the northeast cold vortex pattern. Finally, the synthetic analysis of meteorological fields and backward trajectories are applied to further clarify how these patterns impact particle concentrations. It is demonstrated that air pollution is more or less influenced by high-pressure systems. The relative position~~s~~ of the YRD to the anti-cyclonic circulation~~s~~ ~~are quite~~exerts significant ~~to~~ effects on the air quality of the YRD. The YRD is largely influenced by polluted air masses from the northern and the southern inland areas when it is located at the rear of the East Asian major trough. The s~~S~~ignificant downward motion of air masses results in stable weather conditions, ~~and~~ thereby ~~hinders~~ hindering the diffusion of air pollutants. Thus, the East Asian trough rear pattern is quite favorable for the accumulation of pollutants in the YRD, ~~and causes~~resulting in higher regional mean PM_{10} (116.5±66.9 μg·m-3), $PM_{2.5}$ (75.9±49.9 μg·m-3) and AOD (0.74) values. Moreover, this pattern is also responsible for the ~~most~~ occurrence of most large-scale regional $PM_{2.5}$ (70.4%) and PM_{10} (78.3%) pollution episodes. High wind speed and ~~the~~ clean marine air masses may also play important roles in the mitigation of ~~the~~ pollution in the YRD. Especially when the clean marine air masses account for a large proportion of all trajectories (i.e., when the YRD is controlled by the high-pressure controlled pattern and the northeast cold vortex pattern), the air in the YRD has ~~less~~ a smaller chance of being polluted. The ~~found~~ observed correlation between weather patterns and particle pollution can provide valuable ~~views~~ insight ~~in the~~into making decision~~s-making~~ ~~on~~ about pollution control and mitigation strategies.

Keywords: $PM_{2.5}$; PM_{10}; air pollution meteorology; synoptic weather pattern; the Yangtze River Delta region

1. Introduction

The ~~high~~ common occurrence of regional particle pollution ~~is~~ has acquired worldwide attention in the scientific community (Malm et al., 1994; Putaud et al., 2004; Chan and Yao, 2008) due to its adverse impacts on visibility (Singh and Dey, 2012; Green et al., 2012) and public health (Kappos et al., 2004; Brook et al., 2010). Generally, the causes ~~for~~ of this kind of pollution involve diverse aspects. Two major contributors ~~Among them~~to this pollution, ~~–~~ include the emission of pollutants and weather conditions ~~are two major contributors~~ (Oanh and Leelasakultum, 2011;

Young et al., 2016). Particle pollution in urban agglomerations is primarily attributed to ~~the hugevery~~ very large amounts of the anthropogenic emissions of primary particles and their precursors (e.g., SO_2, NO_x, ~~and~~ VOCs~~, etc.~~). However, these emissions are normally quasi-stable within a certain period of time (Kurokawa et al., 2013). Thus, the pollution level in a certain region generally depends on the regional weather conditions (~~namely~~ namely, weather patterns), which are strongly correlated with ~~the~~ synoptic-scale atmospheric circulation (Buchanan et al., 2002; Chuang et al., 2008; Flocas et al., 2009; Zhang et al., 2012; Zhao et al., 2013; Russo et al., 2014; Grundstrom et al., 2015; Zheng et al., 2015a; 2015b; Li et al., 2016).

~~Until now~~To date, researchers have gained an improved knowledge of the relationship between weather patterns and particle pollution. For example, Buchanan et al. (2002) observed ~~the~~ significantly elevated concentrations of Black Smoke and PM_{10} under the anti-cyclonic, southerly and southeasterly weather types in the city of Edinburgh in the UK between 1981 and 1996. Russo et al. (2014) ~~showed~~ presented an objective classification scheme ~~of~~ for the atmospheric circulation affecting Portugal between 2002 and 2010~~,~~ and revealed that higher concentrations of PM_{10}, O_3 and NO_2 are predominantly associated with synoptic circulation that is characterized by an eastern component and the advection of dry air masses. Previous studies have confirmed that ~~the~~ different levels of air pollution ~~have close relations~~are closely related with weather patterns~~, and also~~ and they ~~showed~~ ascribed its great spatial variability ~~ascribed~~ to the fact that the dominant weather pattern differs ~~among~~ between different regions (Flocas et al., 2009; Grundstrom et al., 2015).

In recent decades, the air pollution caused by PM_{10} and $PM_{2.5}$ has become ~~the~~ an extremely prominent air quality problem in the urban areas of China (Deng et al., 2011; Huang et al., 2012; Ji et al., 2012; Cheng et al., 2013; Kang et al., 2013; Huang et., 2014; Zhang et al., 2014; Xie et al., 2016a; 2016c; Zhu et al., 2017). Many studies have tried to reveal the meteorological contributions ~~of meteorology~~ to these severe particle pollution episodes. Chuang et al. (2008) identified seven weather patterns for aerosol events occurring from March 2002 to February 2005 in the Taipei B~~b~~asin~~,~~ and suggested that weather systems and their associated terrain blocking played important roles in the accumulation of $PM_{2.5}$ ~~accumulation~~ during the days of events~~ days~~. Niu et al. (2010) revealed the potential impacts of the weakening of the East Asian monsoon circulation and increased aerosol loading on the increase ~~of~~ in wintertime fog in China. Zhao et al.

(2013) analyzed a regional haze episode in the North China Plain from 16 to 19 January 2010~~,~~ and ~~pointed out~~noted that ~~the~~ strong temperature inversion, weak surface wind speed and descending air motions in the boundary layer were responsible for the accumulation of pollutants in a shallow layer ~~and~~ that produced high pollutant concentrations within the source region. Zheng et al. (2015a) found that ~~the~~ favorable atmospheric circulation conditions are responsible for the severe winter haze over northeastern China. Li et al. (2016) ~~pointed out~~noted that the fog-haze days over central and eastern China ~~shows a~~exhibited the clear features of inter-annual variations~~,~~ and that the strong (weak) East Asian winter monsoon may result in less (more) fog-haze days ~~across the~~throughout this region.

~~Located in the southeast coastal area of East China, t~~The Yangtze River Delta (YRD) region, which is located in the southeastern coastal area of East China, is one of the most developed urban economic ~~circles~~ regions in the world; it~~,~~ generally includes Shanghai, Jiangsu Province and Zhejiang Province, and it occupies over 20% of China's total gross domestic product (GDP) (Shu et al., 2016; Xie et al., 2016a; 2017). In recent years, ~~like~~ similar to other megacity clusters in China, such as the Beijing-Tianjin-Hebei (BTH) region (He et al., 2001; Chan and Yao, 2008; Ji et al., 2012; Zhang et al., 2012; 2014; Zhao et al., 2013; Zheng et al., 2015a) and the Pearl River Delta (PRD) region (Ho et al., 2003; Chan and Yao, 2008; Xie et al., 2016c; Zhu et al., 2017), the YRD has ~~also been suffering~~suffered from severe air pollution problems ~~brought~~ caused by an ~~accelerated~~ increasing population, urban expansion, and industrialization (Chan and Yao, 2008; Fu et al., 2008; 2010; 2014; Deng et al., 2011; Li et al., 2011; Huang et al., 2012; Kang et al., 2013; Wang et al., 2013; 2014; 2015; Xie et al., 2014; 2016a, 2016b, 2017; Feng et al., 2015; Zheng et al., 2015b; Shu et al., 2016; Xu et al., 2016; Ming et al., 2017). ~~Especially~~In particular, ~~the~~ severe particle pollution episodes are widely recognized as one of the major air pollution issues in the YRD (Fu et al., 2008; 2010; Deng et al., 2011; Huang et al., 2012; Kang et al., 2013; Kong et al., 2013; Wang et al., 2013; 2014; 2015; Fu et al., 2014; Feng et al., 2015; Zheng et al., 2015b; Xu et al., 2016; Ming et al., 2017). Thus, ~~a lot of~~ many ~~researches~~studies have been conducted to ~~figure out~~determine the contamination status (Fu et al., 2010; Kang et al., 2013; Wang et al., 2013; 2015; Feng et al., 2015; Ming et al., 2017), possible source (Fu et al., 2010; 2014; Kong et al., 2013; Wang et al., 2013; 2014; Xu et al., 2016), ~~or~~ and causes ~~and~~ or features (Fu et al., 2008; 2010; Huang et al., 2012; Wang et al., 2015; Zheng et al., 2015a) of these episodes. However, ~~among~~

~~these studies, the work~~studies that have attempted to determine ~~trying to figure out~~ how particle pollution in the YRD is associated with synoptic weather patterns are~~is~~ still quite limited. Zheng et al. (2015b) ~~once~~ summarized the synoptic-scale atmospheric circulations influencing the distribution of particles over eastern China ~~in~~ during autumn from 2001 to 2010. They found that there are six polluted weather types and three clean ones~~,~~ and revealed that heavy pollution events ~~particularly~~ most commonly occur when the study areas are located at the rear of the anticyclone. However, t~~T~~his study considered~~s~~ the influence of pollution in a region that is larger than the YRD, only focused~~s~~ on ~~the~~ pollution in October, and ~~is~~ was mainly ~~on basis~~based ~~of~~ on satellite aerosol optical depth (AOD) data. Ground-based monitoring particle concentration data can better represent the status of particle pollution in the urban atmosphere of the YRD. Thus, to better understand the relationship between ~~the~~ pollution in the planetary boundary layer and the synoptic weather patterns over the YRD, further ~~study~~ studies should be conducted based on surface monitoring ~~the~~ data collected over a time period of at least ~~over a~~ one year ~~from the surface monitoring in~~in the YRD.

This work attempts to enhance ~~the~~ our understanding of particle pollution in the YRD and~~,~~ ~~and~~ provide~~s~~ ~~the~~ scientific knowledge ~~for~~ about the association of regional severe particle pollution and synoptic weather patterns. ~~Firstly,~~ First, we analyze the spatial and temporal distribution of PM_{10}, $PM_{2.5}$ and AOD in the YRD from December 2013 to November 2014 ~~, aimed~~ to illustrate the characteristics of particle pollution over ~~the~~ this region. ~~Secondly,~~ Second, synoptic weather classification is conducted to reveal the weather patterns related to heavy pollution. Finally, the synthetic analyse~~i~~s of meteorological fields and backward trajectories are used to further clarify the impact mechanism. In this paper, Section 2 describes the observed data, the synoptic weather classification method and the trajectory model. Section 3 presents our main findings, including ~~the~~ a detailed analysis of the characteristics of particle pollution in the YRD, the synoptic weather patterns affecting ~~the~~ this pollution, and the mechanism ~~how~~ by which weather systems impact ~~the~~ pollution. ~~In the end~~Finally, a brief summary is ~~addressed~~ presented in Section 4.

2. Data and methods

2.1 Observed data

The observed air quality data used in this study are obtained from the National Environmental Monitoring Center (NEMC) of China. The in situ monitoring data ~~for~~ of the hourly concentrations of $PM_{2.5}$, PM_{10}, CO, NO_2, SO_2 and O_3 ~~can be~~are acquired from the national air quality real-time publishing platform (http://106.37.208.233:20035). Sixteen cities are selected as ~~the~~ representative research ~~objects~~ sites to better reflect the status of particle pollution over the YRD region. ~~They~~ These cities ~~are~~ include Shanghai, Changzhou, Nanjing, Nantong, Suzhou, Taizhoushi, Wuxi, Yangzhou, Zhenjiang, Hangzhou, Huzhou, Jiaxing, Ningbo, Shaoxing, Taizhou, and Zhoushan (here, Taizhou in Jiangsu Province is ~~renamed~~ referred to as Taizhoushi to distinguish it from the city of Taizhou in Zhejiang Province). Fig. 1 shows the locations of the 16 cities in the YRD. In order to better characterize the pollution levels of each city, ~~The~~ the hourly pollutant concentration ~~for~~ of ~~a~~ each city is calculated as the average value of the pollutant concentrations ~~from~~ measured in several of the national monitoring sites in that city~~, which can better characterize the pollution levels of the city~~. The sampling methods and the quality assurance and quality control (QA/QC) procedures used at each site ~~act~~ are in accordance with the Chinese national standard HJ/T193-2005 (State Environmental Protection Administration of China, 2006; Xie et al., 2016b). Furthermore, manual inspection is conducted ~~in~~ during data processing;~~,~~ ~~including~~ this inspection includes the removal of ~~the absent~~missing and ~~the~~ abnormal values (~~such as~~e.g., $PM_{2.5}$ values that are higher than PM_{10} values). ~~The period of this study starts~~The study period lasts from December 2013 to November 2014. In the following analysis, winter refers to the period from December 2013 to February 2014. Accordingly, spring, summer and fall represent the periods from March to May, June to August, and September to November ~~in~~ 2014, respectively.

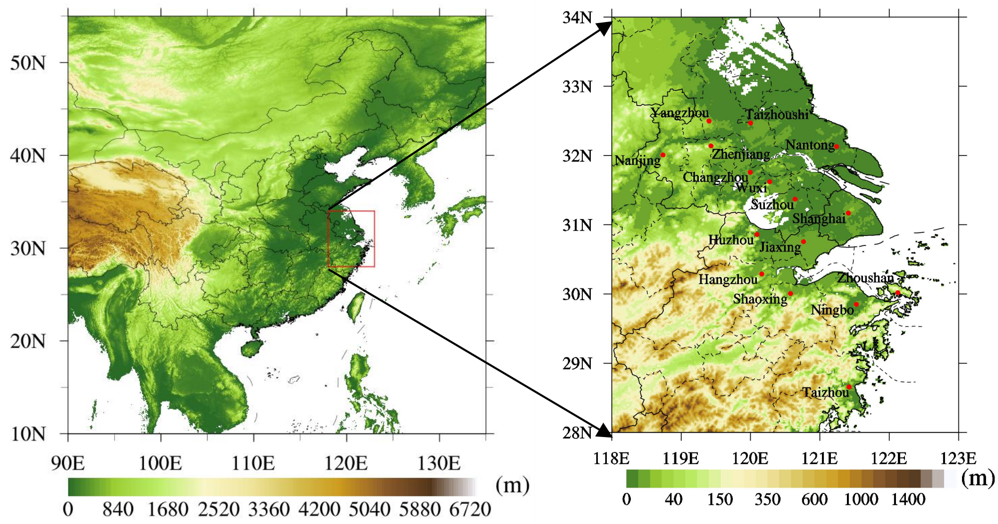

Figure 1. The location of ++the++ YRD in China (a) and 16 typical cities in ++the++ YRD (b), with ~~the~~ terrain elevation~~s~~ data. The terrain elevation~~s~~ data are obtained from the website (https://www.ngdc.noaa.gov/mgg/global/relief/ETOPO1/data/bedrock/cell_registered/).

The ++use of++ Moderate Resolution Imaging Spectroradiometer (MODIS) aerosol products can help ~~to~~ ++us++ comprehensively analyze the spatial and temporal variations ~~of~~ ++in++ aerosol loading over China. In this study, we use the aerosol optical depth (AOD) data ++obtained++ at ++a wavelength of++ 550 nm ~~wavelength~~ in ++the++ Terra/MODIS daily global Level 3 products (MOD08_D3). ~~They~~ ++These data++ can be obtained from ++the++ MODIS collection 6 (C6) dataset (https://ladsweb.nascom.nasa.gov/search/index.html). MODIS aerosol products are derived ~~by~~ ++using++ two entirely independent retrieval algorithms++:++~~,~~ one ++is used++ for deriving aerosols over land (Chu et al, 2002; 2003) and another ++is used++ for ++deriving++ aerosols over the ocean (Remer et al, 2002; 2005; Chu et al., 2005). Here, we use the C6 Deep Blue (DB) products ~~for deriving~~++to derive++ aerosols over land++,++ with ~~the~~ ++a++ spatial resolution of ~~1°~~ ++1°++ × ~~1°~~ ++1°,++ during the period from December 2013 to November 2014. ~~The~~ ++For++ detailed descriptions of the retrieval algorithms ++and their++~~,~~ accuracy and validation++,++ ~~can further~~ refer to the work of Hsu et al. (2013).

~~In order to~~++To++ illustrate ~~the real~~++actual++ weather situation++s++, the hourly monitored meteorological parameter records in each of ++the++ 16 typical cities are ++also++ applied ~~as well~~. The++se++ data include 2 m temperature (T), 2 m relative humidity (RH), 10 m wind speed (WS), 10 m wind direction (WD) and surface air pressure (P). ~~They~~ ++These data++ are collected from the National Meteorological Center (http://www.nmc.cn).

2.2 Synoptic weather classification

Synoptic weather classification refers to the analysis of historical weather charts and the characterization of weather systems. It is more effective for ~~the~~ producing disastrous weather forecasts due to its ability to reveal ~~the~~ atmospheric circulation situations. With the gradual popularization of computer analysis and the ~~greater~~ increased sharing of data, synoptic weather classification has great practical value in ~~many other~~a wide variety of research fields. For example, it has widespread applications in the field of analyzing ~~the~~ weather patterns related to air pollution (Mcgregor and Bamzelis, 1995; Zhang et al., 2012; Santurtún et al., 2015).

Methods of synoptic weather classification can ~~be~~ generally be divided into ~~the~~ objective and ~~the~~ subjective methods (El-Kadi and Simithson, 1992). In this study, we apply the sums-of-squares technique, which is ~~one of the~~an objective classification method~~s~~ ~~and~~ that was established in 1973 by Kirchhofer (Kirchhofer, 1973). The sums-of-squares technique can effectively categorize more than 90% of ~~the~~ analyzed weather maps, which ~~is~~ represents an improvement over ~~the~~ other correlation techniques (Yarnal, 1984). ~~The steps of a~~The application of~~pplying~~ this technique ~~are threefold~~involves three steps. ~~Firstly,~~ First, the daily pressure data at each grid point~~s~~ are normalized as follows:

$$Z_i = \frac{(X_i - \overline{X})}{s} \quad (1)$$

where Z_i is the normalized value of ~~the~~ grid point i, X_i is the value at grid point i, $\overline{X}$ is the mean value of the study domain, and s is the standard deviation. Data normalization removes the effects of the magnitude of pressure ~~magnitude~~ and improves the seasonal comparability of different weather types. ~~Secondly,~~ Second, each normalized grid point is compared to all other grid points~~s~~ ~~on the basis of~~based on the Kirchhofer score (S) ~~for~~ of each grid point:

$$S = \sum_{i=1}^{N} (Z_{ai} - Z_{bi}) \quad (2)$$

where Z_{ai} is the normalized value ~~in~~ of grid point i on ~~the~~ day a, Z_{bi} is the normalized value ~~in~~ of grid point i on ~~the~~ day b, and N is the number of grid points. The Kirchhofer score (S) is calculated for each row (denoted as S_R), each column (S_C) and the entire study domain (S_T) to ensure the pattern similarity between any pair of patterns for all grid points. Finally, all days are separated into one of the identified synoptic weather patterns ~~according to the~~based on these three values and their empirically derived thresholds. ~~Thereinto~~Thus, the values of S_R, S_C and S_T must be lower than their respective threshold values ~~so that~~for these patterns ~~can~~ to be accepted as similar (Barry et al., 1981). For each daily grid, the lowest significant Kirchhofer score (S) is recorded with the associated key day, thus denoting the synoptic type of ~~the~~ that day. All r~~R~~emaining days are considered ~~as~~ to be 'unclassified'.

The ~~dataset of~~ meteorological field dataset used in the sums-of-squares technique ~~is from~~contains NCEP–DOE AMIP-II Reanalysis 2 data (Kanamitsu et al., 2002), which are collected at 00:00, 06:00, 12:00, and 18:00 UTC (universal time coordinated) (https://www.esrl.noaa.gov/psd/data/gridded/data.ncep.reanalysis2.pressure.html). These data have 144×73 horizontal grids ~~of 144×73,~~ with a grid spacing of 2.5°. From the ground level to 10 hPa, there are 17 pressure levels in the vertical direction. The classification of synoptic weather maps is conducted ~~by~~ using the gridded data at ~~the~~ a geopotential height of 850 hPa during the same time period when the air quality data are recorded. The domain of interest is centered over the YRD region, covering an area of 25-40° N in latitude and 110-128°E in longitude.

2.3 HYSPLIT model

Backward trajectories can be adopted to help understand transport paths and identify the source regions of air masses. The Hybrid Single-Particle Lagrangian Integrated Trajectory (HYSPLIT) Model (Version 4) ~~is~~ was developed by the National Oceanic and Atmospheric Administration (NOAA) Air Resources Laboratory (ARL). It is one of the most extensively used atmospheric transport and dispersion models for the study of air parcel trajectories (Draxler and Rolph, 2013; Rolph, 2013; Stein et al., 2016), and it has been ~~well~~ widely applied in simulations of the complex transport, diffusion, chemical transformation and depositional processes ~~simulations~~ of atmospheric pollutants (Mcgowan and Clark, 2008; Wang et al., 2011; Huang et al., 2015; Xie et al., 2016b).

In this study, HYSPLIT is used to compute the ~~air parcel~~ backward trajectories of air parcels, reveal the possible source regions of air masses, and establish ~~the~~ source-receptor relationships for each synoptic weather pattern. For each synoptic weather pattern, the terminus of ~~the~~ each trajectory~~ies~~ is considered to be located at the observation site in Nanjing (32°N, 118.8°E). The 72-h backward trajectories are then calculated and clustered. The ending point is ~~set~~ defined ~~at~~ as

1500 m above sea level. The NCEP reanalysis data (http://ready.arl.noaa.gov/archives.php) are used to drive the backward trajectory calculation. The NCEP data contain 6-hourly basic meteorological fields on pressure surfaces with ~~the~~ a spatial resolution of 2.5°. In this study, these data are also converted to hemispheric 144 by 73 polar stereographic grids;~~,~~ ~~which is~~these data thus have the same grid configuration as the dataset applied in the synoptic weather classification.

3. Results and discussion

3.1 Characteristics of particle pollution in the YRD

3.1.1 Spatial distributions of particle pollution

Fig. 2a displays the annual mean values of AOD observed at a wavelength of 550 nm ~~wavelength in~~throughout most ~~areas~~ of China. The highest values (i.e., larger than 0.6) generally occur in the BTH, the YRD, the Sichuan Basin (SCB), and some of the central and southern provinces in China (i.e., Hubei, Hunan and Guangxi provinces). AOD is mainly governed by fine particles in industrialized urban conditions (Kim et al., 2006);~~,~~ thus, the abovementioned areas should ~~be suffering~~suffer from high columnar aerosol loading. In the YRD, with the development of modern industrialization and urbanization, ~~the~~ contrasts ~~of~~ in the atmospheric pollution levels among ~~the~~ different cities gradually decrease ~~gradually~~, and severe air pollution episodes tend to exhibit significant regional pollution characteristics.

Fig. 2b shows the temporal variations ~~of~~ in the regional average~~d~~ AOD values ~~of AOD~~ in the YRD (covering 16 cities within the area of 25-40°N and 110-128°N). The annual mean value is 0.71±0.57. The maximum seasonal value is 0.98±0.83 in summer, followed by 0.81±0.57 in winter, 0.59±0.24 in spring, and 0.48±0.35 in autumn. ~~Though~~ Although the peak ~~of~~ particle concentrations ~~occurs~~are observed in winter (as shown in Fig. 3 and 5 ~~show~~), the above results demonstrate that the maximum regional mean AOD values occur~~s~~ in summer, ~~with~~ as they reach their~~the~~ highest value of 1.60 in June. ~~The~~ This result is similar to that found by Kim et al. (2006), who~~.~~ ~~It is~~ reported that the value of AOD is not only associated with the pollution levels of fine particles~~, but also~~ but is also strongly affected by other factors (~~such as~~e.g., solar radiation, water vapor ~~and etc.~~). The fact that the maximum AOD values occur in hot seasons should be ascribed to the combined effects of ~~an~~ the increase ~~of~~ in fine aerosol production (i.e., due to secondary aerosol formation by gas-to-particle conversion, the hygroscopic growth of hydrophilic aerosols ~~and~~ or biomass burning emissions) and humid weather (Kim et al., 2006). Consequently, the aerosol optical depth data obtained from satellite observations can reveal the spatial distribution of aerosols to some extent, but they cannot exactly reflect ~~the~~ pollution levels ~~and~~ or replace ~~the~~ concentration data.

Figs. 2c and 2d show the spatial distributions of the annual mean particle concentrations in 16 typical cities over the YRD from December 2013 to November 2014. Generally, the spatial distributions of $PM_{2.5}$ (Fig. 2c) and PM_{10} (Fig. 2d) ~~present a~~exhibit overall similar pattern~~ as a~~s ~~whole~~. The annual mean $PM_{2.5}$ and PM_{10} values decrease progressively ~~along~~ in the northwest-southeast direction, which means that particle concentrations are comparatively high in the northwest inland areas and low in the southeast coastal areas. The pollution levels in most cities ~~have~~ exhibit a positive correlation with their proximity ~~from the city~~ to the sea. The farther ~~the~~ a city is from the sea, the higher ~~the~~ its particle concentrations are. The maximum particle concentrations occur in Nanjing, with ~~the~~ values of 79 μg·m^{-3} for $PM_{2.5}$ and 130 μg·m^{-3} for PM_{10}. ~~Given the p~~Previous ~~researches~~studies ~~on~~ of major climatic features in the YRD have demonstrated that~~,~~ the southeast coastal area is dramatically affected by the land-sea breeze and marine air masses. The clean marine air masses are advantageous to the dilution and ~~the~~ diffusion of atmospheric pollutants, thus ~~leading to~~producing lighter air pollution. However, in the inland region, ~~the~~ clustered cities and ~~the~~ industrial districts tend to emit more pollutants, ~~and~~ thereby resulting in ~~more~~ the accumulation of ~~accumulated~~ more air pollutants around these cities.

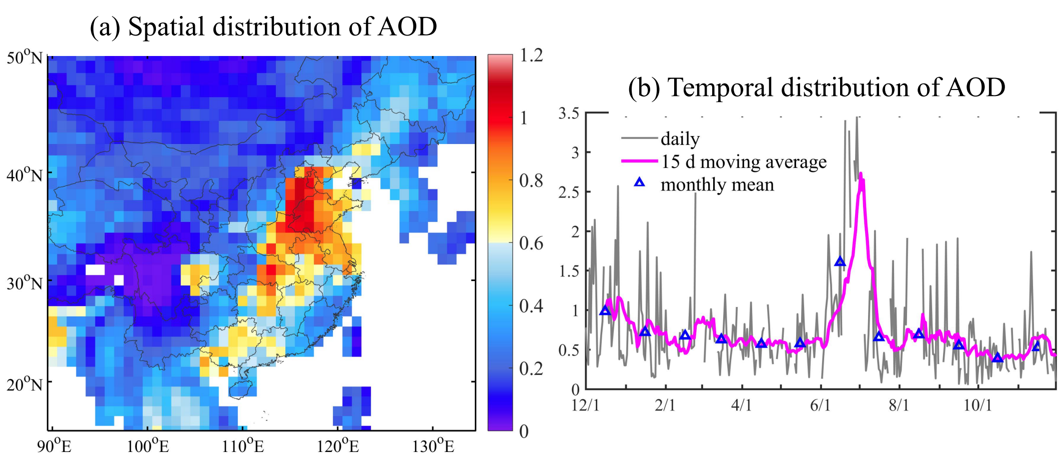

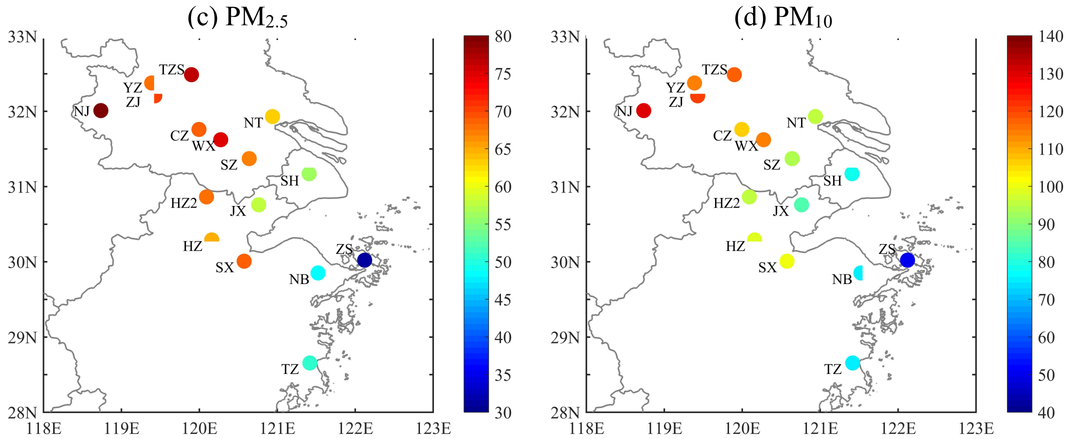

Figure 2. The spatial distribution of annual mean AOD values (at a wavelength of 550 nm ~~wavelength~~) ~~values~~ over the YRD (a);~~,~~ the temporal variations ~~of~~ in regional average~~d~~ AOD values over ~~(~~28-33°N and ~~,~~ 118-123°N~~)~~ (b);~~,~~ the spatial distribution of annual mean $PM_{2.5}$ concentrations (c);~~,~~ and the spatial distribution of annual mean PM_{10} concentrations (d). In (b), the gray line represents the daily value, the blue markers represent the monthly mean values, and the magenta line represents the 15~~-~~day~~s~~ moving average value. In (c) and (d), the acronyms of each city are marked, including Shanghai-SH, Changzhou-CZ, Nanjing-NJ, Nantong-NT, Suzhou-SZ, Taizhoushi-TZS, Wuxi-WX, Yangzhou-YZ, Zhenjiang-ZJ, Hangzhou-HZ, Huzhou-HZ2, Jiaxing-JX, Ningbo-NB, Shaoxing-SX, Taizhou-TZ, and Zhoushan-ZS.

Fig. 3 illustrates the spatial distribution of the seasonal mean $PM_{2.5}$ in 16 cities over the YRD. The pattern observed ~~in~~ during each season is similar to the annual mean pattern (Fig. 2c). The $PM_{2.5}$ pollution levels are much higher in inland cities, and they decrease ~~along~~ in the northwest-southeast direction. ~~For the seasonal variation ,~~ $PM_{2.5}$ concentrations exhibit seasonal variations; they are highest in winter, ~~with the~~reaching a maximum value ~~being up to~~of 120 μg·m^{-3}, and they decrease throughout ~~the~~ spring, ~~and show the~~yielding their lowest values ~~in~~ during summer and autumn. The difference between the $PM_{2.5}$ concentration in summer and that in autumn is relatively small;~~,~~ this difference ranges from~~both~~ ~~with the~~a maximum value of lower than 60 μg·m^{-3} in Nanjing ~~and~~ to ~~the~~ a minimum value of close to 20 μg·m^{-3} in Zhoushan.

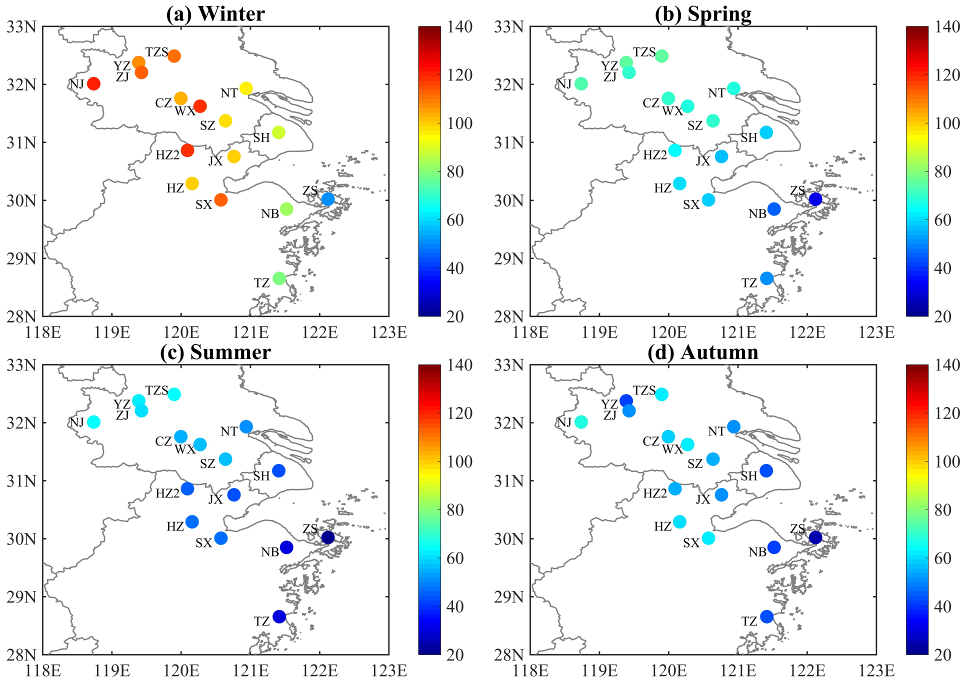

Figure 3. The spatial distribution of seasonal mean $PM_{2.5}$ over the YRD in (a) winter, (b) spring, (c) summer, and (d) autumn. The acronyms for each city are the same as those in Figure 2.

Table 1 quantitatively ~~demonstrates~~ lists the annual mean concentrations of $PM_{2.5}$ and PM_{10} in 16 cities over the YRD. It also ~~shows~~ demonstrates that the particle pollution levels are relatively higher in inland cities ~~are relatively higher~~. The concentrations of $PM_{2.5}$ and PM_{10} in 8 cities ~~of~~ in Jiangsu ~~province~~ Province are all higher than 60 $\mu g \cdot m^{-3}$ ($PM_{2.5}$) and 80 $\mu g \cdot m^{-3}$ (PM_{10}), respectively. However, these concentrations are comparatively lower in the cities located in the coastal area (~~such as~~e.g., Ningbo, Taizhou and Zhoushan) ~~are comparatively lower~~. Only the air quality of Zhoushan meets the national standard, which may be attributed to the fact that it is located on ~~the~~ an island, where ~~the~~ its air is ~~more~~ most likely influenced by ~~the~~ clean marine air masses.

To reveal the important role of $PM_{2.5}$ in particle pollution, the ratios of $PM_{2.5}$ concentration to PM_{10} concentration ($PM_{2.5}/PM_{10}$) are calculated over the YRD. As listed in Table 1, the maximum annual mean value of the $PM_{2.5}/PM_{10}$ ratio is 0.72 in Shanghai, followed by Huzhou and Suzhou (0.71), thus implying that the $PM_{2.5}$ fraction is overwhelmingly dominant ~~of~~ relative to the PM_{10} mass in these cities. The $PM_{2.5}/PM_{10}$ ratios in other cities ~~are between~~range from 0.60 ~~and~~ to 0.69, with ~~the~~ a minimum value of 0.58 in Zhenjiang. These values are comparable to those in other cities, ~~like~~ such as Beijing (He et al., 2001), Shanghai (Wang et al., 2013), Taibei (Chen et al., 1999), and Hong Kong (Ho et al., 2003), thus suggesting that the formation of $PM_{2.5}$ from gases is the most important source of particles in the cities of China. Table 1 also ~~presents~~ indicates that the $PM_{2.5}/PM_{10}$ ratios in all cities exhibit ~~show a~~ distinct seasonal variation. It is remarkable that the values of $PM_{2.5}/PM_{10}$ are much higher in winter than they are in other seasons, ~~with~~ reaching ~~the~~ a maximum value ~~reaching~~ of 0.85 in Shanghai, ~~and~~ followed by a value of 0.82 in Suzhou. The highest concentrations of $PM_{2.5}$ usually occur in winter (Fig. 3a), and high values of the $PM_{2.5}/PM_{10}$ ratio also ~~appear~~ occur ~~in~~ during the same season (Table 1), thus indicating that $PM_{2.5}$ poses a greater threat to human health in cold seasons, ~~that~~ which may be related to ~~the~~ heating activities. In summer, the values of $PM_{2.5}/PM_{10}$ in the 16 cities are medium, with ~~the~~ a mean value of 0.67. The lowest ratios usually occur in spring and autumn, ~~with~~ when the mean ratios of all cities ~~being~~ are 0.61 (spring) and 0.63 (autumn). The minimum value occurs in the autumn ~~of~~ in Yangzhou, with ~~the~~ a value of 0.51, followed by a value of 0.52 in the spring ~~of~~ in Nanjing and the autumn ~~of~~ in Zhenjiang. The above discussion ~~on~~ of the spatial and temporal variations ~~of~~ in $PM_{2.5}/PM_{10}$ ratios also implies that particles originate from various kinds of sources and are variedly emitted.

Table 1. Annual mean concentrations of $PM_{2.5}$ and PM_{10}, and the annual and seasonal mean values of $PM_{2.5}/PM_{10}$ ratio, in 16 cities over the YRD.

Cities		$PM_{2.5}$ ($\mu g \cdot m^{-3}$)	PM_{10} ($\mu g \cdot m^{-3}$)	$PM_{2.5}/PM_{10}$				
				Annual	Winter	Spring	Summer	Autumn
Shanghai		56	78	0.72	0.85	0.68	0.72	0.66
Jiangsu Province	Nanjing	79	130	0.61	0.64	0.52	0.70	0.60
	Changzhou	69	106	0.65	0.73	0.60	0.67	0.62
	Nantong	63	95	0.66	0.72	0.62	0.71	0.64
	Suzhou	67	94	0.71	0.82	0.68	0.71	0.67
	Taizhoushi	76	117	0.65	0.66	0.58	0.72	0.66
	Wuxi	75	114	0.66	0.73	0.59	0.67	0.62
	Yangzhou	68	114	0.60	0.69	0.58	0.59	0.51
	Zhenjiang	70	121	0.58	0.71	0.54	0.58	0.52
Zhejiang Province	Hangzhou	65	99	0.66	0.74	0.59	0.63	0.66
	Huzhou	68	96	0.71	0.78	0.66	0.68	0.69
	Jiaxing	58	84	0.69	0.75	0.65	0.68	0.69
	Ningbo	48	75	0.64	0.69	0.62	0.63	0.62
	Shaoxing	68	100	0.68	0.72	0.62	0.71	0.68

Taizhou	50	75	0.67	0.69	0.66	0.66	0.65
Zhoushan	31	50	0.63	0.66	0.62	0.66	0.55

3.1.2 Temporal variations ~~of~~ in particle pollution

Fig. 4 shows the annual mean diurnal variations ~~of~~ in $PM_{2.5}$ (Fig. 4a) and PM_{10} (Fig. 4b) in 16 cities over the YRD. Obviously, the diurnal cycles of particle concentrations in most cities follow ~~the~~ a similar pattern. The $PM_{2.5}$ concentrations maintain comparably high values from 0:00 to 8:00~~ –~~. ~~From t~~Then~~ on~~, coinciding with more vehicle emissions ~~in~~ during rush hours, these concentrations ~~go up~~increase rapidly from 8:00 to 12:00. After reaching their peak, the $PM_{2.5}$ concentrations decrease and ~~keep the~~remain at low values until ~~the~~ sunset. During ~~the~~ nighttime, the pollutants ~~get~~ accumulated until ~~the~~ midnight, which ~~should~~ can be attributed to the more stable atmospheric stratification in the boundary layer. In comparison, there are two peaks in the diurnal cycles of the PM_{10} concentrations in several cities. The broad morning peak of PM_{10} concentrations is more evident from 8:00 to 12:00, and the evening ~~one~~ peak occurs at ~~around 2~~approximately 20:00. ~~Besides,~~ In addition, the diurnal change ~~of~~ in particle concentrations in the southeast coastal area,~~ like~~ such as Zhoushan, is much smaller. As discussed in Section 3.1.1, ~~the~~ this difference might be related to its special geographic location, which exhibits ~~less~~ fewer emissions of precursors and lower pollution levels.

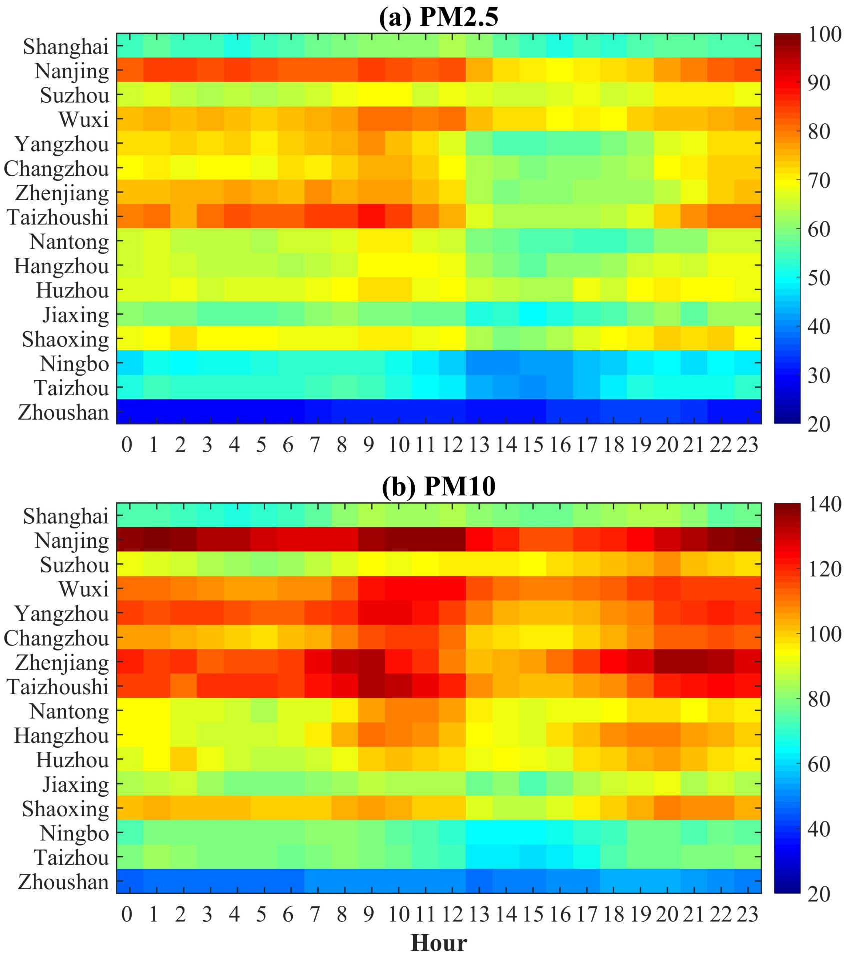

Figure 4. Diurnal variations ~~of~~ in $PM_{2.5}$ (a) and PM_{10} (b) concentrations in 16 cities of the YRD (unit: $\mu g \cdot m^{-3}$).

Fig. 5 ~~demonstrates~~ shows the monthly mean concentrations of $PM_{2.5}$ and PM_{10} in 16 cities of the YRD. As illustrated in ~~the~~ this figure, there are three peaks in the seasonal variations ~~of~~ in particles. These three peaks occur in December, March, and May/June. This monthly variation pattern is more obvious for PM_{10}. The causes resulting in the wintertime peak of particle concentrations can be explained by two factors. One is the enhanced emissions of pollutants ~~emissions~~ from residential heating. The other is the stable and poor meteorological conditions that limit the diffusion of atmospheric pollutants. ~~For~~ The drivers of the peak appearing in March~~,~~ ~~the drivers~~ may be associated with dust storm~~s~~ events in spring (Zhuang et al., 2001; Fu et al., 2010; 2014). As discussed in Section 3.1.1, the values of the $PM_{2.5}/PM_{10}$ ratio in 16 cities are lowest in spring, with ~~the~~ a mean ratio~~s~~ of 0.61. High PM_{10} concentrations during this period further ~~prove~~ demonstrate that dust storms can bring more coarse dust particles to the YRD. ~~For t~~The peak in

May/June~~, it~~ is probably caused by the field burning of crop residue in rural areas of China, which is regarded ~~as~~ to be an important source of biomass burning (Yan et al., 2006; Yang et al., 2007; Zhu et al., 2012).

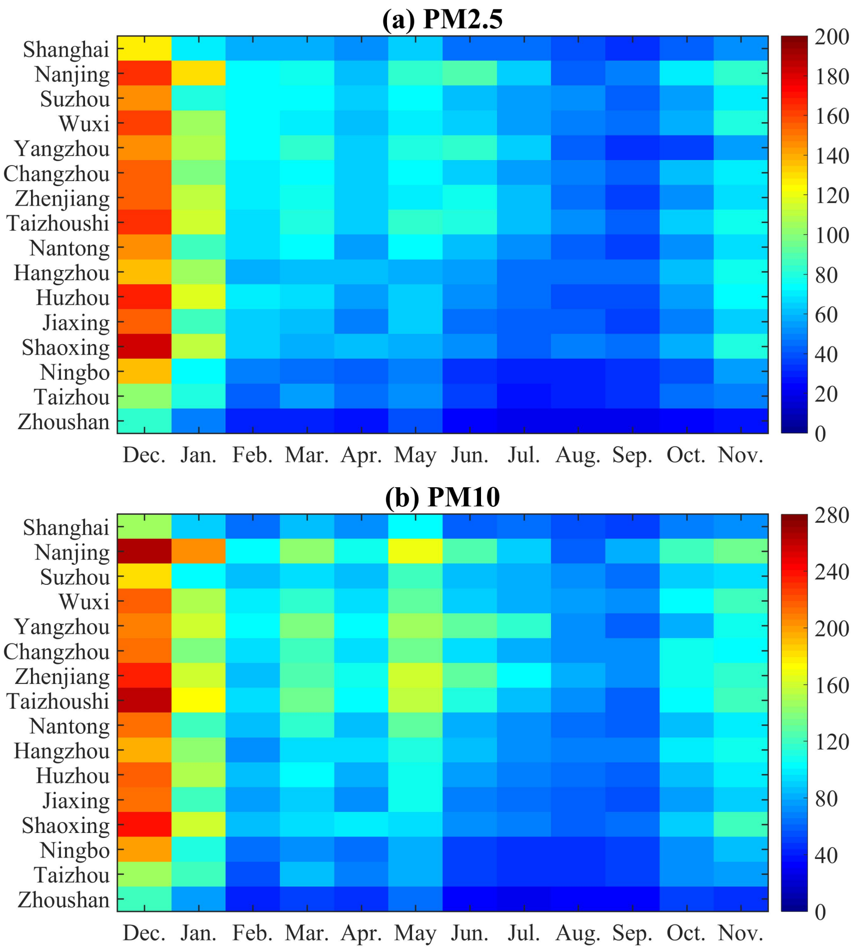

Figure 5. Monthly variations ~~of~~ in $PM_{2.5}$ (a) and PM_{10} (b) concentrations in 16 cities of the YRD (unit: $\mu g \cdot m^{-3}$).

3.1.3 Regional severe particle pollution in the YRD

According to the National Ambient Air Quality Standard (NAAQS) of China, ~~the~~ urban air quality ~~needs to~~ must meet the second standard, with ~~the~~ daily mean concentrations of $PM_{2.5}$ and PM_{10} that are lower than 75 $\mu g \cdot m^{-3}$ and 150 $\mu g \cdot m^{-3}$, respectively. In this study, when the daily mean $PM_{2.5}$ (PM_{10}) concentrations exceed the national air quality standard in most (i.e., 8 or more) of the 16 cities, we define ~~that there is a~~ this as large-scale regional $PM_{2.5}$ (PM_{10}) pollution. Consequently, from December 2013 to November 2014, there were 98 (46) days when ~~the~~ large-scale regional $PM_{2.5}$ (PM_{10}) pollution episodes ~~occurred are~~ were identified. That is, the YRD suffered from ~~the~~ regional $PM_{2.5}$ (PM_{10}) pollution ~~in~~ during nearly 28.0% (13.1%) of the days of the year.

Table 2 shows the typical regional severe particle pollution episodes (that lasted no less than 3 days) in the YRD from December 2013 to November 2014. As illustrated in ~~the~~ this table, ~~there are~~ dozens of continuous large-scale particle pollution episodes occurred. For example, $PM_{2.5}$ concentrations exceeded the national standard in all 16 cities from December 1 to 5, ~~in~~ 2013, and there were more than 14 cities facing heavy PM_{10} pollution at the same time. From May 26 to 30, ~~in~~ 2014, serious $PM_{2.5}$ and PM_{10} pollution episodes were ~~found~~ observed in more than 10 cities. It ~~seems~~ appears that high-~~-~~$PM_{2.5}$ pollution episodes are remarkably associated with high-~~-~~PM_{10} pollution episodes. Moreover, regional $PM_{2.5}$ pollution episodes occurred much more frequently than PM_{10} pollution episodes. ~~It might be owing~~This may be due to the fact that fine particles dominate the composition of particles in the YRD (as discussed in Section 3.1.2).

Table 2. The typical regional severe particle pollution episodes (lasting for no less than 3 days) in the YRD from December 2013 to November 2014.

Episodes of $PM_{2.5}$ pollution	Episodes of PM_{10} pollution
1-6 Dec.	1-6 Dec.
11-15 Dec.	12-15 Dec.
24-26 Dec.	24-26 Dec.
28 Dec. - 6 Jan.	29 Dec. - 5 Jan.
15-20 Jan.	17-20 Dec.
30 Jan. - 2 Feb.	26-30 May
20-24 Feb.	
16-18 Mar.	
8-10 Apr.	
20-22 May	
26-30 May	
5-7 Jun.	
28 Jun. - 1 Jul.	
10-12 Nov.	

3.2 Synoptic weather classification

In this study, ~~To~~ to examine the relationship between regional severe particle pollution in the YRD and weather situations, synoptic weather classification is carried out from December 2013 to November 2014~~ in this work~~. ~~Following~~ Using the method described in Section 2.2, we conduct the classification of the synoptic weather pattern by using the dataset of geopotential height at 850 hPa collected from the NCEP reanalysis data. As shown in Table 3, five weather patterns are finally identified, including the East Asian trough rear pattern (Pattern 1), the depression inverted trough pattern (Pattern 2), the transversal trough pattern (Pattern 3), the high-pressure controlled pattern (Pattern 4), and the northeast cold vortex pattern (Pattern 5). ~~The u~~Unknown ~~type is~~patterns are defined as 'the unclassified pattern'.~~During the study period,~~ The weather situation on 95.6% of the days during the study period is classified as one of the five typical synoptic weather patterns.

Table 3 lists the typical date, ~~the~~ number of days, and seasonal occurrence frequencies of each synoptic weather pattern. As demonstrated in ~~the~~ this table, Pattern 1 is the dominant weather pattern in the YRD, which accounts for 47.6% of all of the days of the year (from December 2013 to November 2014). The occurrence frequencies of Patterns 2 and 3 are 20.0% and 18.1%, respectively. Patterns 4 and 5 are identified on the fewest number of days, with ~~the~~ occurrence frequencies of 4.1% and 5.8%, respectively.

Table 3 also shows the seasonal occurrence frequencies of each pattern from December 2013 to November 2014. Obviously, they are distinctly different. Pattern 1 tends to occur in winter, with ~~the~~ a frequency of 30.5%, followed by spring (25.9%), summer (21.8%) and autumn (21.8%). Pattern 2 is the most popular weather pattern in summer, with ~~the~~ an occurrence frequency of 37.0%, followed by spring (30.1%), autumn (21.9%) and winter (11.0%).~~As for~~ For Pattern 3, the seasonal frequencies ~~are~~ occur in the order of winter (36.4%), spring (27.3%), autumn (19.7%) and summer (16.7%). Both ~~For~~ Pattern 4 and Pattern 5~~,~~ ~~they~~ are ~~both~~ most likely to ~~take place~~occur in autumn, with ~~the~~ occurrence frequencies ~~being~~ of 53.3% and 42.9%, respectively. The occurrence frequencies of Pattern 4 and Pattern 5 ~~in~~ during other seasons account for nearly 50%.

Table 3. The typical date, ~~the~~ number of days, and ~~the~~ seasonal occurrence frequencies of each synoptic weather pattern.

Type	Typical date	Number of days	Occurrence frequency (%)			
			Spring	Summer	Autumn	Winter
East Asian trough rear pattern (Pattern 1)	2014-05-12	174 (47.7%)	25.9	21.8	21.8	30.5
Depression inverted trough pattern (Pattern 2)	2014-05-09	73 (20.0%)	30.1	37.0	21.9	11.0

Transversal trough pattern (Pattern 3)	2014-02-18	66 (18.1%)	27.3	16.7	19.7	36.4
High-pressure controlled pattern (Pattern 4)	2014-10-07	15 (4.1%)	13.3	26.7	53.3	6.7
Northeast cold vortex pattern (Pattern 5)	2014-09-14	21 (5.8%)	19.0	23.8	42.9	14.3
Unclassified pattern	—	16 (4.4%)	—	—	—	—

3.3 Effects of synoptic weather patterns on particle pollution

3.3.1 Relationship between synoptic weather pattern and particle pollution

To ~~figure out~~determine the relationship between synoptic weather patterns and particle pollution, the occurrence frequencies of the five typical synoptic patterns during the regional severe particle pollution episodes are calculated. As shown in Table 4, during the days with regional $PM_{2.5}$ (PM_{10}) pollution episodes~~ days~~, Pattern 1 is the dominant synoptic weather pattern, with ~~the~~ an occurrence frequency of 70.4% (78.3%). ~~For $PM_{2.5}$ pollution,~~ Pattern 2 and Pattern 3 both occur ~~in~~ on 14.3% of the days with $PM_{2.5}$ pollution episodes. ~~For~~ During PM_{10} pollution episodes, Pattern 2 (6.5%) appears less frequently than Pattern 3 (15.2%). The occurrence frequencies of Pattern 4 and Pattern 5 are less than 1%~~,~~ and can thus almost be ignored~~ on that account~~.

According to Table 3 and Table 4, the occurrence frequency of Pattern 1 during ~~the~~ regional particle pollution episodes is obviously higher than its occurrence ~~in~~ during the ~~whole~~ entire year. In contrast, the occurrences of Pattern 2 and Pattern 3 during these episodes are less frequent than those throughout the year. Moreover, Pattern 4 and Pattern 5 appear far less frequently during ~~the~~ regional particle pollution episodes than ~~their appearance~~they do ~~within~~ throughout ~~a~~ the year. ~~To sum up, it suggests~~In summary, these data suggest that the weather situation of Pattern 1 is more beneficial for the formation of large-scale regional particle pollution in the YRD.

Table 4. The occurrence frequencies of synoptic weather patterns during ~~the~~ regional severe $PM_{2.5}$ and PM_{10} pollution episodes

Type	$PM_{2.5}$		PM_{10}	
	Number of days	Frequency (%)	Number of days	Frequency (%)
Pattern 1	69	70.4	36	78.3
Pattern 2	14	14.3	3	6.5
Pattern 3	14	14.3	7	15.2
Pattern 4	0	0%	0	0
Pattern 5	1	1.0	0	0

Fig. 6 shows the whisker-boxbox-and-whisker plot of the mean concentrations of mean air pollutants (PM_{10}, $PM_{2.5}$, O_3, NO_2, SO_2 and CO) concentrations and the meteorological parameters (WS, T, P and RH) of 16 cities under the five synoptic weather patterns, as well as the corresponding spatial distribution of AOD over eastern China. These statistical results are also listed in Table 5 as well.

As shown in Figs. 6a-6f and Table 5, the highest average concentrations of the main air pollutants (except for O_3) averaged forin the 16 cities in the YRD are observed to be associated with Pattern 1. Since aerosols can reflect and absorb solar radiation and thereby cause the decrease of the photochemical production of O_3 to decrease (Kaufman et al, 2002), the O_3 concentration is lowest for Pattern 1 (Fig. 6c). As above mentioned above, Pattern 1 is most likely to occur in during winter (30.5%) and spring (25.9%). Therefore, the weather situation of this pattern features the weakest surface wind, the lowest humidity, the second--highest surface pressure, and low temperature. All of these weather characteristics are conducive to an the accumulation of particles and their precursors (i.e., SO_2, NO_2 and CO). For Pattern 3, the concentrations of PM_{10}, $PM_{2.5}$ NO_2 and SO_2 are the second--highest compared to those of the other patterns. This pattern features the highest surface pressure and much stronger surface wind. The temperature is the lowest, as Pattern 3 also tends to take placeoccur in during winter (37.0%) and spring (30.1%). Under the weather situation of Pattern 1 and Pattern 3, the YRD is both under the control of high -pressure, and likely to suffer serious particle pollution. The strength of the surface wind for different weather patterns plays a key role in the occurrence frequency of regional severe particle pollution episodes. Pattern 1, which With has the weakest surface wind, Pattern 1 is regarded as 'the most polluted pattern'. As for Pattern 2, tThe pollution levels of the main pollutants in Pattern 2 are in the middle and slightly lower than those for of Pattern 3. Due to the its high occurrence frequency in summer (37.0%) and spring (30.1), the weather condition of Pattern 2 is characterized as by its relatively high temperature, low pressure, and the lowest RH. In contrast, Pattern 4 and Pattern 5 are 'the clean patterns', with in which the concentrations of all of their pollutants are distinctly lower than those of the other three patterns. Their conditions of relatively high humidity, high temperature, strong wind (especially for Pattern 5) and much lower surface pressure are also favorable to for the mitigation of pollutants.

Figs. 6k to 6o display the spatial distribution of AOD over eastern China under different synoptic weather patterns. The regional mean values of AOD in the YRD (28-33°N, 118-123°N) are 0.74 for Pattern 1, 0.64 for Pattern 2, 0.81 for Pattern 3, 0.47 for Pattern 4 and 0.49 for Pattern 5~~, respectively~~. ~~It can also be found that~~Additionally, AOD ~~over YRD~~ is higher over the YRD for Pattern 3, Pattern 1 and Pattern 2. For these three patterns, high AOD values usually occur~~s~~ in the BTH, the YRD, and the SCB, as well as the provinces of Shanxi, Shandong, Hubei, Hunan, Anhui and Guangxi. The highest AOD values are mainly found in northeastern China. For Pattern 4 and Pattern 5, high AOD ~~is~~ values are mostly concentrated in the BTH and Shandong ~~province~~ Province, while relatively low AOD ~~is~~ values are found in the YRD. Since AOD is closely related to the concentrations of fine particles~~ concentrations~~, it can be concluded that the YRD is most heavily polluted under the weather situations of Pattern 1 and Pattern 3.

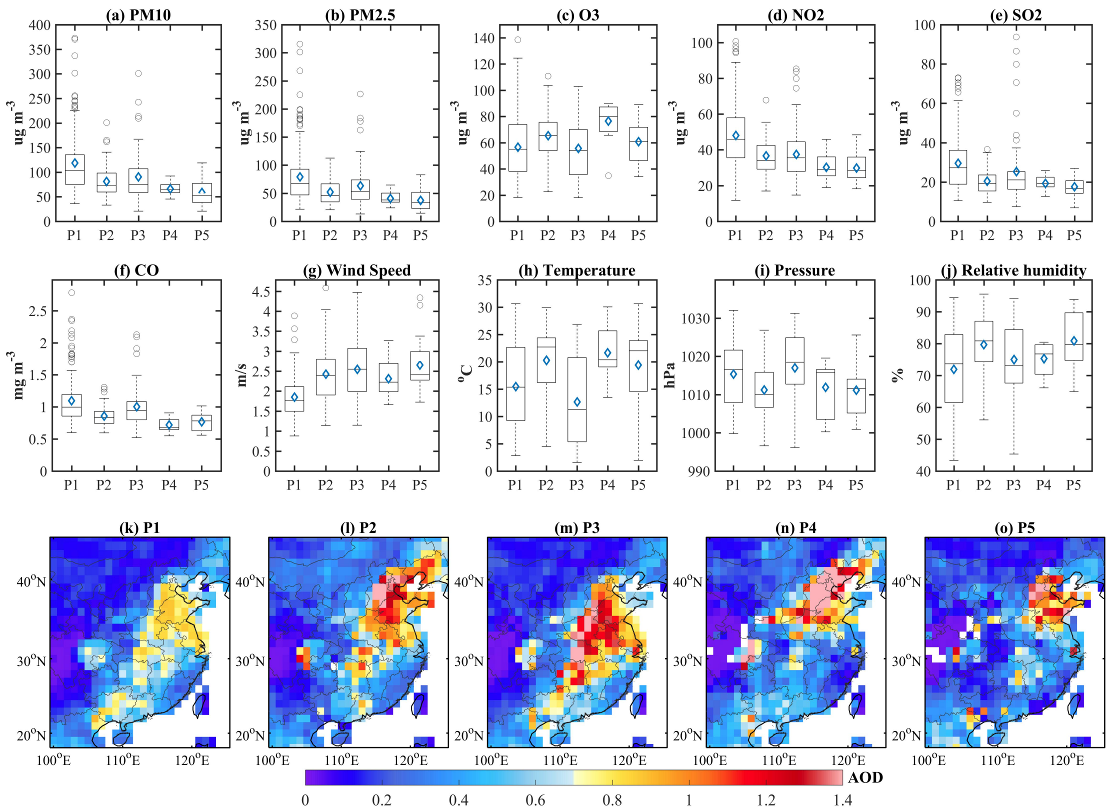

Figure 6. (a-j) ~~Whisker-box~~Box-and-whisker plots for the mean values of air pollutant concentrations and meteorological parameters of 16 typical YRD cities. The edges of each box in (a-j) are the 25th and 75th percentiles;~~,~~ the band inside the box is the median;~~,~~ the diamond is the average;~~,~~ and the whiskers extend to the most extreme data values. (k-p) Spatial distributions of AOD for the five synoptic weather patterns. P1, P2, P3, P4, and P5 represent Pattern 1, Pattern 2, Pattern 3, Pattern 4, and Pattern 5, respectively.

Table 5. The average values of air pollutant concentrations and meteorological factors for the 16 typical YRD cities under the different synoptic weather patterns.

Type	PM_{10}	$PM_{2.5}$	O_3	NO_2	SO_2	CO	SO_2	WS	T	P	RH
Pattern 1	116.5±66.9	75.9±49.9	57.7±27.3	46.9±19.2	29.3±17.1	1.08±0.41	29.3±17.1	1.84±0.67	15.8±7.8	1015.0±8.5	72.3±14.4
Pattern 2	81.5±38.4	52.3±27.4	65.5±23.6	36.1±13.4	20.6±9.9	0.86±0.24	20.6±9.9	2.38±0.88	20.3±6.3	1011.2±6.7	79.8±10.2
Pattern 3	86.9±49.5	59.1±37.3	58.5±25.5	35.1±15.5	23.3±15.9	0.96±0.35	23.3±15.9	2.59±0.87	13.4±8.2	1016.1±9.6	76.0±11.6
Pattern 4	66.1±18.8	40.7±15.9	76.8±19.6	29.4±9.8	19.4±6.4	0.72±0.17	19.4±6.4	2.29±0.64	21.7±4.9	1011.8±7.0	75.4±5.8
Pattern 5	58.7±31.3	37.4±22.5	61.1±20.6	29.1±11.1	17.8±8.4	0.77±0.22	17.8±8.4	2.63±0.93	19.4±8.0	1011.1±6.9	81.0±9.8

3.3.2 The impact mechanism of synoptic weather patterns on severe particle pollution

Figs. 7-11 present the meteorological fields and the backward trajectories under the weather situations of the five synoptic weather patterns. The first two graphs of Figs. 7-11 illustrate the 850 hPa and 500 hPa geopotential height field and wind field, respectively. The third graphs display the sea level pressure field and 1000 hPa wind field. The highlighted boxes depoint outnote the essential areastudy area (i.e., the YRD) that we focus on. The fourth graphs demonstrate the height-latitude cross-sections of vertical velocity over the in the latitudes (of 25-40°N), which is are averaged from the longitudes of 110-128°E in the longitude. The bold black lines show the latitude range of 16 cities (28.6-32.5°N) over the YRD. The positive wind speeds (10^2 Pa s^{-1}) indicate that there arerepresent vertical downward atmospheric motions, while the negative wind speeds represent the upward motions. Besides, In addition, it is well known that the atmospheric pollutant transport trajectories are deeply affected by synoptic systems. As shown in the fifth graphs in Figs. 7-11, to reveal how the typical synoptic weather patterns influence the distribution of particles in the YRD, the 72-h backward trajectories are calculated and then clustered. Given that Nanjing is the most polluted city in the YRD, as described in Section 3.1, the observational site in Nanjing (32°N, 118.8°E) is chosen for the terminus of the trajectoryies for of each synoptic weather pattern.

As illustrated in Fig. 7a, Pattern 1 usually occurs when the YRD is located at the rear of the East Asian major trough and is under the control of a high-pressure ridge at 850 hPa. The center of the high-pressure system is on located in the northwestern Pacific Ocean. Meanwhile, northeastern China is strongly affected by a low-pressure system, namely namely, the Aleutian Low. The strong horizontal northwest wind at the rear of the East Asian major trough can transport the pollutants from the BTH (with high AOD, as shown in Fig. 6k) to the YRD. At the same time, the west and southwest wind at the rear of the high-pressure ridge can also transport ~~the~~ pollutants from central and southwestern China (such as the SCB and Guangxi P~~p~~rovince) to the YRD. The confluence of air flows may cause an accumulation of pollutants in the YRD. Accordingly, the atmospheric circulation at 500 hPa features a shallow through with a west-northwest flow (Fig. 7b). The sea level pressure pattern is ~~almost~~ nearly dominated by a uniform pressure field, ~~with~~ which exhibits relatively weak anti-cyclonic circulation over the YRD (Fig. 7c). The above discussion can be further explained by the 72-h backward trajectories displayed in Fig. 7e. When the YRD is under the control of Pattern 1, the air masses are mainly from northern China (44%), followed by the central ~~region~~ (36%) and ~~the~~ northeastern regions of the YRD (19%). ~~It~~ This suggests that ~~the~~ particle pollution is remarkably affected by the polluted air masses from the BTH and the central city clusters. Surface meteorological observation records also ~~shown~~ indicate that west-northwest-southwest surface winds ~~dominate~~ are dominant in Nanjing (Fig. 7f)~~,~~ and that high $PM_{2.5}$ is closely associated with the transport of polluted air masses in these wind directions. In the vertical section (Fig. 7d), the relatively weak upward air flows ~~dominate~~ are dominant ~~in~~ to the south of 30°N, while ~~the~~ clear downward air flows ~~prevail~~ are prevalent ~~in~~ to the north of 30°N. The largest descending velocity (~8×10^{-2} Pa s^{-1}) appears at ~~the~~ an altitude of 500 hPa and ~~in~~ athe latitude of 37.5°N. Downward motion ~~dominates~~ is dominant above the YRD, which is in accordance with the 850 hPa circulation pattern represented by a high-pressure ridge. ~~For this reason~~Thus, the weather conditions are relatively stable near the surface~~,~~ ~~and~~ which is beneficial to the local accumulation of pollutants. Overall, Pattern 1 represents a stable synoptic weather pattern that ~~, and this weather situation~~ is extremely conduc~~t~~ive to the build~~t~~-up of atmospheric pollutants over the YRD. This result is consistent with the findings of Zheng et al (2015b).

Pattern 1

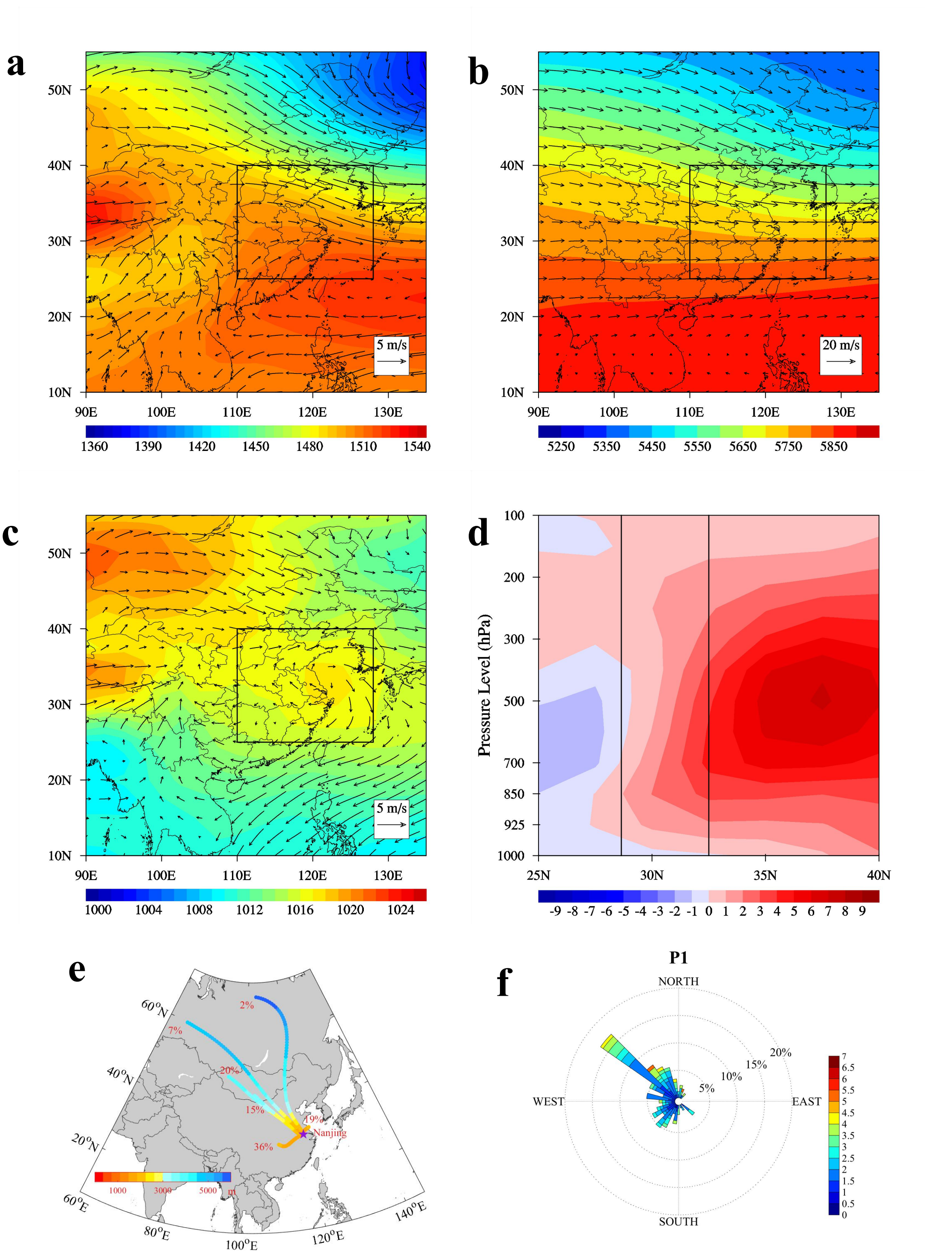

Figure 7. Weather condition in Pattern 1. (a) 850 hPa geopotential height field and wind field; ~~,~~ (b) 500 hPa geopotential height field and wind field;~~,~~ (c) sea level pressure field and 1000 hPa wind field;~~,~~ (d) height-latitude cross-sections of vertical velocity (unit: 10^{-2} Pa/s) averaged from longitude of 110-128°E;~~,~~ (e) 72-h backward trajectory ending at ~~the~~ a height of 1500 m;~~,~~ and (f) observation wind rose plots in Nanjing. In (a)-(c), the highlighted boxes ~~depoint out~~note the ~~essential~~ study area (i.e., the YRD)~~ that we focus on~~. In (d), the black rectangular region represents the 16 cities in the YRD (28.6-32.5°N). In (e), the purple marker indicates the location of Nanjing (32°N, 118.8°E). These data ~~is~~ represent averages~~d~~ for all days

corresponding to Pattern 1.

~~As fo~~In~~r~~ Pattern 2, a low-pressure center (the Southeast Vortex) is centered in the SCB, the East China Sea is influenced by a high-pressure system, and a depression inverted trough extends and covers the YRD region ~~in~~ at a latitude at 850 hPa (Fig. 8a). Consequently, in the YRD, the strong southwest air flows from southern China meet with the southeast air flows from the East China Sea. After the convergence of these air masses, they jointly transport pollutants northwestward. ~~While~~ In contrast, at the surface (Fig. 8c), the study ~~domain~~ area is located at the bottom of a high-pressure system and is impacted by a strong southeast wind. In the middle troposphere (Fig. 8b), the sparse isopleths indicate that there is a small geopotential height gradient, while the shallow ridge causes westerly flows. Fig. 8e also illustrates these air pollutant transport paths. For the days when Pattern 2 ~~dominates~~is dominant, ~~about 4~~approximately 42% of the air masses are from the southwest and the south of China, and 15% are from the East China Sea. The air masses from the East China Sea are very important~~,~~ because the clean marine air masses may dilute the particle concentrations in the YRD. ~~Besides,~~ In addition, ~~there are~~ nearly 43% of air masses originat~~i~~e~~ng~~ from the local sources of the YRD, which may be related to ~~the~~ their short-range transport in the northwest direction. This is also in accordance with the dominant northwest surface wind in Nanjing (Fig. 8f). ~~When it comes to~~In regard to ~~the~~ its vertical structure (Fig. 8d), Pattern 2 is obviously different ~~from~~ than Pattern 1, as ~~the~~ upward air flows ~~dominate~~ are dominant ~~in~~ to the south of 37.5°N. The largest updraft~~s~~ zone (~7×10^{-2} Pa s^{-1}) appears above the YRD and between the altitudes of 700 hPa and 500 hPa. The vertical velocity close to the surface is ~~relatively~~ weaker ~~compared to~~than that at higher levels over the YRD. ~~Meantime~~Meanwhile, ~~there is~~ stronger upward motion occurs near the surface ~~in the~~at a latitude of 37.5°N, with weak downward motion occurring above the 700 hPa layer. The above discussion suggests that atmospheric pollutants in the YRD are horizontally transported northwestward to a higher latitude~~,~~ and vertically transported upward to higher layers. Therefore, despite the transport of abundant pollutants to the YRD via southwest air flows and the short-range northwest transport of polluted air masses, the strong surface southeast wind and upward motion under the weather situation of Pattern 2 ~~determine that there~~result ~~is~~ in much ~~slighter~~ less particle pollution over the YRD compared to Pattern 1.

Pattern 2

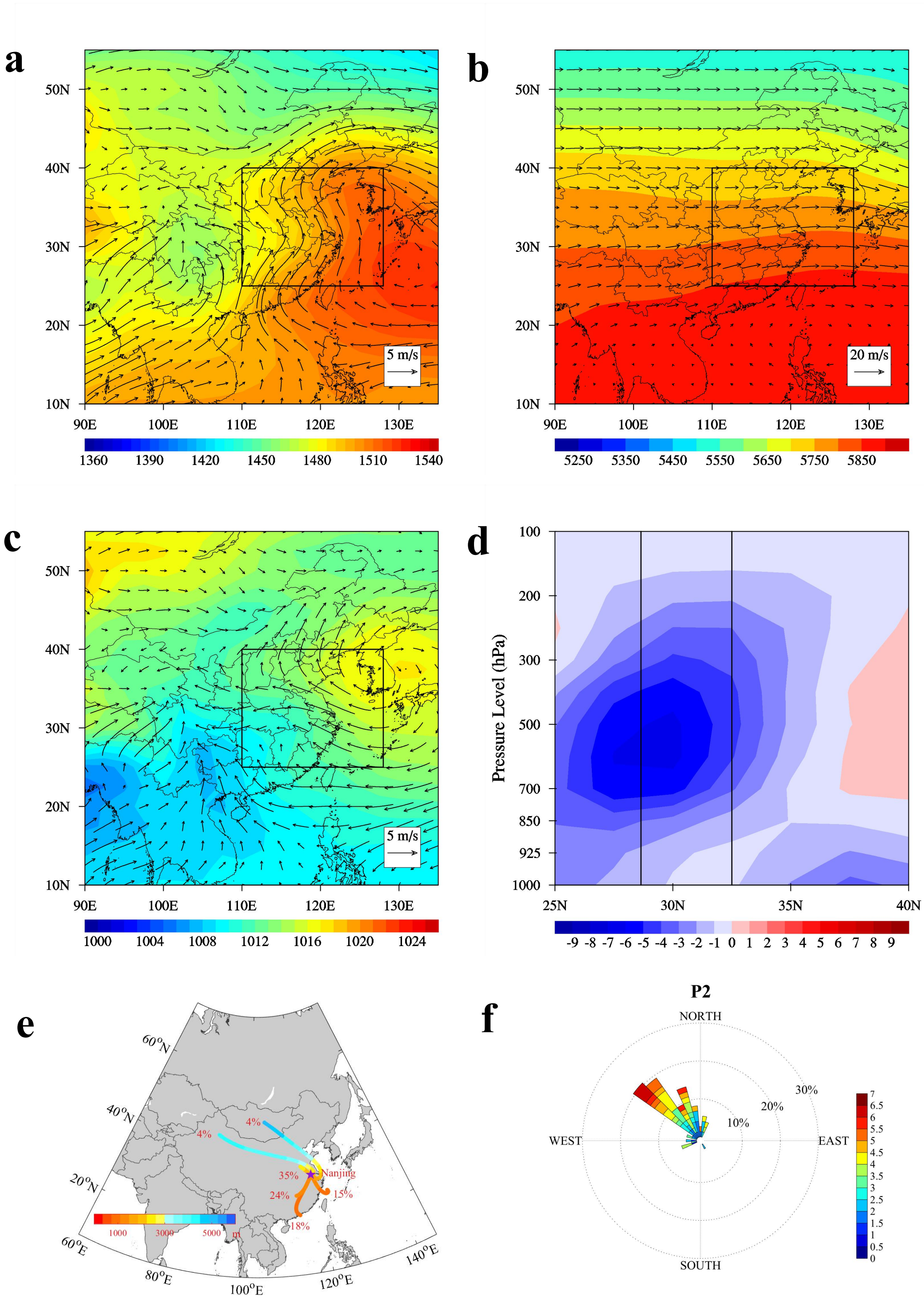

Figure 8. As in Fig. 7, but for Pattern 2.

For Pattern 3, it tends to occur in winter (36.4%, as displayed in Table 3). Under this circumstance, the YRD is mainly controlled by a high-pressure system that is centered in central China (Fig. 9a). Meanwhile, northeastern China is under the steering influence of the northwest air flows at the rear of the East Asian major trough, with its trough axis appearing along the eastern coastline of China. Affected by the strong northwest winds coming from northern China, the polluted air masses from the BTH are easily transported to the YRD. At the higher layer of 500 hPa (Fig. 9b), the circulation structure patterns are similar to those ~~for~~ of Pattern 1. A trough appears in the upper atmosphere, resulting in relatively strong west-northwest flows. The presence of dense isopleths indicates that there is a large geopotential height gradient and strong downward flows. ~~While a~~At the surface layer (Fig. 9c), the presence of strong northerly wind is also evident, and the YRD is located at the bottom of a high-pressure system centered in the remote Mongolian region. The above discussion is further ~~proved~~ supported by the results ~~from~~ of back trajectory calculations. As suggested in Fig. 9e, most air masses in clusters are from the Loess Plateau~~, with the percentage of~~(i.e., 31%). The transport path of this cluster is relatively short, which ~~might~~ may be attributed to ~~the~~ its strong anti-cyclonic circulation. Due to the strong northerly wind, the long-range transport of air masses from remote Mongolia and northern China account~~s~~ for 22% and 18% of all trajectories, respectively. ~~Besides,~~ In addition, the local transport of air masses from the southeast coastal area in the YRD accounts for 26% of all trajectories~~.~~, and ~~The~~ the marine air masses cluster that originates from the western Pacific via the Yellow Sea accounts for 4% of all trajectories. For the vertical structure (Fig. 9d), the distribution of the vertical flow field is similar to that of Pattern 1, whereas the vertical wind is slightly stronger ~~for~~ in the weather systems ~~in~~ of Pattern 3. Due to the influence of the high-pressure system, ~~it is observed that evident~~ downward air flows ~~dominate~~ are dominant ~~in~~ to the north of ~~around 2~~approximately 28°N (including the YRD) below ~~the~~ an altitude of 300 hPa. The largest descending velocity (~9×10^{-2} Pa s^{-1}) also appears at ~~the~~ an altitude of 500 hPa, covering the latitude of 35-40°N. However, ~~in spite of~~despite the higher surface pressure (Figs. 6i and 9c) and stronger downward motion (Fig. 9d), the surface wind is also much stronger for Pattern 3 ~~as well~~ (Figs. 6g, 9a and 9c), which alleviates the problems of air pollution over the YRD compared to Pattern 1. ~~In all~~Overall, under the weather situation of Pattern 3, the strong northwest wind in the front of the high-pressure system usually leads to the transport of polluted air masses from the BTH to the YRD. Nevertheless, the strong surface wind is conducive to the mitigation of pollutants, which plays a significant role in the level of air pollution over the YRD.

Pattern 3

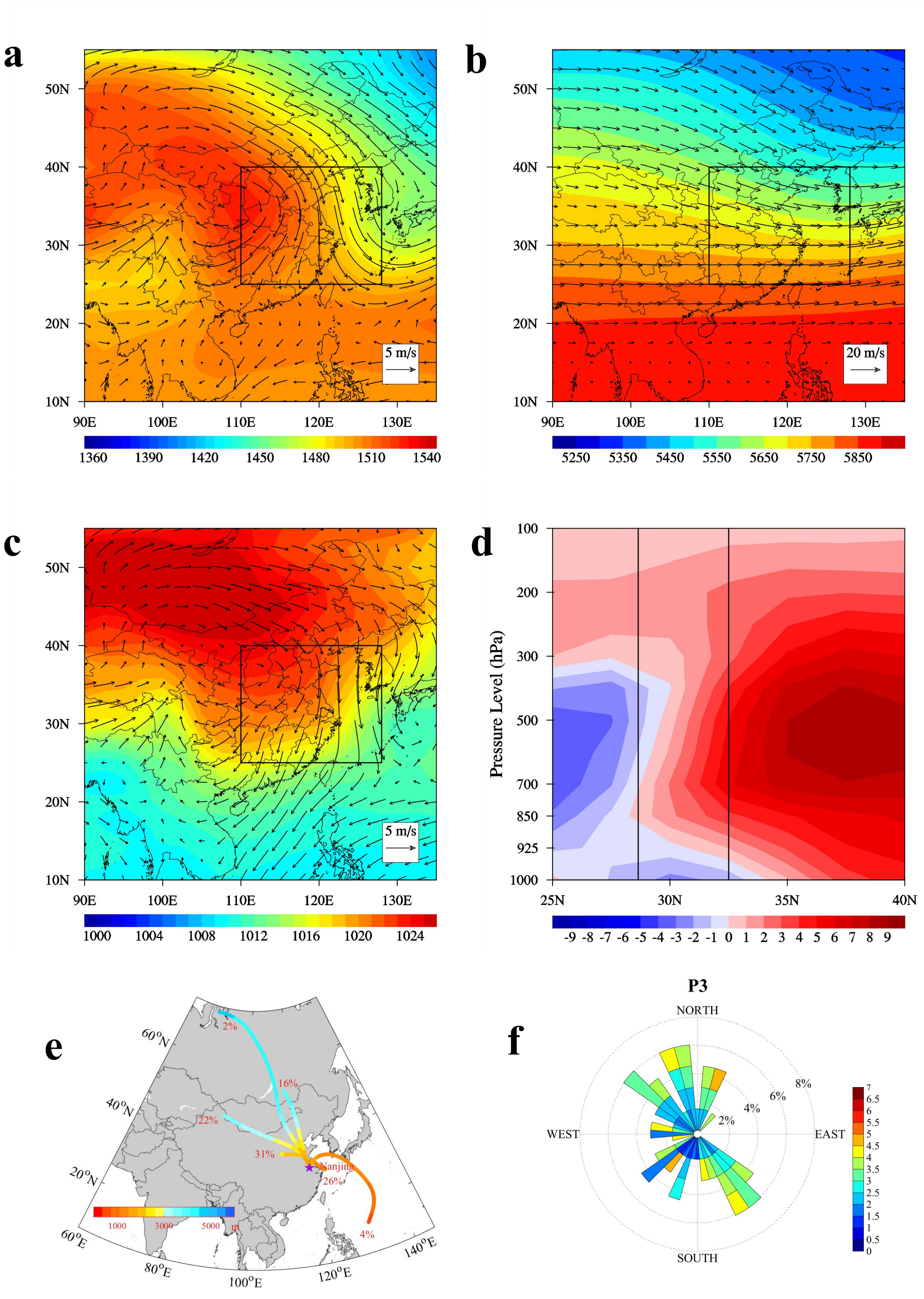

Figure 9. As in Fig. 7, but for Pattern 3.

~~With respect to~~In Pattern 4, on both the surface and at the 850 hPa level, the study ~~domain~~ area is under the control of a high-pressure system (Figs. 10a and 10c). The center of the high-pressure system is located ~~on~~ in the Sea of Japan, while a cyclonic circulation occurs over the

Philippine Sea. ~~The a~~Anti-cyclonic circulation prevails over the YRD and horizontally brings the clean marine air masses to the land. Meanwhile, the sparse isopleths represent a small geopotential height gradient in the middle troposphere, which is accompanied by a much weaker west wind compared to the other patterns (Fig. 10b). Accordingly, influenced by the high-pressure system, ~~the~~ downward atmospheric motion ~~dominates~~ is clearly dominant in the vertical direction ~~obviously~~ (Fig. 10d). The strongest downward motion (~6×10^{-2} Pa s^{-1}) appears between the altitudes of 300 hPa and 500 hPa ~~and~~ at ~~the~~ a latitude of 35°N. The weak updrafts near the surface may be related to the regional thermodynamic circulation. As shown in Fig. 10e, the cluster with the largest frequency of 32% ~~stands for~~represents the local transport of air masses from the southern adjacent areas in the YRD. Additionally, the air masses originating from northern China via the Bohai Bay (25%), from Japan via the Yellow Sea (23%), and from the Philippines via the East China Sea (5%) are also representative. In total, ~~These~~ the clusters ~~passing~~ that pass over the ocean areas ~~totally~~ account for more than 50% of all trajectories. Therefore, under this weather situation, ~~it is confirmed that~~ the dilution effects of clean marine air masses play ~~great~~ a large role~~s~~ in the particle pollution over the YRD.

Pattern 5 features one of the most complex circulation situations at 850 hPa (Fig. 11a). The YRD is located between the bottom of the northern high-pressure system and the top of the southern weak low-pressure system. ~~For this reason~~Thus, the strong horizontal ~~strong~~ east wind prevails and easily carries clean marine air masses from the East China Sea to the YRD. The corresponding circulation structure at the surface layer is similar to that at the 850 hPa layer (Fig. 11c), while ~~the~~ east-northeast flows ~~prevails~~are prevalent over the study domain. In the upper troposphere, a ridge appears in the east due to the tropical cyclonic system, thus leading to the west-southwest flows over the region. ~~Owing~~ Due to the ~~above-mentioned~~abovementioned two opposite pressure systems (Fig. 11a), strong upward air flows are dominant ~~in~~ to the south of the latitude of 35 °N, while ~~the~~ downward motion is obvious in the north (Fig. 11d). The largest ascending velocity (~ -9×10^{-2} Pa s^{-1}) appears ~~in~~ at ~~the~~ a latitude of ~~around 2~~approximately 27.5 °N in the upper troposphere. ~~The~~ This strong upward motion facilitates the diffusion and removal of the accumulated pollutants from the surface layer. According to Fig. 11e, the cluster with the largest frequency of 45% consists of the wet air parcels originating from Japan via the Yellow Sea. Only 5% of the trajectories originate~~s~~ from the Philippines and pass over the East China Sea. ~~On~~

~~the whole~~Overall, under the weather situation ~~for~~ of Pattern 5, the transport of clean marine air masses and favorable diffusion conditions contribute to the good air quality over the YRD.

Pattern 4

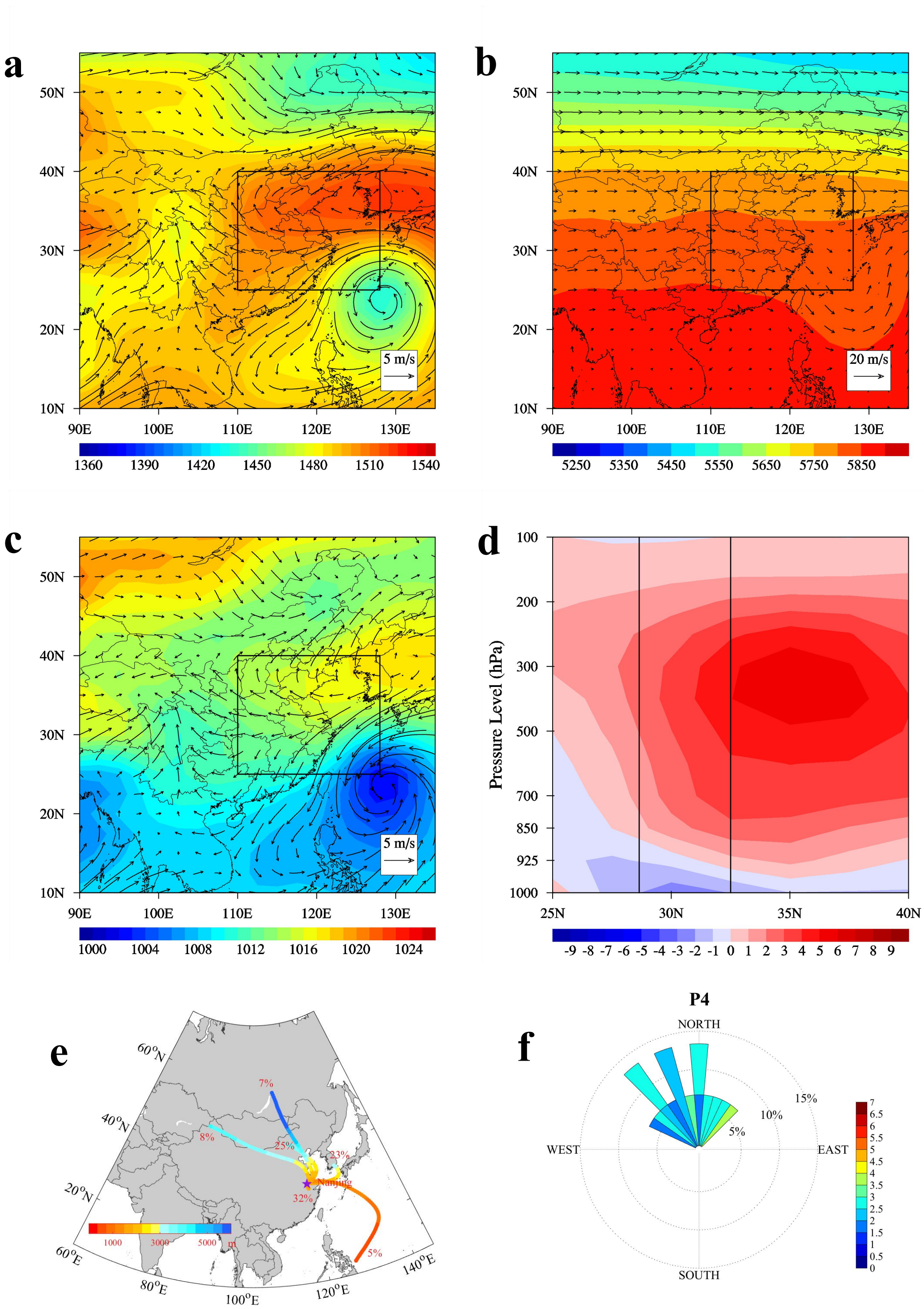

Figure 10. As in Fig. 7, but for Pattern 4.

Pattern 5

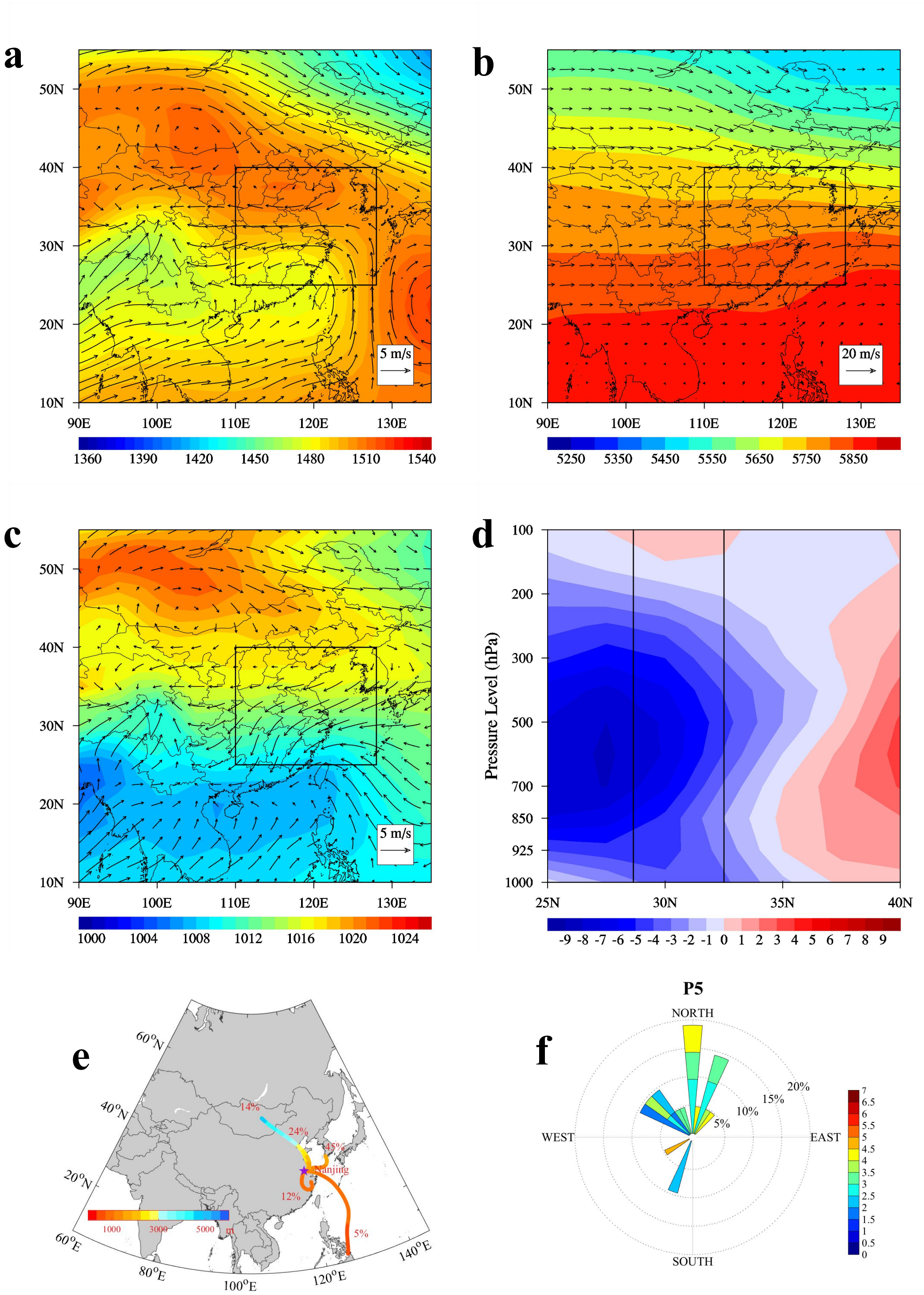

Figure 11. As in Fig. 7, but for Pattern 5.

To ~~sum up~~summarize, the weather situations for Patterns 1-5 are more or less affected by a high-pressure system. However, the relative positions of the study ~~domain~~ area to the anti-cyclonic circulation system ~~are~~ have ~~quite~~ significant ~~to~~ effects on the air quality of the YRD. These differences determine the wind speed and wind direction, and the latter further determines whether the YRD is influenced by the clean marine air masses. ~~For~~ In both Pattern 1 and Pattern 3, the YRD ~~are both~~is impacted by the northwest air flows at the rear of the East Asian major trough, which transport abundant air pollutants from other regions (such as the BTH and the SCB) to the YRD and cause severe particle pollution (as well as high AOD value~~s as well~~) in the YRD. In contrast, the weaker local surface wind ~~for~~ in Pattern 1 is extremely conducive to the local accumulation of pollutants. For this reason, Pattern 1 is 'the most polluted pattern', and it is responsible for ~~the~~ most of the large-scale particle pollution episodes over the YRD. ~~Owning~~ Due to ~~the~~ its stronger surface wind, Pattern 3 is 'the second-most polluted pattern'. ~~As for~~ In Pattern 2, the polluted air masses mainly travel from the southern inland areas~~,~~ and synchronously meet with the clean marine air masses in the YRD. To some extent, this weather situation ~~is helpful to the mitigation of~~helps mitigate particle pollution in the YRD. ~~With respect to~~In Pattern 4 and Pattern 5, the YRD is directly influenced by ~~the~~ air flows traveling from the ocean areas, and it ~~has little chance of being~~is thus unlikely to be polluted. Thus, Pattern 4 and Pattern 5 can be identified as 'the clean patterns'. ~~It~~ These data suggest~~s~~ that the clean marine air masses can ~~have great dilution impacts on~~substantially dilute the particle pollution over the YRD.

4. Conclusions

In this study, the spatial and temporal distributions of particle pollution in 16 YRD cities are characterized from December 2013 to November 2014. Meanwhile, ~~the~~ synoptic weather classification is conducted to identify the dominant weather patterns over the YRD. The meteorological fields and 72-h backward trajectories are analyzed to reveal the potential impacts of weather systems on ~~the~~ regional severe particle pollution episodes.

~~From the~~O~~o~~bservational records~~, it is shown~~ indicate that the concentrations of $PM_{2.5}$ and PM_{10} decrease progressively ~~along~~ in the northwest-southeast direction. The pollution levels are comparatively higher in ~~the~~ Jiangsu Province and much lower in the southeast coastal area (i.e., Ningbo, Taizhou and Zhoushan). The highest particle concentrations occur~~s~~ in Nanjing, ~~with~~ where the concentrations of $PM_{2.5}$ and PM_{10} ~~being~~ are 79 and 130 $\mu g \cdot m^{-3}$, respectively. The $PM_{2.5}/PM_{10}$ ratios are high in the YRD, especially in winter. The seasonal mean $PM_{2.5}/PM_{10}$ ratios are 0.73 (winter), 0.61 (spring), 0.67 (summer) and 0.63 (autumn)~~, respectively~~. These high

$PM_{2.5}/PM_{10}$ ratios suggest that the $PM_{2.5}$ fraction is extraordinarily dominant in the PM_{10} mass in the YRD. ~~Besides,~~ In addition, high AOD ~~is~~ values are also found in the YRD, with ~~the~~ an annual mean value of 0.71±0.57 and ~~the~~ a maximum seasonal mean value of 0.98±0.83 in summer. The diurnal cycles of the particle concentrations in most cities follow the same pattern, ~~with~~ reaching a morning peak from 8:00 to 12:00. There are three peaks in seasonal variations (December, March, and May or June). The wintertime peak is closely related to ~~the~~ enhanced emissions ~~in~~ during the heating season and poor meteorological conditions. Moreover, the YRD suffers from ~~the~~ $PM_{2.5}$ (PM_{10}) pollution ~~in~~ on nearly 28.0% (13.1%) of the days of the year. ~~The c~~Continuous large-scale regional $PM_{2.5}$ pollution episodes occur much more frequently than ~~the~~ PM_{10} pollution episodes.

Based on the sums-of-squares technique, five typical synoptic weather patterns are objectively identified in the YRD, including the East Asia major trough rear pattern (Pattern 1, ~~occurs~~ which occurs on 47.7% of all days), the depression inverted trough pattern (Pattern 2, 20.0%), the transversal trough pattern (Pattern 3, 18.1%), the high-pressure controlled pattern (Pattern 4, 4.1%) and the northeast cold vortex pattern (Pattern 5, 5.8%). Each pattern differs from the other in respect to the relative position of the YRD to the main synoptic system (i.e., the anti-cyclonic circulation system). ~~The~~ This difference determines the wind speed and wind direction, which play ~~an~~ important roles in the air quality level of the YRD. ~~Especially~~In particular, the wind direction is closely associated with ~~the situation~~determining whether the YRD is influenced by clean marine air masses. ~~Under~~ In the patterns ~~when~~ in which the YRD is located at the rear of the East Asian major trough at 850 hPa (i.e., Pattern 1 and Pattern 3), ~~the~~ strong northwest wind can easily transport air pollutants from other polluted areas to the YRD, thus leading to serious particle pollution in the YRD. Due to the high-pressure system, significant vertical downward motion ~~dominates~~ is dominant above the YRD, resulting in relatively stable weather conditions at the surface. With weak local surface wind, the worst polluted weather pattern (Pattern 1) features the highest regional mean PM_{10} (116.5±66.9 $\mu g \cdot m^{-3}$), $PM_{2.5}$ (75.9±49.9 $\mu g \cdot m^{-3}$) and high AOD (0.74) values. Pattern 1 is also responsible for ~~the~~ most of the large-scale regional $PM_{2.5}$ (70.4%) and PM_{10} (78.3%) pollution episodes in the YRD. ~~As for~~ In Pattern 3, the strongest surface wind is conducive to the mitigation of pollution, thus resulting in the second-~~-~~highest PM_{10} (86.9±49.5 $\mu g \cdot m^{-3}$) and $PM_{2.5}$ (59.1±37.3 $\mu g \cdot m^{-3}$) values. In contrast, under the weather system of other synoptic patterns (especially Pattern 4 and Pattern 5), the clean marine air masses, which are transported via the east-southeast wind, play a crucial role in the mitigation of pollution over the YRD. Therefore, the YRD has a much ~~less~~ smaller chance of being polluted.

In summary, the above results reveal that ~~the~~ particle pollution in China is ~~no longer~~ a thorny issue not only over a single city~~,~~ but also ~~over~~ on a regional scale. This study can enhance ~~the~~ our understanding of the features of particle pollution in East Asia. Meanwhile, ~~it is~~these results also confirm~~ed~~ that large-scale synoptic weather systems ~~have~~ exert ~~great~~ large impacts on regional particle pollution. Therefore, ~~the establishment of the~~establishing potential links between different levels of particle pollution and predominant synoptic patterns can provide ~~an insightful view~~insight ~~on~~ into formulating pollution control and mitigation strategies.

5. Data availability

The air quality monitoring records are available at http://106.37.208.233:20035. The meteorological data are available at http://www.nmc.cn. The MODIS/AOD records are available at https://ladsweb.nascom.nasa.gov/search/index.html. The NCEP reanalysis data are available at https://www.esrl.noaa.gov/psd/data/gridded/data.ncep.reanalysis2.pressure.html an~~d~~ ~~h~~d http://ready.arl.noaa.gov/archives.php.

Acknowledgments

This work was supported by the National Natural Science Foundation of China (41475122, 91544230, 91537102, 41621005), the National Key Research and Development Program of China (2016YFC0203303, 2016YFC0208504, 2016YFA0602104), and the open research fund of the Chongqing Meteorological Bureau (KFJJ-201607). The authors would ~~like to thank~~ like to thank the anonymous reviewers for their constructive and ~~precious~~ valuable comments on this manuscript.

LANGUAGE EDITING

CERTIFICATE

This document certifies that the manuscript listed below was edited for proper English language, grammar, punctuation, spelling, and overall style by one or more of the highly qualified native English speaking editors at Wiley Editing Services.

Manuscript title:

Regional severe particle pollution and its association with synoptic weather patterns in the Yangtze River Delta region, China

Authors:

Lei Shu, Min Xie, Da Gao, Tijian Wang, Dexian Fang, Qian Liu, Anning Huang, Liwen Peng

Date Issued:

September 3, 2017

Certificate Verification Key:

02A8-9799-C450-AD88-F648

This certificate may be verified at https://secure.wileyeditingservices.com/certificate. This document certifies that the manuscript listed above was edited for proper English language, grammar, punctuation, spelling, and overall style. Neither the research content nor the authors' intentions were altered in any way during the editing process. Documents receiving this certification should be English-ready for publication; however, the author has the ability to accept or reject our suggestions and changes. If you have any questions or concerns about this document or certification, please contact help@wileyeditingservices.com.

CERTIFIED

Wiley Editing Services